U.PORTO

FEUP FACULDADE DE ENGENHARIA
UNIVERSIDADE DO PORTO

STUDY OF THE DYNAMIC SOIL-STRUCTURE INTERACTION OF A BUILDING ON ELASTIC FOUNDATION

JOÃO PAULO TRAVANCA DE OLIVEIRA

Dissertação submetida para satisfação parcial dos requisitos do grau de

MESTRE EM ENGENHARIA CIVIL — ESPECIALIZAÇÃO EM ESTRUTURAS

Rui Manuel Menezes Carneiro de Barros

JANEIRO DE 2010

MESTRADO INTEGRADO EM ENGENHARIA CIVIL 2009/2010

DEPARTAMENTO DE ENGENHARIA CIVIL

Tel. +351-22-508 1901

Fax +351-22-508 1446

✉ miec@fe.up.pt

Editado por

FACULDADE DE ENGENHARIA DA UNIVERSIDADE DO PORTO

Rua Dr. Roberto Frias

4200-465 PORTO

Portugal

Tel. +351-22-508 1400

Fax +351-22-508 1440

✉ feup@fe.up.pt

http://www.fe.up.pt

To my sister Lara

ACKNOWLEDGEMENTS

First and above all, I would like to thank God for granting me the grace of giving one more step ahead in my life.

Many people have played an important role not only in the process of writing a dissertation, but also during this long and intense endeavor of 5 years of my academic achievements. I would therefore like to offer my sincere thanks to all of them:

- I want to express my deep thanks to Professor Rui Carneiro Barros for accepting to be my supervisor, as well as for his guidance, motivation, time, attention and help with the bibliography;
- I would like to thank Mag. Michael Österreicher for sharing his large experience and knowledge, for his support with the software concerning signal analysis as well as his help in FLAC modeling, and for his endless patience in staying awake along many nights or even available during holiday periods;
- I am grateful to Dr. Wolfgang Unterberger and the IC Consulenten for receiving me as a trainee and for letting me take part in one of their projects where this dissertation was based on;
- To my university colleagues and friends with whom I spent countless hours preparing examination after examination, I thank them for making such times and the atmosphere more pleasant;
- I must not forget my friend António Gonçalves for his continued moral support, assistance, advices and sapience;
- I cannot finish without thanking my family for being my essential support in all aspects of my life.

ABSTRACT

The saturation of the urban areas over recent years and the increasingly limited space for the construction has led this activity sometimes to be done in more critical areas than usual. On the other hand, the expansion and development of the public transport systems, such as railways, has been responsible for the increase in these critical areas. A building which is relatively close to a railway will undergo higher vibrations, where the soil is their propagation mean. The case of study reports a building to be built under these conditions.

For the structural requirements and scope of human comfort are fulfilled, an elastic foundation model was adopted in order to reduce the incoming vibrations from the railway traffic propagated through the ground.

The purpose of this work is to predict the impact of such vibrations, by trying to design a finite element model, where issues such as interaction between soil and structure and the chosen material for the elastic foundation should be taken into account in such modelling due to their influence.

Regarding the analysis, it was done in the frequency domain and the comparison between theoretical and practical results was made by means of transfer functions, due to the specific characteristics of such type of dynamic actions.

KEYWORDS: soil-structure interaction, dynamics, elastic foundation, transfer function, frequency.

RESUMO

A saturação das áreas urbanas ao longo dos últimos anos e a cada vez mais escassez de espaço para a construção tem levado a que esta actividade se desenvolva por vezes em áreas mais críticas que o habitual. Por outro lado, a expansão e desenvolvimento dos sistemas de transporte público, como por exemplo as linhas férreas, tem sido responsável pelo aumento dessas áreas críticas. Um edifício relativamente próximo a uma via-férrea estará sujeito a maiores vibrações, sendo o solo o meio de propagação das mesmas. O caso de estudo reporta um edifício a ser construído nessas mesmas condições.

Para que os requisitos estruturais e do âmbito do conforto humano sejam preenchidos, foi adoptado um modelo de fundação elástica com o propósito de atenuar as vibrações provenientes do tráfego ferroviário propagadas através do solo.

O objectivo do trabalho passa por prever os efeitos dessas mesmas vibrações, através da tentativa de idealização de um modelo de elementos finitos, onde aspectos como a interacção entre o solo e a estrutura e o material escolhido para a fundação elástica deverão ser tidos em conta nessa mesma modelação devido à sua influência.

No que toca à análise, a mesma é feita no domínio da frequência e a comparação entre resultados teóricos e práticos feita por meio de funções de transferência, devido às características específicas deste tipo de acções dinâmicas.

PALAVRAS-CHAVE: interacção solo-estrutura, dinâmica, fundação elástica, função de transferência, frequência.

TABLE OF CONTENTS

FIGURE LIST

TABLE LIST

SYMBOLS AND ABBREVIATIONS

a_{max} – maximum acceleration [m/s^2]

a_{eff} – effective acceleration [m/s^2]

c – dashpot [kN/m/s]

c' – cohesion angle [º]

c_c – critical dashpot [kN/m/s]

f – exciting frequency [Hz]

f_0 – central frequency [Hz]

f_1 – lower frequency limit of a third octave band [Hz]

f_2 - upper frequency limit of a third octave band [Hz]

f_0 – natural frequency [Hz]

k – stiffness [kN/m]

m – mass [kg]

r – frequency ratio [-]

t – time [s]

v – velocity [m/s] or velocity level [dB]

v_p – P-wave velocity [m/s]

v_s – S-wave velocity [m/s]

x – displacement [m]

x_h – homogeneous solution [m]

x_p – particular solution [m]

$\dot{x}$ - velocity [m/s]

$\ddot{x}$ - acceleration [m/s^2]

[C] – damping matrix [kN/m/s]

E – elastic modulus [Pa]

F – force [kN]

{F} – vector of forces [kN]

K – bulk modulus [Pa]

[K] – stiffness matrix [kN/m]

G – shear modulus [Pa]

[M] – mass matrix [kg]

[M_1] – mass system matrix without the mass of the structure[kg]

$[M_2]$ – mass matrix without the soil [kg]

T – period [s]

{U} – absolute displacement vector [m]

X – dynamic amplitude [m]

X_0 – static deflection [m]

{X'} – relative displacement vector [m]

{Y} – modal displacement vector [m]

α – Rayleigh damping constant [1/s] or [rad/s]

β – Rayleigh damping constant [s] or [rad.s]

Δz_{min} – smallest width of an adjoining zone in the normal direction to the interface [m]

ε – volumetric expansion [-]

ν – Poisson's ratio [-]

Ø – phase angle [rad]

ø – friction anlge [º]

σ – normal stress [Pa]

τ – shear stress [Pa]

γ – angular distortion [-]

η – loss factor [-]

ζ – damping ratio [-]

ω – excitation frequency [rad/s]

ω_n – natural frequency [rad/s]

DFT – Discrete Fourier Transformation

FFT – Fast Fourier Transformation

SSI – Soil Structure Interaction

TF – Transfer Function

1

Introduction

1.1. BACKGROUND

During the past few decades, extensive investments have been made in creating new infrastructures. This rapid expansion took place almost simultaneously in many European and some other countries. More and more, the lack of space has led the activity of construction to be carried out in sites with/in special conditions which engineers so far had never dealt with. For instance, many design guidelines related to vibration problems have been responsible for a high number of research and applications all over the world. The subject of dynamics in structures has a very wide field of application, and it is hard to define standards due to several and specific situations, thus digressing from statics. Either of problems has its own particularities and its own nature. For instance, problems concerning blasting and construction activities, offshore and earthquake problems have significantly different dynamic characteristics than those caused by train traffic. Also the nature of the soil constitutes itself another issue: different types of soils have influence on vibration propagation and on the interaction with the structure in different ways.

Vibrations can affect buildings, installations and cause nuisance, which may disturb people. Under unfavorable conditions, these can also damage sensitive structures and installations in and on the ground.

In spite of the increasing practical importance of vibration problems caused by human activities and the advances in soil dynamic research, practicing engineers have limited knowledge of vibration problems and how these can be analyzed and included in design.

Moreover, because of the special nature of rail-bound transportation systems, which usually need to pass through highly populated areas (the train weight had to be increased significantly, while at the same time, modern communication required trains to travel faster, resulting in higher vibration amplitudes), new technical and environmental challenges have to be dealt with.

The erection of a habitation building 20 meters away from a buried/tunneled train track, supported on an elastic foundation composed by two concrete plates with 1 meter of thickness each and an elastic material lying between represents so far a noticeable case of study. The dynamic soil-structure-interaction, as well as the efficiency of the elastic material, structure and human response are the points where the work is going to be focused on.

Since the dynamic SSI must be considered due to its influence on the structure and therefore human response, a correct modeling of such phenomenon, as well as any eventual improvements on it can be ensured from several measurements both in the ground and structure (foundation), with which the theoretical results are then compared. The same procedure may be taken for a subsystem involving the elastic material, whereas this time the geophones are set up on the two different plates of the

foundation. Once the accuracy of the theoretical models is verified, an estimation of what to expect for the storeys not yet built, regarding the human perception, can be done. By adopting such sort of elastic foundation for a building under the mentioned conditions, it is desired that the effects of the train induced vibrations will decrease enough so that the human comfort will be guaranteed.

1.2. CONTENTS AND ORGANIZATION OF THE REPORT

The introduction in Chapter 1 gives a background and describes the objectives of the report. The present work is essentially focused on the analysis and verification of the accuracy for future projects concerning similar characteristics/solutions.

Chapter 2 presents some fundamentals concerning vibration terms, signal analysis and ground vibration. For a good comprehension of modeling, dynamic analysis and all the procedures that were carried out for calculations, it is important for any reader to be acquainted with the basic concepts of dynamics and the way how they relate each other. Thus, the singly mass system formulation is firstly approached. This initial subchapter will also introduce the reader to signal analyzing via Fourier Transformation. Although such subject is often associated to other branches of engineering, the equipment used for the measurements, as well as the theoretical calculations, implied the tasks to be carried out in both time and frequency domains. Hence, in order to understand how the equipment and auxiliary software act some aspects of signal analysis shall be presented. Another factor to take into account due to its influence is the soil. Any case of study of the dynamic soil-structure-interaction matter is obviously based on the two subsystems, soil and structure, and the way how their interaction influences and affects the structure when the soil is under motion. A few words are then devoted to soil vibration, wave types and ahead to the soil performance as propagation path. In the last topics of the chapter, also the vibration source and the receiver are briefly described thus giving to the reader a clearer idea of the entire phenomena of rail induced vibrations.

Chapter 3 gives an overview of vibration analysis of SSI, since the first solutions obtained till the present. The state of the art provides one the evaluation and different ways in modeling, which also constitutes a base for the intended models of the report.

Chapter 4 indicates the area where the measurements were done and describes the equipment and software used for data processing, as well as the steps considered for the data treatment.

In chapter 5, the different phases of modeling are described and the FE model is executed. Together, the limitations and characteristics of the software and the real case of study implied specific settings in the model creation. Every theory behind some theoretical assumptions is also explained. Different sub-models aimed to test and predict the dynamic SSI phenomena, the elastic foundation behavior, wave propagation and structure and human response are presented. The theoretical results are then compared to the practical ones in order to verify the accuracy and utility of the defined models. Ahead, the results are discussed.

Finally, in chapter 6 a global appreciation of the work is done, as well as some suggestions are given for future works.

2
Fundamentals

2.1. SINGLE-DEGREE-OF-FREEDOM SYSTEM

The single-degree-of-freedom system represents the simplest model that one can consider in order to predict or analyse the response of a vibratory system. This designation may be used since it is possible to specify the position of the mass, at any time, by using a single coordinate. Such system is shown in Figure 2.1. No external forces are applied to the mass. Thus, the motion from any disturbance will result in a free vibration. Equally, there is no element that causes the dissipation of the energy as long as the motion is performed, which means that the amplitude of the motion will remain constant with time. Therefore, the idealized system consists of a linear spring with a spring constant *k* and a body with a mass *m* (Figure 2.1):

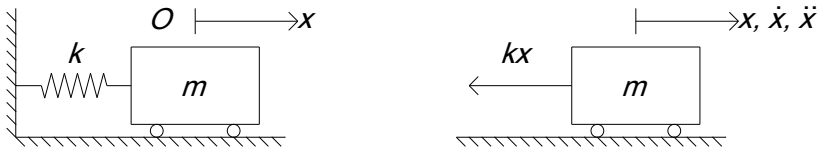

Figure 2.1 – Single DOF system

2.1.1. FREE VIBRATION OF AN UNDAMPED TRANSLATIONAL SYSTEM

According to Figure 2.1, it is possible to obtain the differential equation of motion by using, for instance, the Newton's second law, which states that a force applied to a body produces a proportional acceleration:

$$\vec{F} = m\ddot{\vec{x}} \qquad (2.1)$$

where

$$\ddot{\vec{x}} = \frac{d^2\vec{x}(t)}{dt^2} \qquad (2.2)$$

is the acceleration of the mass.

By applying it to the system shown in Figure 2.1, one will have:

$$F(t) = -kx = m\ddot{x} \qquad (2.3)$$

or

$$m\ddot{x} + kx = 0 \qquad (2.4)$$

where the mass *m*, displaced a distance *x* from its static equilibrium position, generates a spring force of *kx*.

Nevertheless, other several methods may be taken into account when it comes to derivate the equations of motion: D'Alembert's Principle, the Principle of Conservation of Energy, among many others.

The solution:

$$x(t) = Ce^{st} \qquad (2.5)$$

satisfaes the Equation (2.6). The constants *C* and *s* are to be determined. The substitution of Equation (2.7) into Equation (2.6) gives

$$C\left(ms^2 + k\right) = 0 \qquad (2.6)$$

Since *C* is different than zero

$$s = \pm\sqrt{\frac{k}{m}} = \pm i\omega_n \qquad (2.7)$$

where *s* represents the two roots of the characteristic equation (Equation (2.4)), also called *eigenvalues* of the system, and ω_n is the natural angular frequency $(2\pi f)$. The general solution of Equation (2.4) can thus be expressed as

$$x(t) = C_1 e^{i\omega_n t} + C_2 e^{-i\omega_n t} \qquad (2.10)$$

and rewritten either as

$$x(t) = A\left(\cos\phi\cos\omega_n t + \sin\phi\sin\omega_n t\right) \qquad (2.11)$$

or

$$x(t) = A\cos\left(\omega_n t - \phi\right) \qquad (2.12)$$

where *ø* is the phase angle and *A* is the amplitude which is function of the initial conditions of the system.

The scheme discribed in Figure 2.1 can thus be associated to a *harmonic oscillator*, whose motion is graphically described in Figure 2.2:

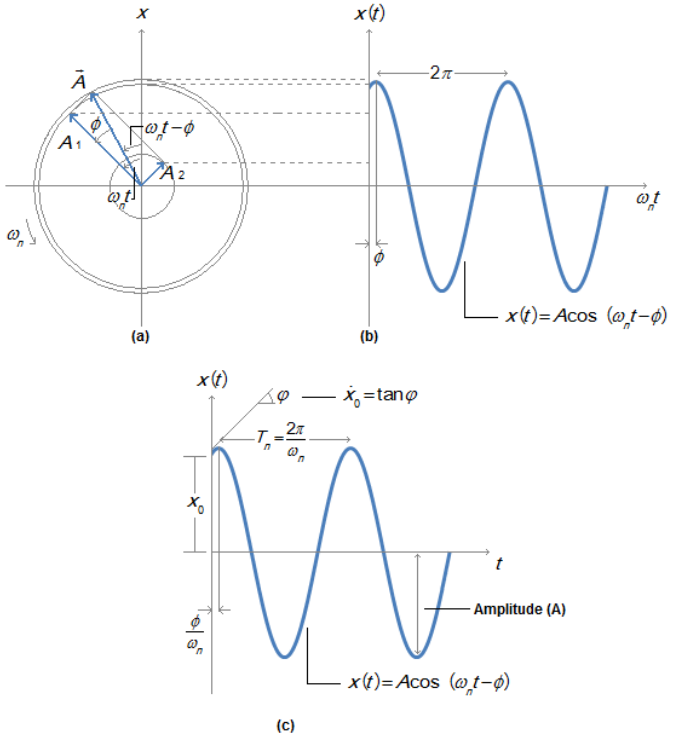

Figure 2.2 – Graphical representation of the motion of a harmonic oscillator (Rao, 1991)

2.1.2. Free Vibration with Viscous Damping

A viscous damper will be now added to the system initially portrayed. Dampers are assumed to have neither mass nor elasticity. Their force is proportional to the velocity and has the opposite direction of it. Furthermore, damping force only exists if there is relative velocity between the two ends of the damper. Once the free vibration motion takes place, the resistance, offered by the damper, causes energy to be dissipated. Figure 2.3 shows the single degree of freedom with the viscous damper:

Figure 2.3 – Single DOF system with damping

Yielded by the second Newton's law, the equation of motion will come:

$$m\ddot{x} = -c\dot{x} - kx \qquad (2.13)$$

or

$$m\ddot{x} + c\dot{x} + kx = 0 \qquad (2.14)$$

The solution

$$x(t) = Ce^{st} \qquad (2.15)$$

can also be adopted to solve Equation (2.13). Once more the constants *C* and *s* are to be determined. The characteristic equation is obtained by introducing the meant solution into Equation (2.14), from which the general solution comes

$$x(t) = C_1 e^{s_1 t} + C_2 e^{s_2 t} \qquad (2.16)$$

The characteristic equation also provides one the critical damping value (c_c):

$$c_c = 2\sqrt{km} = 2m\omega_n \qquad (2.17)$$

Whenever a system is damped, a damping ratio (ζ) is defined as the ratio between the damping constant and the critical damping constant.

Regarding the damping, the system can be underdamped, critically damped or overdamped.

Figure 2.4 represents the vibration behaviour for the critical damping situation. It is perceptible that *x* decreases exponentially without changing its sign, which means that no oscillations occur.

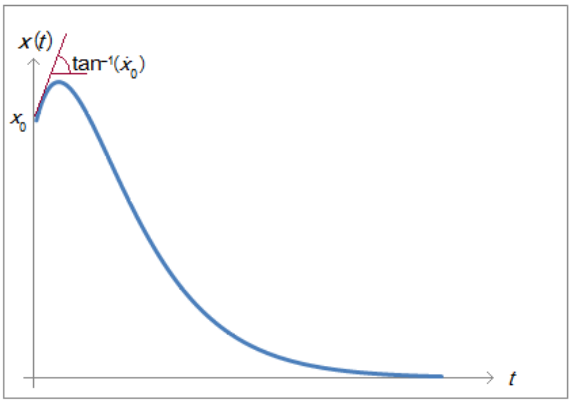

Figure 2.4 – Free vibration for critical damping

For different real solutions the system is said to be *overdamped*. The graphical aspect of the motion will be somewhat similar to figure 2.4, although *x* converges slower to zero.

When the damping is less than critical damping, the solutions of the system are complex. For such *underdamped* system the solution becomes:

$$x(t) = e^{-\zeta\omega_n t}\left\{x_0 \cos\sqrt{1-\zeta^2}\,\omega_n t + \frac{\dot{x}_0 + \zeta\omega_n x_0}{\sqrt{1-\zeta^2}\,\omega_n}\sin\sqrt{1-\zeta^2}\,\omega_n t\right\} \qquad (2.18)$$

Where x_0 and $\dot{x}_0$ are the initial conditions of the system.

The motion for an *underdamped* system, illustrated in Figure 2.5, describes a harmonic function, where the amplitude decreases with time.

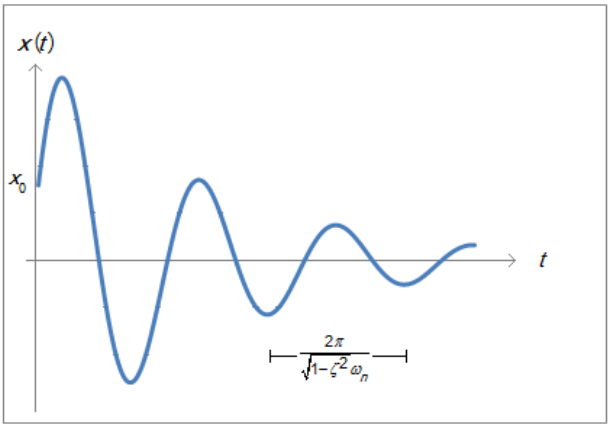

Figure 2.5 – Free vibration of an *underdamped* system

2.1.3. RESPONSE OF A SYSTEM UNDER VIBRATION

Whenever external energy comes into a system during vibration, the system is said to undergo forced vibration. Either these applied forces or displacement excitations may have several natures: harmonic, periodic, non-periodic, random, etc.

2.1.3.1 Harmonic vibration

Let one assume the following harmonic force

$$f(t) = F_0 \cos \omega t \qquad (2.19)$$

acting on an undamped system of mass *m*. The equation of motion reduces to:

$$m\ddot{x} + kx = F_0 \cos \omega t \qquad (2.20)$$

and the homogeneous solution is:

$$x_h(t) = C_1 \cos \omega_n t + C_2 \sin \omega_n t \qquad (2.21)$$

As the excitation is harmonic, the particular solution will also be harmonic and with the same frequency ω

$$x_p = X \cos \omega t \qquad (2.22)$$

Once replaced *x* (Equation (2.20)) by the particular solution, one has:

$$X = \frac{F_0}{k - m\omega^2} = \frac{F_0}{k} \times \frac{1}{1 - \left(\frac{\omega}{\omega_n}\right)^2} \qquad (2.23)$$

By assuming

$$X_0 = \frac{F_0}{k} \qquad (2.24)$$

is the static deflection, and

$$r = \frac{\omega}{\omega_n} \qquad (2.25)$$

is the frequency ratio. The general solution becomes:

$$x(t) = \left(x_0 - X_0 \frac{1}{1 - r^2} \right) \cos \omega_n t + \frac{\dot{x}_0}{\omega_n} \sin \omega_n t + \frac{X_0}{1 - r^2} \cos \omega t \qquad (2.26)$$

From Equation (2.27) one can obtain the ratio between the dynamic and static amplitude of the motion

$$\frac{X}{X_0} = \frac{1}{1 - r^2} \qquad (2.27)$$

denominated amplification factor. Thus, the response of the system can be of three different types:

- For $0 < r < 1$, the amplification factor is positive and the response is performed without any change. Both harmonic response of the system x_p and the external force are said to be in phase.
- If $r > 1$, the amplification factor has a negative sign. Therefore x_p and $f(t)$ have opposite signs, i.e., the response is said to be 180º out of phase with the excitation. For very high frequencies of the external force, the response of the system is close to zero.
- At last, when $r = 1$ the amplitude of the motion becomes infinitive. Whenever the frequency of the force and the natural frequency are equal, resonance takes place. For such case, the response at resonance comes:

$$x(t) = x_0 \cos \omega_n t + \frac{\dot{x}_0}{\omega_n} \sin \omega_n t + X_0 \frac{\omega_n t}{2} \sin \omega_n t \qquad (2.28)$$

and it is graphically represented as:

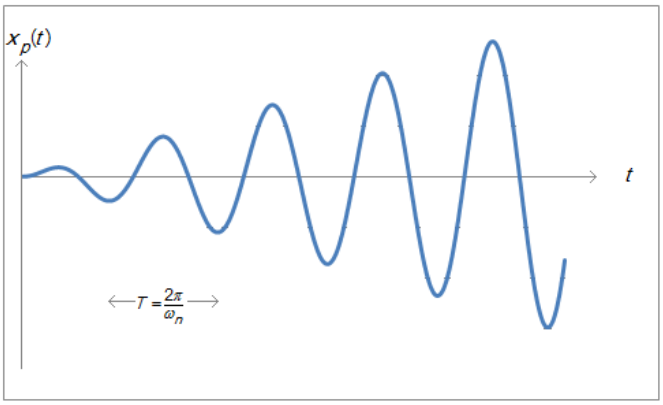

Figure 2.6 – Response of a system under resonance

In case the system is damped, Figure 2.7 relates the amplitude factor with the damping:

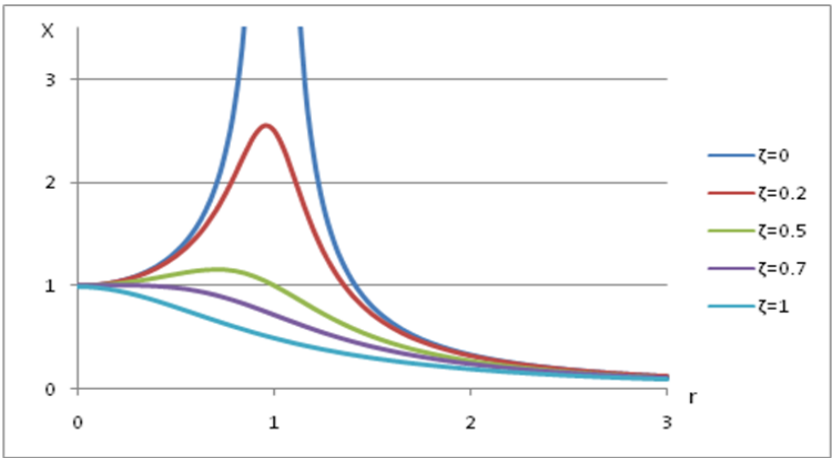

Figure 2.7 – Amplitude factor (*X*) versus *r* for different damping values

From Figure 2.7 some conclusions may be taken

- Any amount of damping (ζ) reduces the amplitude for all values of the forcing frequency;
- The higher the value of damping is, the lower the value of *X* is;
- *X* has sharp reductions ($\zeta > 0$) when near resonance.

For the phase angle one can conclude that:

- And undamped system ($\zeta=0$) has a phase angle of zero since there is no resonance;
- Undamped systems where $0 < r < 1$ have a phase angle ranged]0; 90[;
- Undamped systems where r > 1 have a phase angle ranged]90; 180[;
- An undamped system at resonance has a phase angle of 90º;
- For very high values of *r* in an undamped system the phase angle approaches 180º.

The general solution for an *underdamped* system submitted to a harmonic excitation will come

$$x(t) = x_h(t) + x_p(t) \qquad (2.29)$$

where $x_h(t)$ is given in Equation (2.18). The general solution will be

$$x(t) = x_0 \cos\sqrt{1-\zeta^2}\omega_n t + \frac{\dot{x}_0 + \zeta\omega_n x_0}{\sqrt{1-\zeta^2}\omega_n} \sin\sqrt{1-\zeta^2}\omega_n t + \frac{F_0}{k} \cdot \frac{1}{\sqrt{\left(1-r^2\right)^2 + \left(2\zeta r\right)^2}} \qquad (2.30)$$

2.1.3.2 General forcing conditions

When there is a periodic but non-harmonic function, it is possible to replace it by a sum of harmonic functions using, for instance, the Fourier series. The Fourier series consist of the superposing of individual harmonic functions, and they are given by:

$$f(t) = \frac{a_0}{2} + \sum_{m=1}^{\infty} a_m \cos m\omega t + b_m \sin m\omega t \qquad (2.31)$$

where $\omega = \frac{2\pi}{T}$ is the angular frequency and

$$\begin{aligned} a_0 &= \frac{2}{T}\int_0^T f(t)dt \\ a_m &= \frac{2}{T}\int_0^T f(t)\cos m\omega t dt \\ b_m &= \frac{2}{T}\int_0^T f(t)\sin m\omega t dt \end{aligned} \qquad (2.32)$$

are constant coefficients. From Figure 2.8 it is possible to observe the approximations of the first terms to square wave.

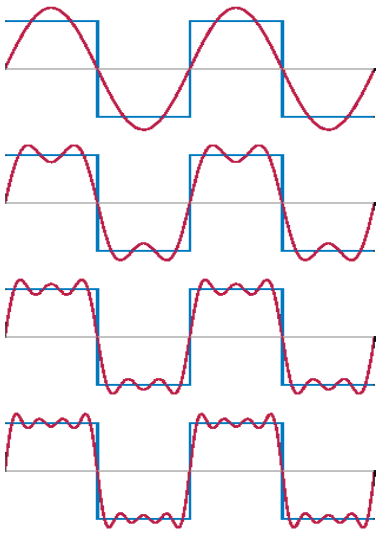

Figure 2.8 – First four Fourier series approximations for a square wave (*Wikipedia*)

Fourier series can also be represented in complex notation.

$$f(t) = \sum_{m=1}^{\infty} F_m e^{im\omega t} \qquad (2.33)$$

where

$$F_m = \frac{a_m}{2} + \frac{b_m}{2i} = \frac{1}{T}\int_0^T f(t)\frac{e^{im\omega t} + e^{-im\omega t}}{2}dt + \frac{1}{Ti}\int_0^T f(t)\frac{e^{im\omega t} - e^{-im\omega t}}{2i}dt = \frac{1}{T}\int_0^T f(t)e^{-im\omega t}dt \qquad (2.34)$$

There are, however, some cases where the system undergoes an irregular force. Let one consider the following non-periodic action (Figure 2.9):

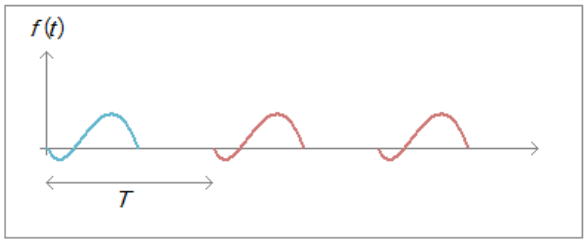

Figure 2.9 – Transformation of a function into a periodic one

The function represented in Figure 2.9 can be imagined with periodic repetitions over the time. If t tends to infinity then one will have an isolated function. Therefore, as $t \to \infty$, $\Delta w \to \partial w$ and:

$$\begin{aligned} &\frac{1}{T} \equiv \frac{\Delta\omega}{2\pi} \\ &m\omega = m\Delta\omega \equiv \omega_m \\ &F_m = \frac{1}{T}F(\omega_m) = \frac{\Delta\omega}{2\pi}F(\omega_m) \end{aligned} \qquad (2.35)$$

wherefrom Equation (2.34)

$$F(\omega_m) = \int_0^T f(t)e^{-i\omega_m t}dt \qquad (2.36)$$

and thus

$$f(t) = \frac{\Delta\omega}{2\pi}\sum_{m=-\infty}^{\infty} F(\omega_m)e^{i\omega_m t} = \frac{1}{2\pi}\sum_{m=-\infty}^{\infty} F(\omega_m)e^{i\omega_m t}\Delta\omega$$

$$F(\omega_m) = TF_m = \int_{-\frac{T}{2}}^{\frac{T}{2}} f(t)e^{-i\omega_m t}dt \qquad (2.37)$$

The limit of Equations (2.37) leads to the Fourier integral

$$f(\omega) = \frac{1}{2\pi}\int_{-\infty}^{\infty} F(\omega)e^{i\omega t}d\omega = \int_{-\infty}^{\infty}\frac{F(\omega)e^{i\omega t}}{2\pi}d\omega \qquad (2.38)$$

and the amplitude function

$$F(\omega) = \int_{-\infty}^{\infty} f(t) e^{-i\omega t} dt \qquad (2.39)$$

Equations (2.38) and (2.39) represent the Fourier transform pairs.

2.2. SIGNAL ANALYSIS

The Fourier - Transformation (referred to hereafter as FT) is a fundamental analytical tool for solving various problems in signal processing. The Fourier series have shown that it is possible to describe any periodic function by using either the time domain or the frequency domain (Figure 2.10).

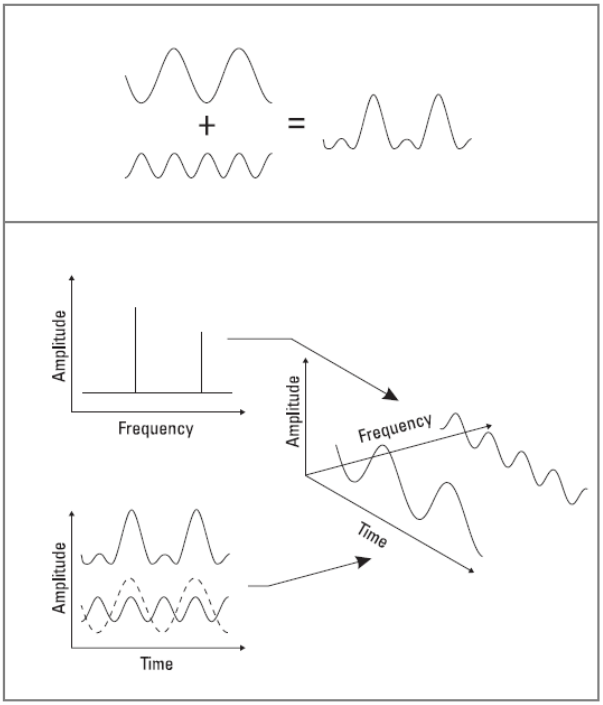

Figure 2.10 – Signal representation in both time and frequency domain (*Agilent Technologies*)

The frequency domain representation contains the axis of amplitude versus frequency. At the frequency domain, each wave separated from the input appears a vertical line, its height represents its amplitude and its position represents its frequency. Although the traditional way of observing signals is to view them in the time domain, the frequency domain is useful whenever the frequency of a signal is of interest.

The frequency domain representation of a signal is called *spectrum* of the signal. Each wave of spectrum is called a component of the total signal. Figure 2.10 illustrates a property of Fourier transformation: a discrete equally spaced signal which is periodic and exists for all time has a discrete frequency *spectrum*. If a signal has continuous *spectrum* then it means that the sine waves that generate it are spaced infinitesimally close together.

For numerical calculations the transform pair is used in its discrete form because the measured signals are also of a discrete form. Based on the discrete Fourier transform pairs there is the Fast Fourier Transformation (FFT), of which algorithm converts *N* equally spaced lines at the time line into *N/2* equally spaced lines at the frequency time.

The FFT is considerably faster than the conventional solution of the discrete Fourier transformation. The expression for the increase of speed in a $N = 2n$ points sampled time function is given by:

$$f_{FFT} = 2.\frac{N}{n} \qquad (2.40)$$

where f_{FFT} is the speed increase of FFT, N is the number of points in the series and n is the exponent of 2, $N = 2n$.

Figure 2.11 shows a comparison of the necessary computational steps of the FFT compared to that for the DFT as a factor of the speed increase.

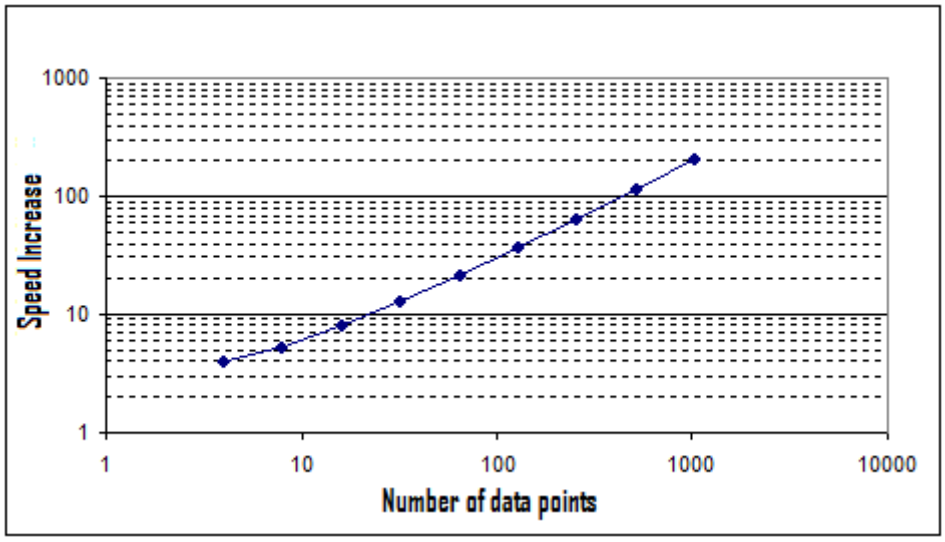

Figure 2.11 – Speed increase of the FFT over the DFT

As visible from Figure 2.11, at an amount of 1024 data points the calculation by means of FFT is 200 times faster than the calculation by means of DFT.

The condition to calculate the FFT is that the number of grid points (samples) in the signal is $N = 2n$. There are several methods to achieve this in case of practical measurements.

- Interpolation
- Populate with zeros until the next power of 2
- Data reduction by means of deleting several data points

When interpolating the number of data points to the next power of 2 between every *n* data points in the original data an additional interpolated data point is added. Although the interpolation method depends on the data, it is in many cases just the average of the two neighbor points.

The padding of the signal with "zeros" to the next power of 2 is the most common method, since this can be carried out with little effort and complexity.

Modern measuring instruments or analog-digital converters (AD converters) also offer the possibility of a more or less arbitrary selection of the sampling rate. Thus, with knowledge of the signal length a

suitable choice of sampling rate can be achieved so that the signal after the digitization satisfies the condition $N = 2n$.

Another important point relating to the FFT is the sampling theorem. The sampling theorem states that a function *h (t)* described by *n*-values is only accurate and complete if it has no frequency components higher than a cutoff frequency f_{max}. The relationship between the cutoff frequency and the sampling rate can be described as follows:

$$\Delta t = \frac{1}{2} f_{max} \qquad (2.41)$$

In other words, the maximum frequency that can be calculated by the FFT is one half of the sampling frequency:

$$f_{Ny} = \frac{1}{2} \Delta t \qquad (2.42)$$

This frequency is called the Nyquist frequency and it is a fundamental value regarding the signal analysis.

The DFT requires not only a periodicity in the time domain but also in the frequency range. That means that if a function is sampled with Δt, then the Fourier transform of this function is repeated in the frequency interval $1/\Delta t$. If one chooses a too large Δt, there will be an overlap in the frequency range called "aliasing" of each transform and the result will be distorted.

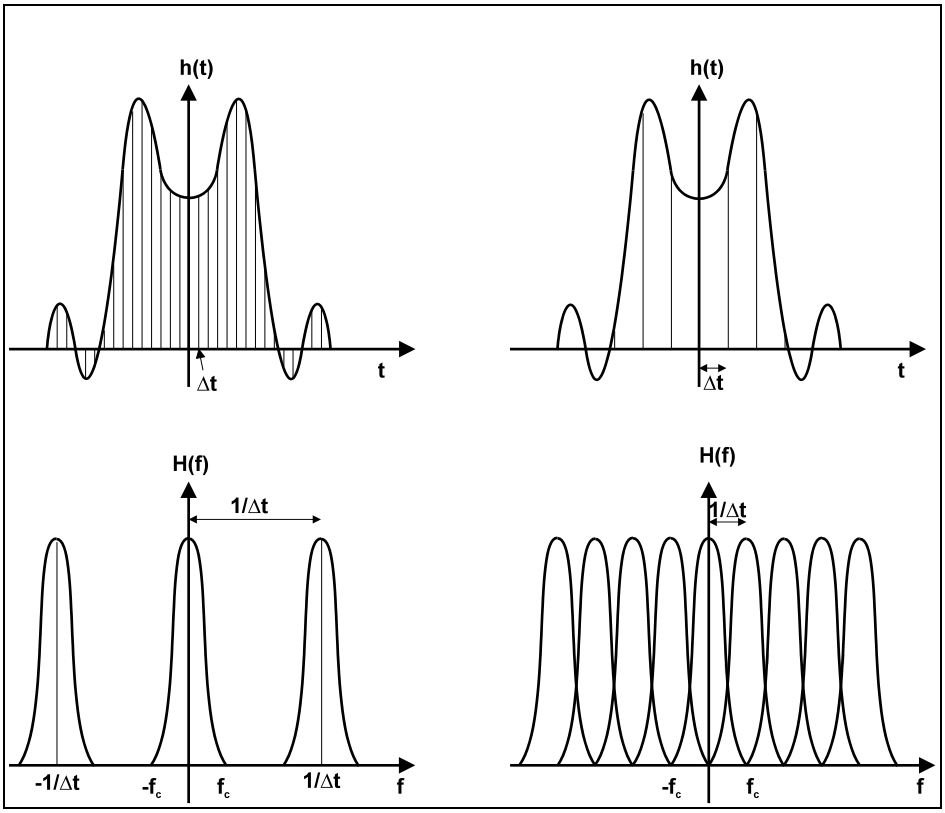

Figure 2.12 – A not sufficiently dense sampled function and its Fourier Transform (Brigham, 1987)

However, the error (aliasing effect) will disappear as soon as the Nyquist frequency of sampling is greater than the highest frequency of the function.

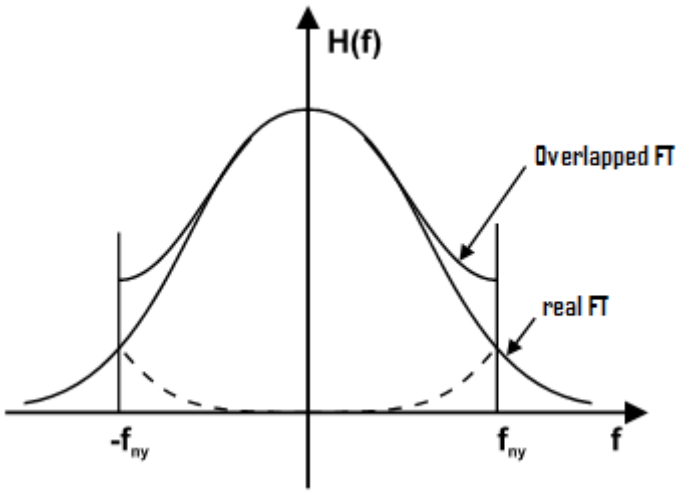

Figure 2.13 - Distortion of the discrete Fourier transform function by a non-Bandwidth overlap (Brigham, 1987)

The sampling rate should therefore always be chosen so that the Nyquist frequency is well above the highest significant frequency (ideally a factor of 10) of the problem.

Another problem related to the DFT results is the limited number of samples which are present in a finite time series. A finite time series analysis obtained by the limited number of samples leads to discrete frequency values. The signal at the beginning and end of a timeframe is zero and therefore results in a periodic continuation of a discontinuity at these points (see Figure 2.13).

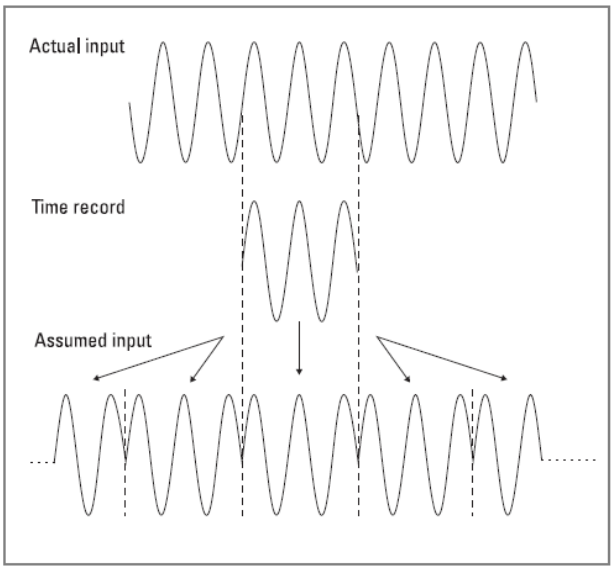

Figure 2.14 – Incorrect assumption of an input generating a distorted waveform (*Agilent Technologies*)

In order to avoid the discontinuity at the beginning and at the end of the time slot, a window function with a suitable amplitude series is applied. Practically, there is the possibility to use any function which satisfies certain mathematical conditions. The following window functions are often used:

- Barlett - Windows

- Hamming - Windows
- From Hann - Windows
- Blackman - Windows

The selection of the right window function depends on the requirements of the evaluation. It mainly depends on what is more important, i.e. the amplitude information or the frequency content of a signal.

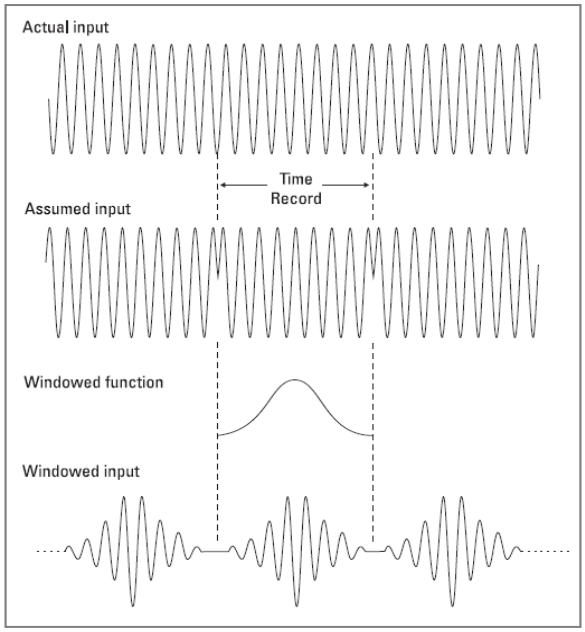

Figure 2.15 – Windowing (*Agilent Technologies*)

As an example of a window function there is the *Hann* function, the van-hann window is plotted below in Figure 2.16.

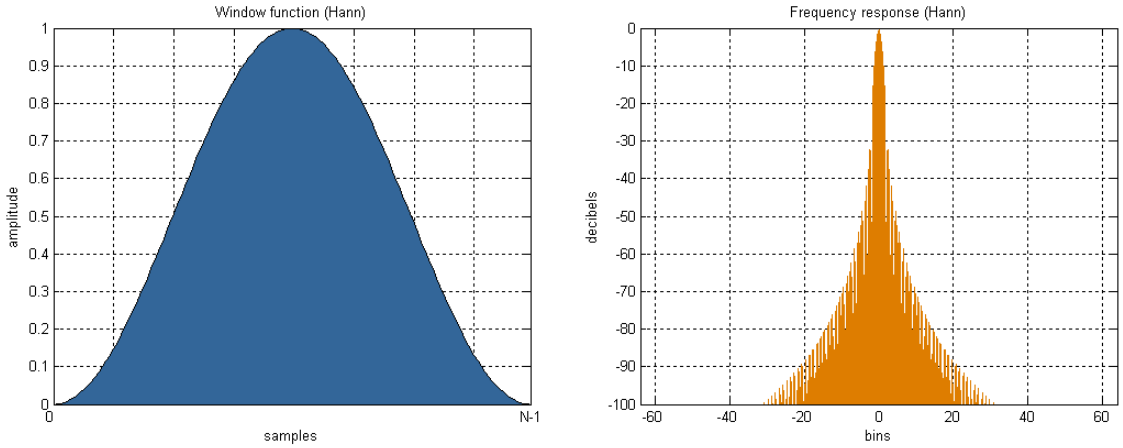

Figure 2.16 – Hann window function (*Wikipedia*)

The Fourier transform is nowadays used in almost all disciplines of science and technology for analysis and processing of particular time series, as well as or the improvement and manipulation of images.

To ensure the quality to improve in terms of identifying individual frequency components of a frequency spectrum, there are basically between two different approaches:

- Methods in the time domain, i.e. before the FT
- Methods in the frequency domain

For the methods in the time domain the digital filtering is one of the most important methods. For instance, electrical noise or some other sources may disturb a signal at certain frequencies. Thus, if the frequencies are known they can be taken out of the signal through the digital filtering.

Below, Figure 2.17 illustrates this process with an example with Gaussian noise.

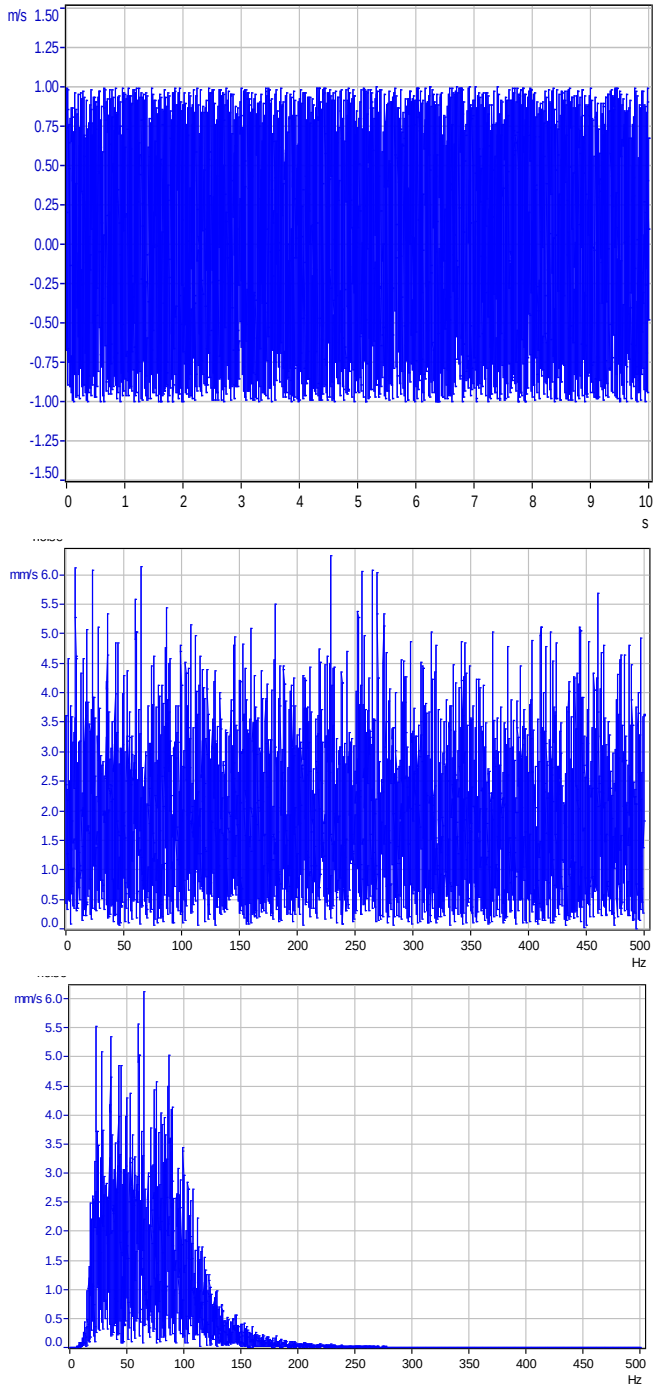

Figure 2.17 - Influence of frequency filtering on the frequency spectrum (on the top – output signal; in the middle – frequency spectrum after the output signal; on the bottom – band pass filtered of the frequency spectrum)

The upper part of Figure 2.17 shows the output signal. As the starting signal is a noise signal (Gaussian noise, with a signal length of 10 seconds and a sampling rate of 0.001 seconds, a sampling frequency of 1000Hz is selected). The middle graph shows the frequency spectrum of the original signal. As one can see, the frequency spectrum of the Gaussian noise shows a spectrum with more or less constant amplitude components of the whole frequency area between 0 Hz and the half sampling frequency. The bottom graph shows exemplarily the frequency spectrum, for the time domain filtered output signal.

How strong the amplitudes outside the frequency bounds of the filter decrease depends on the type of the filter, the ripple of the filter and the slope of the filter. Thus, similarly to the selection of the window functions for a spectral problem, the choice of the appropriate filter is of importance.

Another way to improve the quality of a time series that contains signal components (frequencies) is to remove them directly with a narrow band filter method. However, this requires a detailed knowledge of the expected signal and the frequency content, and it is just possible manually in most of cases.

To improve the quality of the spectrum after the FFT, the improvement of the signal to noise ratio (SNR Signal to Noise Ratio) is performed. For this purpose a smooth filtering method is used. The simplest case of smoothing is the moving average filter. The following example (Figure 2.18) illustrates this process.

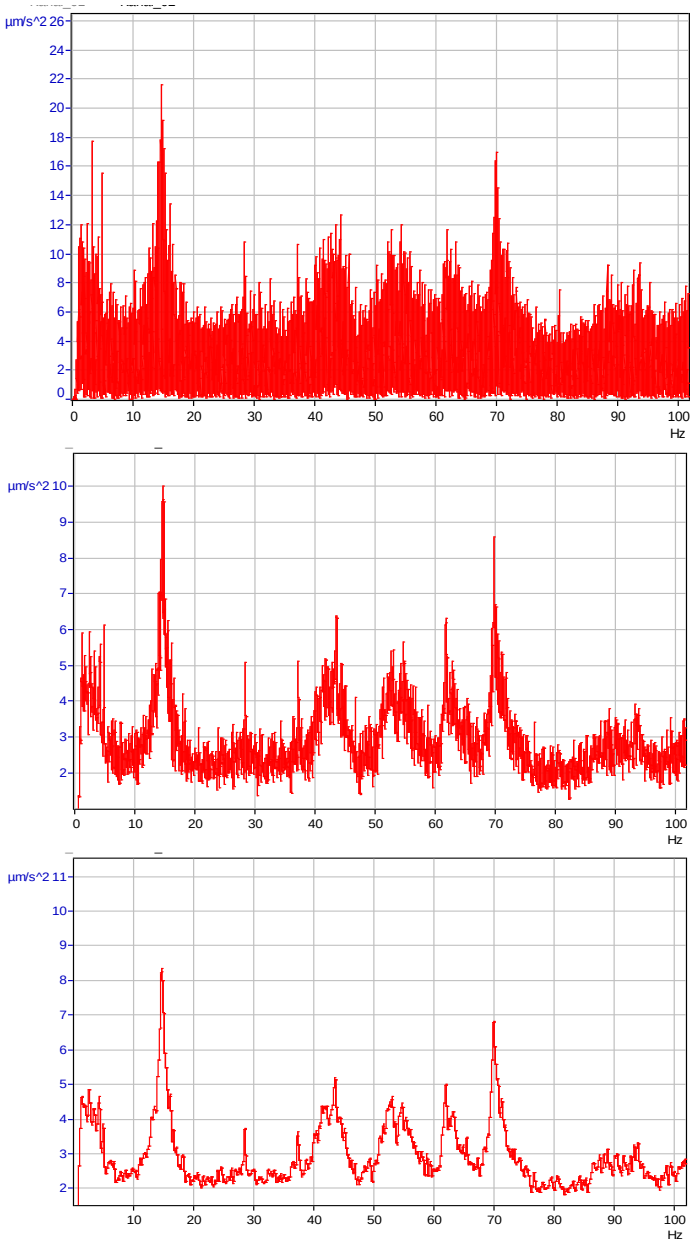

Figure 2.18 – Smoothing of a frequency spectrum with different frequency parameters

The first diagram of Figure 2.18 shows the frequency spectrum of the signal of an acceleration measurement on a bridge structure. The signal for a period of 320 seconds has a sampling rate of 1000 Hz. Each of the diagrams in the lower part of Figure 2.18 shows different smoothing filters. As it can be seen from the two diagrams of the smoothed spectra, it is easy to implement a mean filter to get a significant improvement of the signal quality of the spectrum.

2.3. SEISMIC VIBRATIONS

The surface of the Earth undergoes the motion arising from man-made disturbances, wind induced vibrations or even effects of sea storms. The records of a seismometer have, from time to time, some disturbances within its irregular pattern of records, described as wave trains. Such disturbances feature seismic waves and may come from natural or human sources.

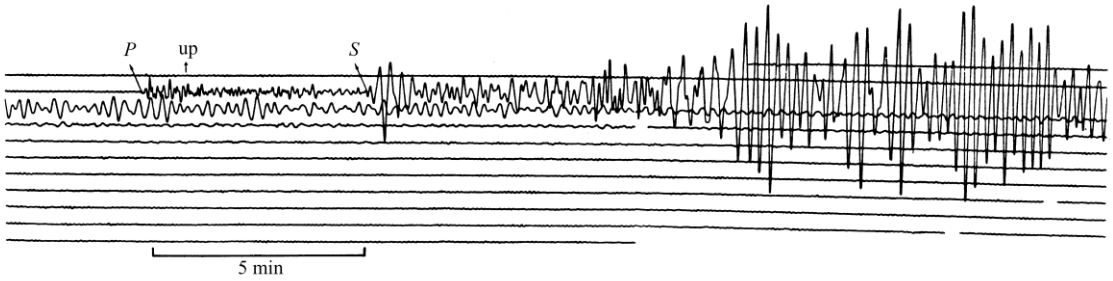

Figure 2.19 – Seismogram sample showing a wave train (B.L.N. Kennet)

Most of the times generated by earthquakes, the seismic waves with frequency ranges from 0.001 Hz to 4 Hz can be detected even far away from the source. The train vibrations, in turn, vary from 5 Hz to 100 Hz.

The records of seismic events obtained at the Earth's surface represent the primary sources of information in seismology which means a too limited sampling of the whole seismic wave-field in the Earth. However, further on the detailed nature of the source that generates the seismic waves, the elastic parameter distribution within the Earth should be tried to be determined. Therefore, the entire process whereby the seismic energy reaches the recording site must cover the generation of elements by the source, the passage of the waves through the Earth to the neighborhood of the receiver and the detection and recording characteristics of the receiver itself. The character parameters will depend on the elastic parameter distribution within the Earth and the scale of the paths of interest thus resulting in a wide diversity of the phenomena.

2.3.1. SEISMIC WAVES

For a simple approach concerning the main types of waves, the equations of motion for a differential element of the subsoil will be considered for a unit mass ρ undergoing normal stresses (σ_x, σ_y, σ_z), shear stresses (τ_{xy}, τ_{xz}, τ_{yx}), angular distortions (γ_{xy}, γ_{xz}, γ_{yz}) and displacements (u, v, w). Thus, from the theory of elasticity, the dynamic equations will come:

$$\begin{aligned}
(\lambda+G)\frac{\partial\theta}{\partial x}+G\nabla^2 u &= \rho\frac{\partial^2 u}{\partial t^2}\\
(\lambda+G)\frac{\partial\theta}{\partial y}+G\nabla^2 v &= \rho\frac{\partial^2 v}{\partial t^2}\\
(\lambda+G)\frac{\partial\theta}{\partial z}+G\nabla^2 w &= \rho\frac{\partial^2 w}{\partial t^2}
\end{aligned} \qquad (2.43)$$

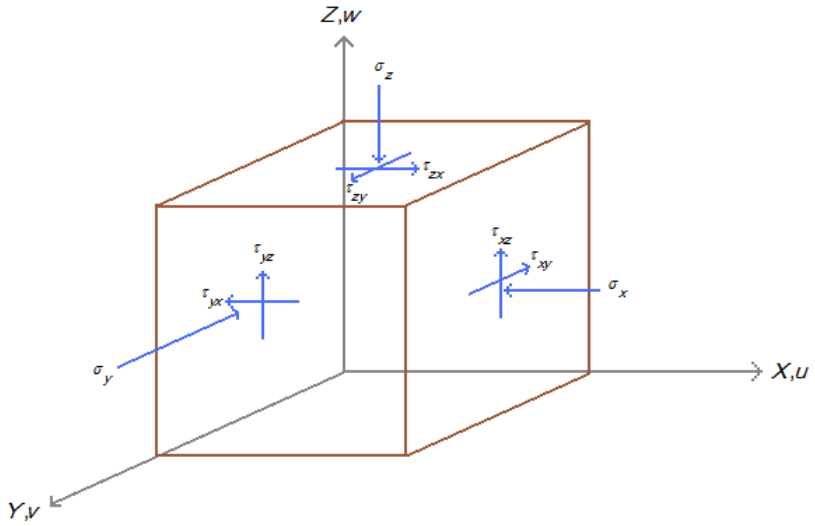

Figure 2.20 – State of stresses at a point (Zeevaert, 1979)

in which θ is the volumetric expansion or compression due to dynamic state of stresses, and is equal to

$$\varepsilon_x + \varepsilon_y + \varepsilon_z$$

λ comes from

$$\lambda = \frac{\nu E}{(1+\nu)(1-2\nu)} \qquad (2.44)$$

where E is the modulus of elasticity (σ/ε) and ν is the Poisson's ratio, defined as

$$\varepsilon_x = \varepsilon_y = -\nu \frac{\sigma_z}{E} \qquad (2.45)$$

The relationship between the shear modulus (τ/γ) and E is

$$G = \frac{E}{2(1+\nu)} \qquad (2.46)$$

The symbol (∇^2) represents a gradient for the elastic range

$$\nabla^2 = \frac{\partial^2}{\partial x^2} + \frac{\partial^2}{\partial y^2} + \frac{\partial^2}{\partial z^2} \qquad (2.47)$$

The strains are defined as

$$\varepsilon_x = \frac{\partial u}{\partial x}$$
$$\varepsilon_y = \frac{\partial v}{\partial y} \qquad (2.48)$$
$$\varepsilon_z = \frac{\partial w}{\partial z}$$

The distortions as

$$\gamma_{xy} = \frac{\partial u}{\partial y} + \frac{\partial v}{\partial x}$$
$$\gamma_{xz} = \frac{\partial u}{\partial z} + \frac{\partial w}{\partial x} \qquad (2.49)$$
$$\gamma_{yz} = \frac{\partial v}{\partial z} + \frac{\partial w}{\partial y}$$

And the rotations as

$$w_x = \frac{1}{2}\left(\frac{\partial w}{\partial y} - \frac{\partial v}{\partial z}\right)$$
$$w_y = \frac{1}{2}\left(\frac{\partial u}{\partial z} - \frac{\partial w}{\partial x}\right) \qquad (2.50)$$
$$w_z = \frac{1}{2}\left(\frac{\partial v}{\partial x} - \frac{\partial u}{\partial y}\right)$$

The types of seismic waves can be divided into two groups; the body waves and the surface waves. There are, however, several other modes of wave propagation than these, even though they are less significant. The equations of motion can be studied according to the mentioned definitions.

2.3.1.1. Body waves

Body waves are waves that travel through the interior of the elastic media. As long as the raypaths they follow depend on the density and stiffness of the Earth's interior, their density and modulus, in turn, depend on the temperature, composition and phase.

If one considers the existence of an irrotational movement, by considering that w_x, w_y, and w_z are zero-valued, then:

$$\frac{\partial \theta}{\partial x} = \nabla^2 u$$
$$\frac{\partial \theta}{\partial y} = \nabla^2 v \qquad (2.51)$$
$$\frac{\partial \theta}{\partial z} = \nabla^2 w$$

And dynamic equations reduce to

$$\begin{aligned}(\lambda+2G)\nabla^2 u &= \rho\frac{\partial^2 u}{\partial t^2}\\ (\lambda+2G)\nabla^2 v &= \rho\frac{\partial^2 v}{\partial t^2}\\ (\lambda+2G)\nabla^2 w &= \rho\frac{\partial^2 w}{\partial t^2}\end{aligned} \qquad (2.52)$$

Those waves are required to be longitudinal or compressional, which means that the ground is alternately compressed and dilated with the same direction of the propagation. Their velocity is

$$v_\rho = \sqrt{\frac{\lambda+2G}{\rho}} \qquad (2.53)$$

After the wave passes, the ground returns to its original shape.

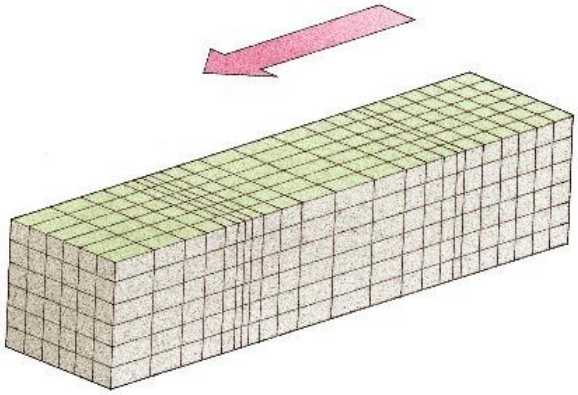

Figure 2.21 – P-wave. URL http://www.dkimages.com

When the waves do not produce volume change, one has:

$$\frac{\partial\theta}{\partial x}+\frac{\partial\theta}{\partial y}+\frac{\partial\theta}{\partial z}=0 \qquad (2.54)$$

which means that the ground is displaced perpendicularly to the direction of propagation, once the material only undergoes angular distortions and rotations. The dynamic equations become:

$$\begin{aligned}\mu\nabla^2 u &= \rho\frac{\partial^2 u}{\partial t^2}\\ \mu\nabla^2 v &= \rho\frac{\partial^2 v}{\partial t^2}\\ \mu\nabla^2 w &= \rho\frac{\partial^2 w}{\partial t^2}\end{aligned} \qquad (2.55)$$

And the velocity of such distortion or shear waves is:

$$v_s = \sqrt{\frac{G}{\rho}} \qquad (2.56)$$

Compared to the longitudinal waves, the shear waves have lower velocities in solid materials and, thereby, they arrive to the seismogram after the P-waves. From Equation (2.56) it is possible to notice that the velocity of longitudinal waves is function of Poisson's ratio. In shear waves, in turn, the velocity does not depend on Poisson's ratio, which means a higher precision for problems where the shear wave velocity is present is greater than those where it is necessary to determine the Poisson's ratio for the soil mass. Concerning the frequency values, shear waves have lower frequencies than P-waves.

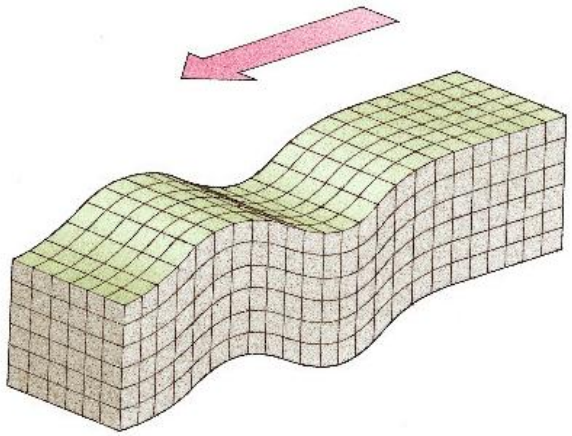

Figure 2.22 – S-wave. URL http://www.dkimages.com

2.3.1.2. Surface waves

The surface waves are waves that propagate only through the Earth's surface. They travel slower than body waves. With low frequencies, long durations and higher amplitudes, these waves can be the most destructive seismic waves. The surface waves can be divided into Rayleigh and Love waves. The Love waves are generated from great amplitudes, thus the approach to such surface waves gains more importance when it comes to earthquake studying. As the present work is not focused on this subject, the approach will restrict itself to the Rayleigh waves.

If compared to the waves on the surface of the water, the differences in Rayleigh waves reside in a retrograde particle motion at shallow depths and an elastic restoring of the force instead of gravitational. The amplitudes of Rayleigh waves generally decrease with depth in the Earth and they are slower than body waves.

Figure 2.23 illustrates a Rayleigh wave:

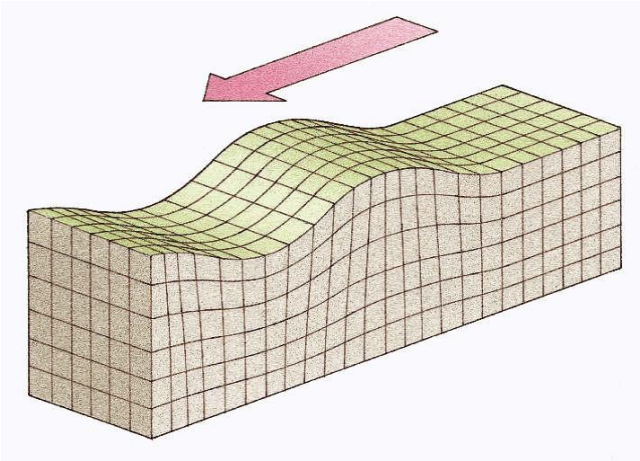

Figure 2.23 – R-wave. URL http://www.dkimages.com

It is generally assumed that R-waves are caused by refraction of P and S-waves at the surface. It consists of a vertical and a horizontal vibration component and their amplitudes decay quickly with depth, as can be seen in Figure 2.24. These horizontal and vertical amplitudes are affected by the *Poisson*'s ratio. The relationship between the propagation velocity of an R-wave (v_r) and an S-wave (v_s) is given by

$$v_r = v_s \frac{1}{1.135 - 0.182\nu} \qquad (2.57)$$

The Rayleigh wave propagation is practically unaffected by the ground water, except indirectly as a result of the increase in the soil density due to the pore water.

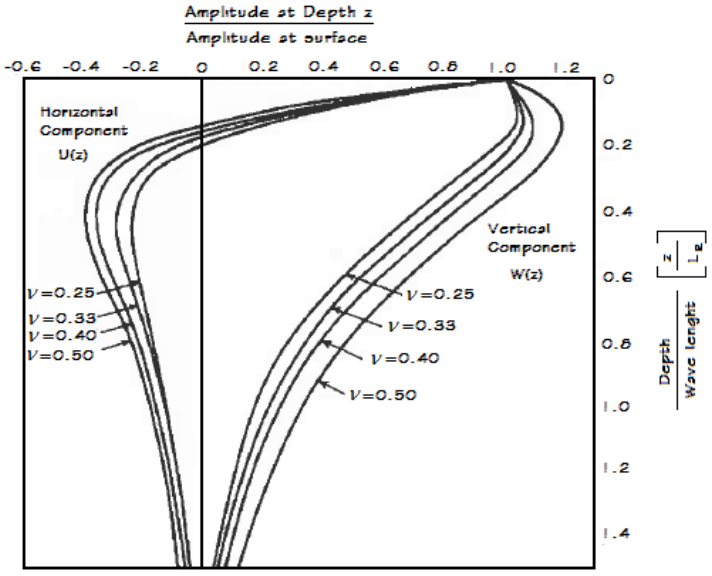

Figure 2.24 – Normalized amplitude according to the depth for Rayleigh waves (Flesch, 1993)

2.4. GROUND-BORNE VIBRATION DUE TO TRAIN TRAFFIC

The understanding of how the source, the path and the receiver perform under excessive ground-borne vibration due to train constitutes the issue in prediction and mitigation of the problem. It is worth to refer that the present work is essentially focused on the receiver. Anyway the other two links can be briefly approached.

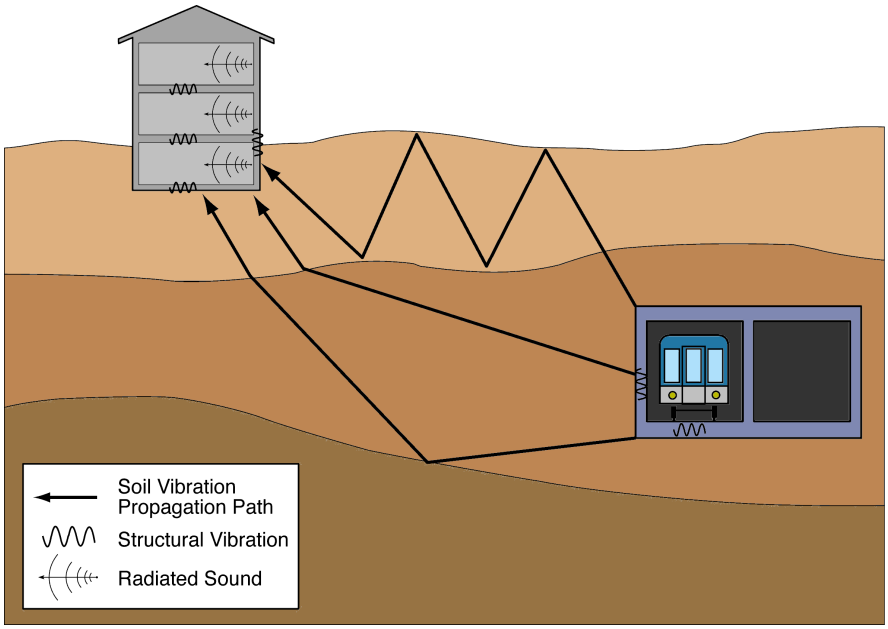

Figure 2.25 – Scheme of ground-borne vibrations caused by a train

2.4.1. VIBRATION SOURCE

Generally it is believed that the vibration is generated due to interaction of the moving train with the track which lies on the underlying soil.

In Figure 2.26 the main parts of the train in terms of vibration generation are shown.

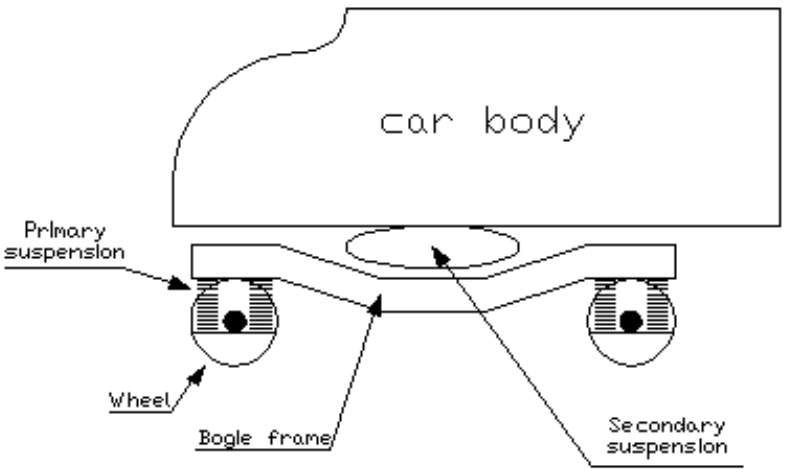

Figure 2.26 – Main parts of a train bogie (Bahrekazemi, 2004)

The car body is connected to the bogie via secondary suspension. The weight of the car body is taken transferred to the wheels through a bogie frame that is connected to the wheels by a primary suspension system. The wheels in turn transfer the load to the rails as shown in Figure 2.27.

Figure 2.27 – Vertical and horizontal contact forces between wheel and rail, (Andersson et al., 2002)

Figure 2.28 shows different parts of the track in a schematic way. As seen in it the railway track consists of the rails, rail pads and rail fasteners, sleepers, ballast and sub-ballast. The different parts of the track may vary their specifications according to the type of the traffic.

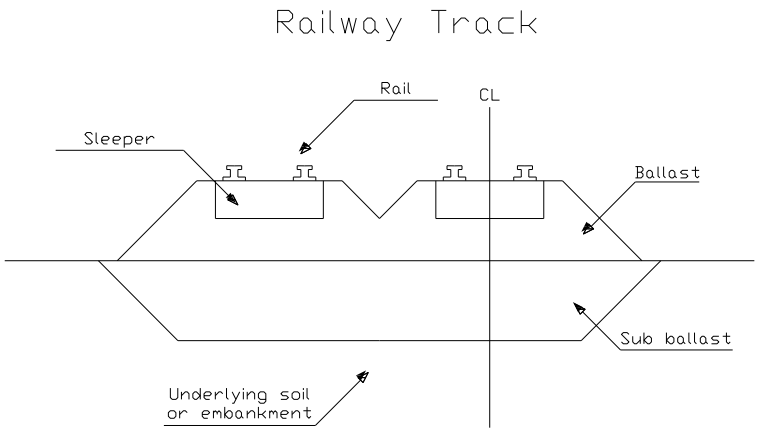

Figure 2.28 – Schematic picture of railway track and description of its different parts (Bahrekazemi, 2004)

According to *Dawn* and *Stanworth* (1979), the vibration energy is not shared equally among the modes and most of the energy is carried by *Rayleigh* waves at significant distances from the train. It is mentioned that if the trains were to travel faster than the propagation velocity of the ground vibration, the shock wave which is performed in the ground would seriously affect the nearby buildings. From some experimental results, it is suggested by them that the excitation of the ground vibration, especially at low frequencies, depends on the total vehicle mass, not just the unsprung mass of the wheel-set.

A report from *Hannelius* (1974) indicates that the significant frequency range for ground vibration is in the range of 0-10 Hz for cohesive soils, and higher frequencies for soils or friction material. It is further noticed that vibration in the ground increases with decreasing mass of the bank-fill material, and increasing depth to bedrock.

Fujikake (1986) refers that peaks in the ground vibration spectra occur at the axle-passing frequency and its overtones.

Krylov and *Ferguson* (1994) discuss the theory of generation of low-frequency ground vibrations due to quasi-static pressure from the wheels. Considering the soil as elastic foundation, the generation of vibrations due to passage of the deflection curve from each sleeper and the vibration induced by each sleeper in the ground has been formulated. Expressing that the major part of the energy is carried by Rayleigh waves, only these waves have been considered in determining the spectral density of the vertical vibrations. It has been concluded that the vibration spectra strongly depend on the axel road.

2.4.2. PROPAGATION PATH

After being generated in the track, the vibration propagates to the surrounding through the media. *Hannelius* (1978) suggests that *Rayleigh* waves dominate at a distance from the track, while body waves are significant within the first 20 m, approximately.
Equation (2.58), *Nelson* and *Saurenman* (1983), yields the propagation attenuation of waves in linear elastic half space, where n is given by Table 2.1 and some examples of α are given by Table 2.2. the R-waves are considered important, especially at greater distances from the track, since the body waves decay more rapidly by geometric spreading than the *Rayleigh* wave.

$$v = v_0 \cdot \left(\frac{r}{r_0}\right)^{-n} \cdot e^{-\alpha(r-r_0)} \qquad (2.58)$$

Where v_0 is the particle velocity at the source, r_0 is the distance from the source to the reference point on the ground, r is the source from the distance to the receiver, n is the power of geometric attenuation and α is the factor of material damping.

Table 2.1 – Power of geometric attenuation of waves in linear halfspace

Wave type	Point source	Line source
Shear waves	1	0.5
Compression waves	1	0.5
Rayleigh waves	0.5	0.5
Love waves	0.5	0.5

Table 2.2 – Factor of material damping

Soil Type	Soil attenuation, α [m^{-1}]
Water-saturated clay	0.04-0.12
Losses and loessial soil	0.10
Sand and silt	0.04

From a series of experiments on the screening effect of open trenches in very controlled conditions, in a 2-layer soil environment, *Woods* (1968) argues that 67% of the energy is carried by *Rayleigh* waves and its wavelength in the media is used for a dimensionless study of the issue. A few sheet-walls of steel and aluminum have also been studied in order to show that open trenches would be more effective as wave barriers. The results show that in a symmetric area about a radius from the source of excitation through the center of one trench, bounded laterally by two radial lines extending from the center of the source through of the arc reduction of AR=0.25 (amplitude reduction factor, which is the

ratio of vibration at a point with the barrier to that with the barrier absent) was obtained when the depth fulfilled $d/\lambda_r \geq 6$, where d is the depth and λ_r is the *Rayleigh* wavelength. According to him the trench width has little influence on the effectiveness of open trenches. Based on a literature review he has illustrated the attenuation of different types of waves as shown in Figure 2.29:

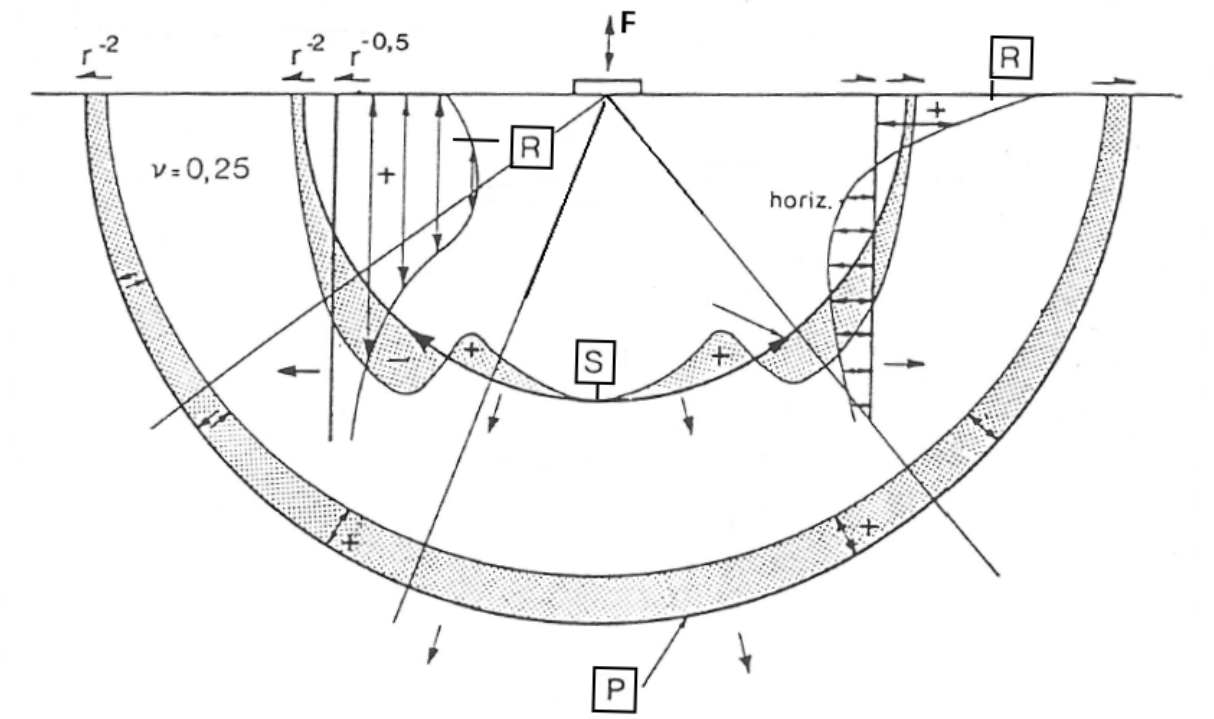

Figure 2.29 – Different types of waves from a circular footing and their theoretical geometrical damping (Woods, 1968)

2.4.3. RECEIVER

After generated in the track, and propagating through the media, the vibrations are received by the foundations nearby buildings. From the foundations, the vibrations then propagate to the other parts of the buildings.

According to *Hannelius* (1974), resonance of the whole building usually occurs below 10 Hz, while resonances of walls and ceilings occur in the 40-60 Hz range. *Jones* (1994), summarizes the response of the building to the vibrations as typically having resonances of the whole building on the foundation at about 4 Hz, floors at about 20-30 Hz, and walls and windows above 40 Hz. *Jonsson* (2000) concluded from a case study that only the low-frequency content of the vibrations is effectively transmitted into the building foundation.

A review of the reports on vibration related damages to buildings (*Nelson* and *Saurenman*, 1983) has shown that there is only 5% probability that buildings would receive structural damages due to particle velocities less than 50 mm/s and no case had been reported of structural damage to buildings for particle velocities less than 25 mm/s. The same review states that there is no risk of architectural damage to normal buildings due to vibration less than 15 mm/s.

Jonsson (2000) has presented experimental and theoretical investigation carried out to characterize and explain low-frequency ground and structural vibrations related to railway traffic. It has been concluded from a case study that only the low-frequency content of the vibrations is effectively transmitted into the building foundation.

2.4.4. MITIGATION METHODS

In order to reduce the train induced ground-borne vibration at a distance from the track, several issues such as generation of the vibration at the source, its propagation through the media, and interaction with the structure at the receiver should be considered.

The mitigation methods in the source that can be used for avoiding excessive vibrations in the railway structure can be of several types, such as welded rail, modification of car design, resilient wheels, wheel truing, rail grinding, resilient direct fixation rail fasteners, stabilization of soil under the embankment, floating slabs, reduction of train speed… A combination of two or more of these methods is usually used. Each method is mostly effective within certain frequency range. As long as the truing of the wheel and the rail grinding methods are effective at frequencies above 100 Hz, the floating slabs usually is effective at frequencies above 15-20 Hz.

Concerning mitigation methods in the path, barriers in the way of waves propagating from the source to the receiver are used. An important disadvantage of the method in soft clay soils is due to the relatively low frequency content vibrations in this type of soils which is corresponding to very long wave lengths. Therefore in order to be effective, the trench must be very deep.

If only a few buildings are affected by the excessive ground-borne vibration from the railway, alternative methods such as building isolation way prove to be suitable and economical.
Isolation of the building foundations from the ground using elastic support systems as shown in Figure 2.30 is a method that has been used in some cases in order to mitigate ground-borne vibration. In this method the building is considered as a rigid body supported on a number of springs and dampers. The natural frequency of the system must be designed to be quite below the lowest frequency of the vibration that must be mitigated as seen for a single degree of freedom system (Figure 2.30).

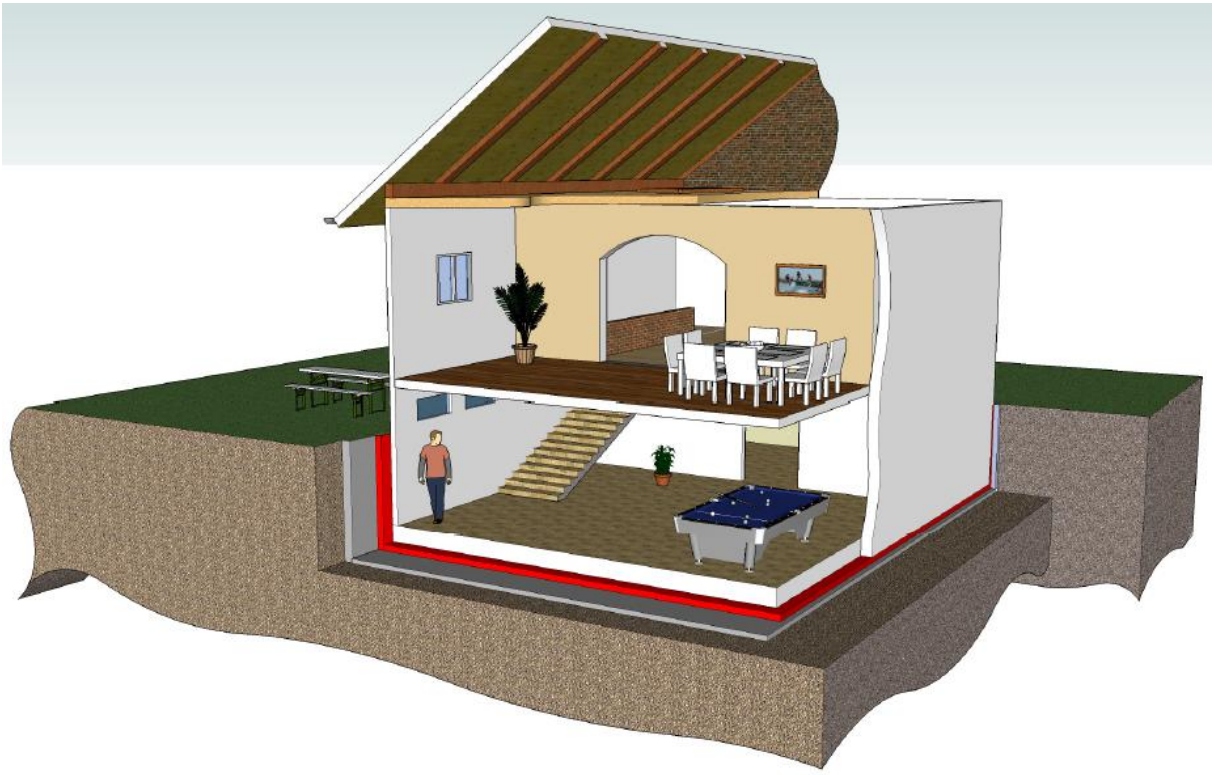

Figure 2.30 – Building elastically supported

3

Dynamic SSI models

3.1. INTRODUCTION

The seismic excitations experienced by structures are functions of the earthquake source, travel path effects, local site effects and soil structure interaction effects. Together, the first three mentioned factors result in a free field motion of the ground. The process in which the response of the soil influences the motion of the structure and the motion of the structure influences the motion of the soil is named as soil structure interaction (SSI).

When a lightweight flexible structure is built on a very stiff rock foundation, a valid assumption is that the input motion at the base of the structure is the same as the free field equation motion. However, if the structure is very stiff and the foundation relatively soft, the motion at the base of the structure may be significantly different than the free field surface motion. Even for this case, the most significant interaction effects will take place near the structure and at some finite distance from the base of the structure the displacements will converge to the free field equation motion.

The soil structure interaction can be divided into two mechanisms: the kinematic interaction and the inertial interaction.

When the soil is displaced by an earthquake ground motion, the stiff foundation elements on or in the soil will not follow the free field motion as a result of the ground motion incoherence, wave inclination, or foundation embedment. This inability of the foundation to match the free field equation causes the kinematic effects. Such effects relate the free field motion to the motion that would occur on the base of the structure if the structure was massless.

On the other hand, the inertia developed in the structure due its own vibrations transmits the inertial force to the soil giving rise to base shear and moment, causing, thereby, further deformation in the soil. These phenomena represent the inertial interaction.

The inertial interaction can be the most important effect for foundations without large, rigid base slabs or deep embedment. It is also the dominant effect for stronger vibrations, where near-field soil modulus degradation, soil-pile gapping, limit radiation damping and inertial interaction become predominant causing excessive displacements and bending strains concentrated near the ground surface resulting in pile damage near the ground level.

The kinematic interaction, in turn, is more dominant at low levels of the ground shaking, causing lengthening of the period and increase in radiation damping.

3.2. MODELS FOR VIBRATION OF SSI

Finding an exact solution for a dynamic SSI problem is only possible for a too small number of particular cases. The necessity of solving real engineering problems has led to take some simplifying assumptions. According to such assumptions, the models for seismic analysis can be divided into three groups: models using mass-spring-damper systems, elastically bedded beam models and FE models.

3.2.1. MODELS USING MASS-SPRING-DAMPER SYSTEMS

In the models consisting of mass-spring-damper systems the soil is replaced by a system of springs and dampers applied to each freedom degree of the "infinite rigid" foundation. The soil is admitted to be perfectly homogeneous, elastic and isotropic.

Since the first solutions obtained from a foundation subjected to a dynamic load (Lamb, 1904), many approximated solutions have been adopted. Figures 3.1 and 3.2 show such approximations by using models with mass-spring-damper systems.

SPRING-DAMPER-SYSTEMS OF SOIL-STRUCTURE SYSTEMS

halfspace theory

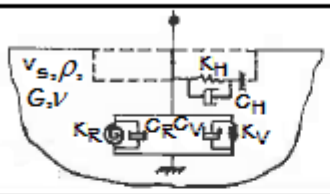

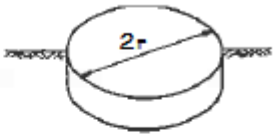

circular foundations

Model Parameters	Vibration Type	RICHART (and others), 1967	RICHART (and others), 1970	YAMAHARA	TAJIMI
K_H	horizontal	$\frac{32(1-\nu)Gr}{7-8\nu}$		$\frac{8Gr}{2-\nu}$	$\frac{2\pi Gr}{2-\nu}$
K_V	vertical	$\frac{4Gr}{1-\nu}$			
K_R	Rotation (around horizontal axes)	$\frac{8G^3r}{3(1-\nu)}$			$\frac{\pi G^3 r}{(1-\nu)}$
C_H	horizontal	$\frac{0.288}{(B_H)^{0.5}}$	$\frac{0.576K_H r}{v_s}$	$\rho v_s A$	
C_V	vertical	$\frac{0.425}{(B_V)^{0.5}}$	$\frac{0.85K_V r}{v_s}$	$\rho v_p A$	
C_R	Rotation (around horizontal axes)	$\frac{0.150}{(1+B_R)(B_R)^{0.5}}$	$\frac{0.30K_R r}{(1+B_R)v_s}$	$\rho v_p I_R$	

Constants and their meaning

$$B_H = \frac{(7-8\nu)m}{32(1-\nu)\rho r^3}$$

$$B_V = \frac{(1-\nu)m}{4\rho r^3}$$

$$B_R = \frac{3(1-\nu)I}{8\rho r^5}$$

B_H, B_V, B_R - mass ratio values

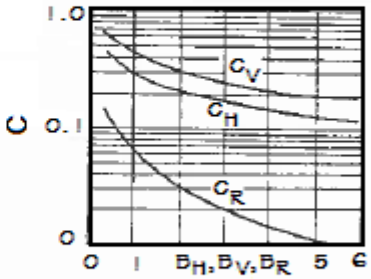

G - shear modulus
ρ - density
ν - Poisson's ratio
A - foundation area
I_R - moment of inertia

v_s - shear wave velocity
v_p - compression wave velocity

$$v_s = \left(G/\rho\right)^{0.5} \qquad v_p = \left[2(1-\nu)/(1-2\nu)\right]^{0.5} \cdot v_s$$

Figure 3.1 – Mass-spring-damper system approximations for circular foundation models (Flesch, 1993)

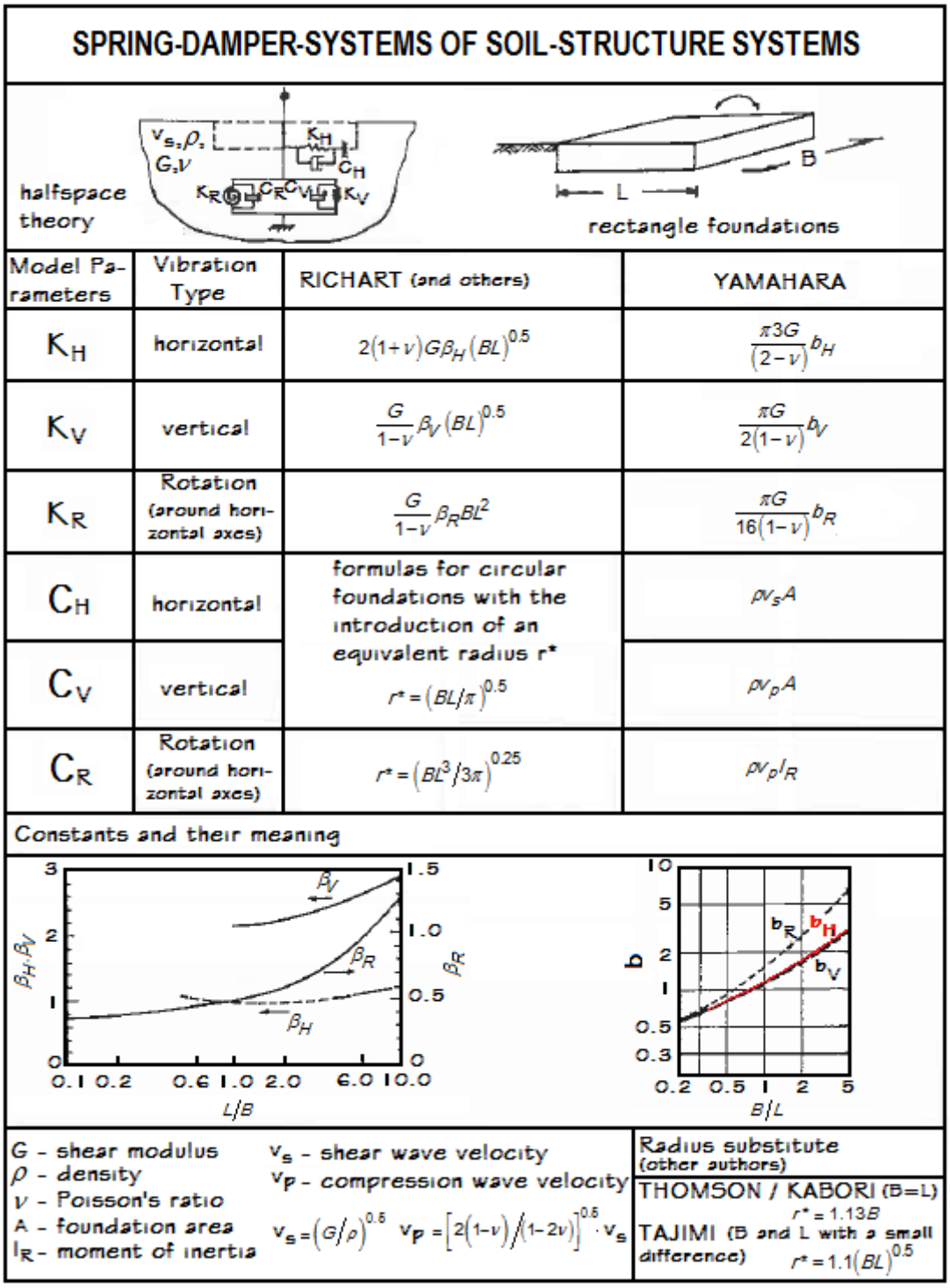

Figure 3.2 – Mass-spring-damper system approximations for rectangular foundation models (Flesch, 1993)

It is possible to notice, by Figures 3.1 and 3.2, that the represented models have some limitations: one can only analyze settled foundations on homogeneous soils; the damping of the soil and the influence of adjacent structures cannot be taken into account; only linear analyzes are possible, once no information of the soil is available. Due to these uncertainties, these and other tables shall be used for simplified analysis.

The direct analysis using mass-spring-damper systems will be described forward.

3.2.2. ELASTICALLY BEDDED BEAM MODELS

The elastically bedded beam models are especially appropriated for pile foundations, once they are a generalization of the Winkler assumption for the dynamic case. Therefore, the soil reaction depends not only on the displacements, but also on the velocities and accelerations of the common points between the beam and the soil.

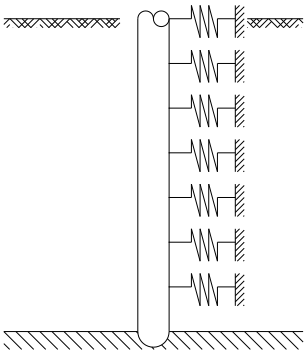

Figure 3.3 – Elastically bedded beam model

The results are obtained by taking several layers of infinitesimal thickness, infinitely extended. The piles are admitted to be vertical and independents from each other. Each point between the soil and the structure undergoes harmonic vibrations, with both horizontal (u) and vertical (w) components:

$$\begin{aligned} u &= u_0 e^{i\omega t} \\ w &= w_0 e^{i\omega t} \end{aligned} \qquad (3.1)$$

The soil reactions are given by

$$\begin{aligned} p_u &= G\left(S_{u1} + iS_{u2}\right)\cdot u_0 e^{i\omega t} \\ p_w &= G\left(S_{w1} + iS_{w2}\right)\cdot w_0 e^{i\omega t} \end{aligned} \qquad (3.2)$$

where ω is the circular frequency of the excitation, G is the shear modulus of the soil and the parameters S were determined (*Beredugo* and *Novak*), for different values of *Poisson*'s ratio, as function of the dimensionless frequency.

It should be noted that by taking the independence of the deformation of each infinitesimal thick layer, the shear deformations between layers are neglected. Therefore, the resonance of the natural frequencies of the soil is not taken into account.

Similarly to the solutions using mass-spring-damper systems for the shallow foundations, several methods have arisen, where the soil is replaced by a system of masses, springs and dampers distributed throughout the pile. Despite when taking into account the soil-pile interaction in the dynamic response analysis of pile foundations the Winkler models are the simplest and numerically most efficient ones, most of those models have been developed without a logical base and thus often fail to produce the computed results consistent with mother nature. The Matlock model (*Matlock*, 1978) and the Novak model (*Novak*, 1976) may be classified as conventional Winkler models often used in the dynamic response of pile foundations, while the Nogami model is a Winkler model recently developed for the dynamic and nonlinear response analysis (*Nogami* 1983, 1985, 1987).

The Matlock model is basically viewed as a system of a frequency-independent nonlinear spring and linear dashpot as shown in Figure 3.4:

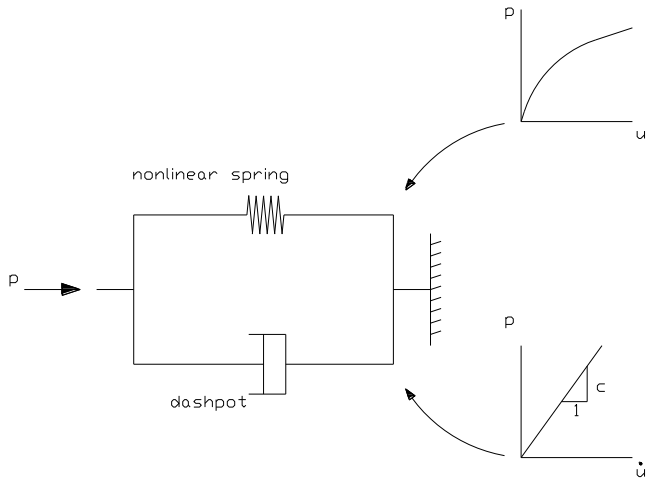

Figure 3.4 – Matlock Model (Nogami, 1991)

The force-displacement relationship of the nonlinear spring is defined by a so-called unit load transfer curve and the dashpot taken into account for the radiation damping. When a steady-state harmonic response is assumed, the force-displacement relationships at two different frequencies are illustrated in Figure 3.5 for $\omega_1 < \omega_2$.

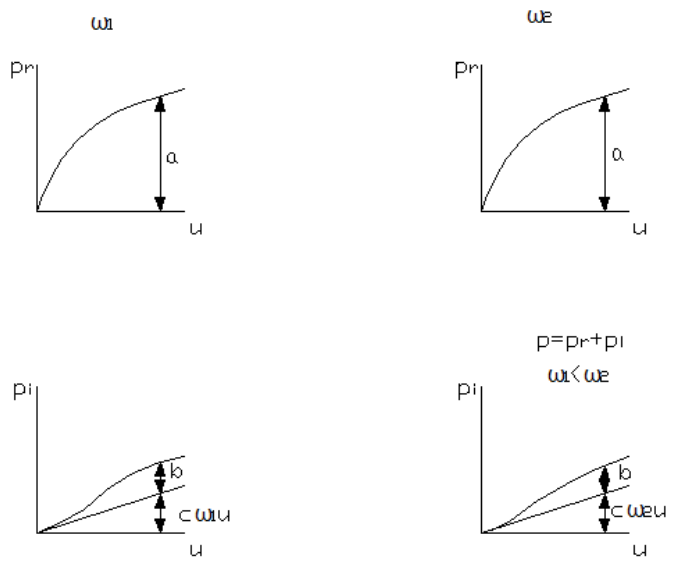

Figure 3.5 – Force-Displacement relationship of Matlock Model (Nogami, 1991)

The nonlinear spring generates both the real and imaginary parts of the force independent of frequency. The dashpot generates only the imaginary part of the force linearly proportional to the frequency. The force induced in the Matlock model is summation of those spring and dashpot forces. The real part of the force generated by the Matlock model is therefore independent of the frequency. The imaginary part of the force in the elastic range results entirely from the dashpot force. As the displacement level increases beyond the elastic range, the imaginary part always increases due to generation of hysteresis damping in the spring.

The Novak model is limited to linear elastic conditions and steady-state harmonic motion. The model is made of a frequency dependent complex spring (Figure 3.6).

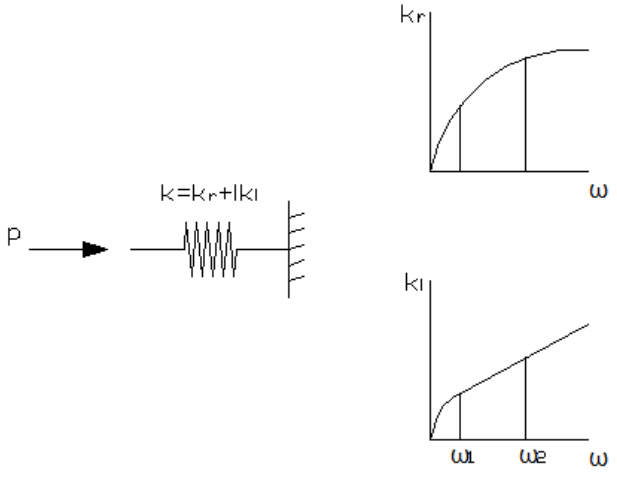

Figure 3.6 – Novak Model (Nogami, 1991)

The stiffness of the spring is defined from the analytical formulation obtained for the vibration of an infinitely long vertical massless rigid cylinder embedded in an infinite elastic medium. Such

conditions yield plane strain conditions, in which medium displacements do not vary along vertical direction and hence body waves generated in the medium propagate only in the horizontal direction.

The force displacement relationships of the Novak model at two different frequencies are shown in Figure 3.7:

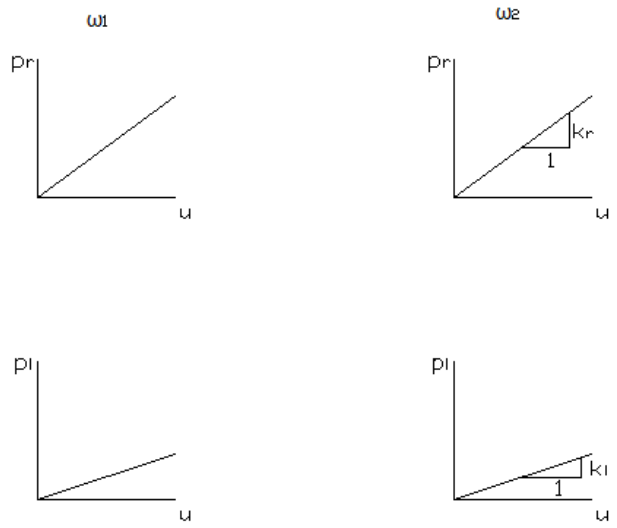

Figure 3.7 – Force-Displacement Relationship of Novak Model (Nogami, 1991)

The model cannot produce the nonlinear behavior, but can do the dynamic behavior rationally for linear elastic conditions.

The Nogami model is conceptually viewed as a combination of the Matlock model and Novak model and is capable of properly produce the nonlinear behavior coupled with the dynamic behavior. The model consists of the near-field element made of nonlinear spring and the mass represents the soil in the vicinity of the shaft. The nonlinear spring is defined by providing a static unit load transfer curve such as that used in the Matlock model (*Nogami*, 1987, 1991) and the mass is attached to produce the dynamic effects in the near-field response. The far field element produces the effects of linear elastic behavior of the far-field soil outside the near-field. Since nonlinear response to random loading must be analyzed in the time-domain, the far-field element is modeled by frequency independent springs, dashpots and mass as shown in Figure 3.8.

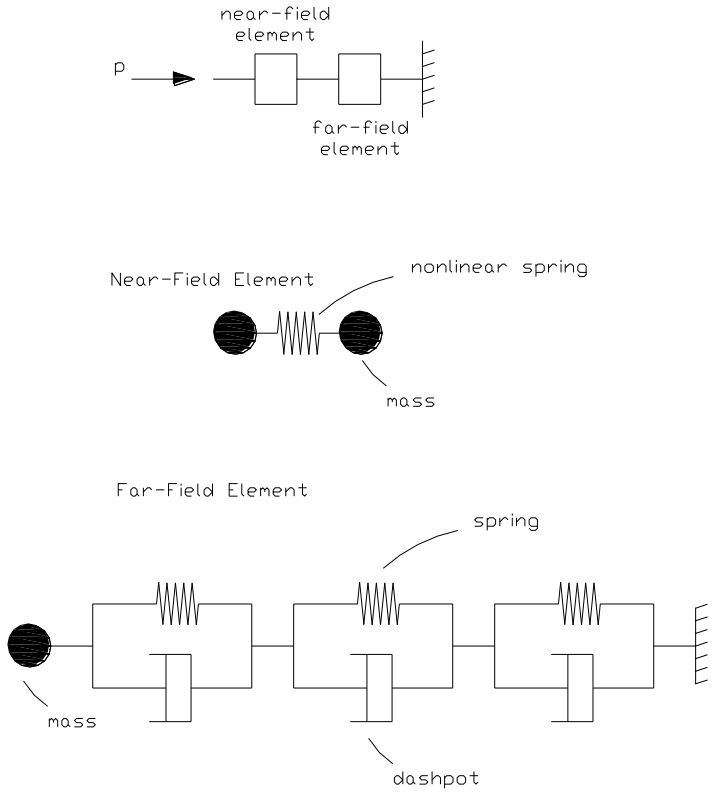

Figure 3.8 – Nogami Model (Nogami, 1991)

This far-field model is developed in a rational manner from the analytical formulations of the Novak model so that it behaves closely to the Novak model under the steady-state harmonic motion (*Nogami* 1986, 1988). When the linear elastic region of the provided unit load transfer curve is reasonable, the Nogami model behaves very closely to the Novak model except at very low frequencies as illustrated in Figure 3.9:

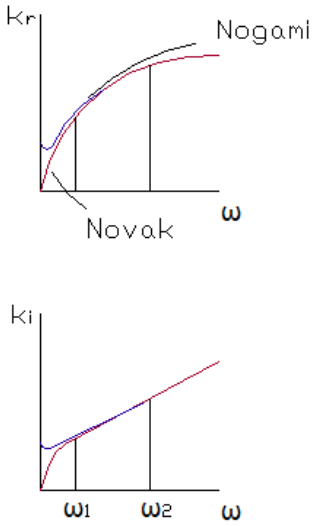

Figure 3.9 – Linear elastic conditions (Nogami, 1991)

It is noted, however, that the Novak model is based on plane strain conditions and thus does not behave realistically at those very low frequencies. Given an identical unit load transfer curve to the Nogami and Matlock models, the force-displacement relationship of the Nogami model is identical to the Matlock model under static conditions. Under dynamic conditions, however, these methods behave quite differently from each other (as illustrated in Figure 3.10), in which two frequencies, ω_1 and ω_2, correspond to the frequencies indicated in Figure 3.10.

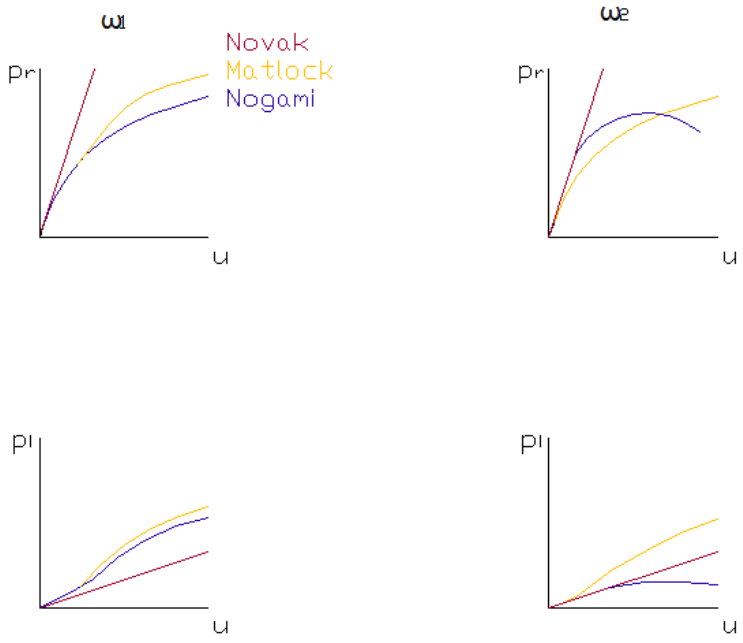

Figure 3.10 – Inelastic conditions (Nogami, 1991)

Dynamic conditions stiffen the spring characteristics of the Nogami model in the elastic range as seen in the real part, whereas that of the Matlock model is frequency independent. Significant difference between the two model behaviors is seen in the damping (imaginary part of the curve). As stated earlier, the Matlock model increases the damping at any frequency as soil nonlinearity develops. Contrary to this, the Nogami model increases the damping at low frequencies but decreases at high frequencies. The damping results from both hysteresis damping value due to non-elastic behavior and radiation damping. When nonlinearity develops in the vicinity of the shaft, the soil generates the hysteresis damping but reduces the radiation damping by reducing the energy transmitted to the far-field soil. The change in the damping doe to soil nonlinearity is the net of those trends.

3.2.3. FINITE ELEMENT MODELS

The FE models are the latest approach for the SSI models, together with the boundary elements for the halfspace approach.

In a FE model the integration domain of differential equations of motion is divided into a finite number of regions, in which the geometrical contour is defined by a determined number of nodal points. The compatible models obtain the displacements field of each element through interpolation functions, as from the displacements of the nodal points (Equation 3.3).

$$\{X\} = [a][q] \quad (3.3)$$

where $\{X\}$ is the displacement vector in the center of the element, $[a]$ is the interpolation function matrix and $[q]$ is the displacement matrix of the nodal point.

Based on this assumption, the dynamic problem is transformed into the system of differential equations:

$$[M]\{\ddot{X}\} + [C]\{\dot{X}\} + [K]\{X\} = \{F\} \quad (3.4)$$

in which $[M]$, $[C]$, $[K]$ and $\{F\}$ represent, respectively, the mass, damping and stiffness matrices and the vector of forces.

The stiffness matrix is given by

$$[K] = \int_V [a']^T [E][a'] dv \quad (3.5)$$

where $[a']$ transforms the nodal displacements into specific deformations

$$\{\varepsilon\} = [a'][q] \quad (3.6)$$

and $[E]$ transforms the specific deformations into stresses

$$\{\sigma\} = [E][\varepsilon] \quad (3.7)$$

The matrices of consistent mass and the vector of consistent forces come, respectively, from

$$[m] = \int_V \mu [a]^T [a] dv \quad (3.8)$$

And

$$\{f\} = \int_V [a]^T \{f_m\} dv + \int_S [a]^T \{f_s\} ds \qquad (3.9)$$

where $\{f_m\}$ is the volumetric load vector and $\{f_s\}$ is the superficial load vector.

The global matrices are then assembled from the local matrices, respecting the common nodes to various elements.

With the boundary elements, the structure and the soil in the vicinity are modeled using finite elements connected to other elements that represent the halfspace. The stiffness matrix obtained from such boundary elements depends strongly on the frequency excitation. Therefore, the analysis at the frequency domain must be done.

3.3. CURRENT APPROACHES

3.3.1. EMPIRICAL APPROACH

The empirical way to predict the vibrations inside a building due to seismic ground vibrations is performed by measuring and correlating the vibrations of two different points: one located at the free-field ground and the other at the foundation or any other point of the structure. The time series, usually velocity versus time charts for the train induced vibrations, are then converted to the domain time through the FFT. From the ratios between the obtained spectrum at the structure point and the spectrum at the ground point transfer functions are described. These transfer functions indicate the factors to which the vibrations from the source are subjected for a frequency amount: for higher values than 1, an amplification factor will increase the amplitudes; if the transform function is ranged from 0 to 1, then there will be a reduction factor over the amplitudes; a zero-valued transform function means that, for the respective frequency, the vibration affects are suppressed. Figure 3.11 illustrates the steps of the described measurement approach.

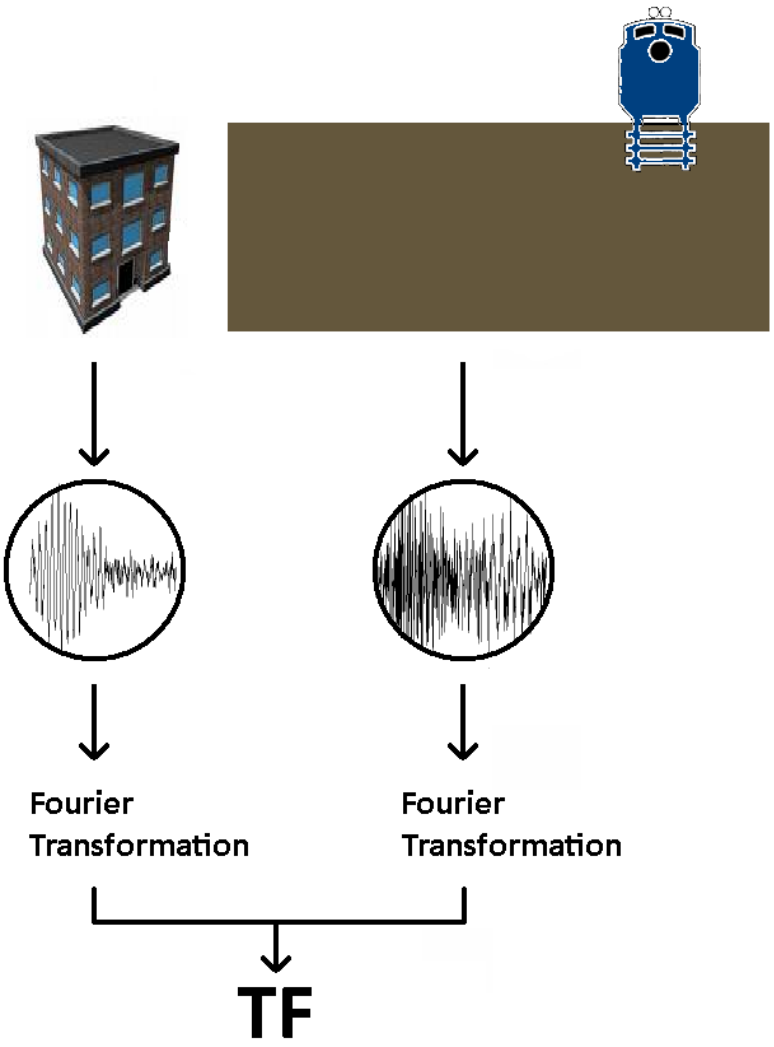

Figure 3.11 – Empirical procedure for vibration predictions

With the study of the transfer functions, it is proposed that the vibrations inside similar buildings can be predicted given a known ground motion outside. As a transfer function depends on many factors, like the soil type, bedrock depth, adjacent structures, etc, the more measures are performed, the more accurate the predictions will be.

3.3.2. Substructure Approach

The theoretical approach consists on the division of the system into two substructures: soil and structure. As mentioned in subchapter 3.2, such approach considers a direct analysis using mass-spring-damper systems that implies that the presence of the structure does not have influence on the soil displacements. This assumption might not be true for buried structures. Thus, the solution for the problem may be obtained by dividing the calculations into three steps:

- Firstly, the calculations are performed either for the dynamic loading acting on the structure only represented by its stiffness (*Kausel*) or by taking only the soil subjected to the seismic excitation without the presence of the structure (*Clough*). It is the kinematic interaction;

- The second step is to determine the stiffness and dashpot coefficients that will substitute the soil in the third step;
- In the last step, the considered loadings are the accelerations obtained in the kinematic interaction and these are applied to the mass of the structure (inertial interaction).

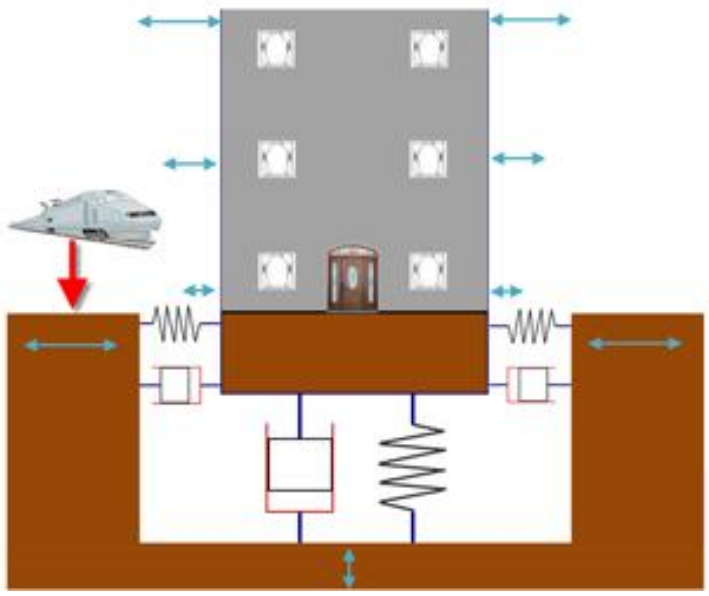

Figure 3.12 – Considered model for the theoretical substructure approach. URL http://www.norsonic.no

The superposition method demonstrates the equivalence between this three step solution and the complete solution.

Let one consider the differential equations of motion in its matrix form:

$$[M]\{\ddot{U}\}+[C]\{\dot{X}'\}+[K]\{X'\}=\{0\} \qquad (3.10)$$

The matrices $[M]$, $[C]$ and $[K]$ are the matrices of the system. The vectors $\{U\}$ and $\{X'\}$ are the vectors of absolute and relative displacements relatively to an axis system connected to the soil.

For the *Kausel* superposition, the equation of the motion for the kinematic interaction will come:

$$[M_1]\{\ddot{X}_1'\}+[C]\{\dot{X}_1'\}+[K]\{X_1'\}=-[M_1]\{\ddot{U}_g\} \qquad (3.11)$$

where $[M_1]$ is the mass matrix of the system without the mass of the structure, $\{\ddot{U}_g\}$ is the vector for the absolute acceleration of an axis system connected to the base and $\{X_1'\}$ represents the kinematic interaction solution. The vector of absolute accelerations for the first step is given by:

$$\{\ddot{U}_1\} = \{\ddot{X}_1'\} + \{\ddot{U}_g\} \qquad (3.12)$$

Hence, the motion for the inertial interaction becomes:

$$[M]\{\ddot{X}_2'\} + [C]\{\dot{X}_2'\} + [K]\{X_2'\} = -[M_2]\{\ddot{U}_1\} \qquad (3.13)$$

The matrix mass of the system without the mass of the soil is $[M_2]$, $\{X_2'\}$ is the inertial interaction solution, and:

$$\{X'\} = \{X_1'\} + \{X_2'\} \qquad (3.14)$$

The sum of Equations (3.11) and (3.13) will result in Equation (3.15):

$$[M_1]\left(\{\ddot{X}_1'\} + \{\ddot{U}_g\}\right) + [M_2]\{\ddot{U}_1\} + [M]\{\ddot{X}_2'\} + [C]\left(\{\dot{X}_1'\} + \{\dot{X}_2'\}\right) + [K]\left(\{X_1'\} + \{X_2'\}\right) = \{0\} \qquad (3.15)$$

From Equations (3.14) and (3.15) and $[M_1] + [M_2] = [M]$ one has:

$$[M]\left(\{\ddot{U}_1\} + \{\ddot{X}_2'\}\right) + [C]\{\dot{X}'\} + [K]\{X'\} = \{0\} \qquad (3.16)$$

where

$$\{\ddot{U}_1\} + \{\ddot{X}_2'\} = \{\ddot{X}'\} + \{\ddot{U}_g\} = \{\ddot{U}\} \qquad (3.17)$$

For the *Clough* superposition, the stiffness and damping matrices of the structure will be partitioned, similarly to the matrix of mass, into sub-matrices in which either the structure properties ($[C_1], [K_1]$) or the soil properties ($[C_2], [K_2]$) are excluded.

The equation of the motion for the kinematic interaction will be:

$$[M_1]\{\ddot{U}_1\}+[C_1]\{\dot{U}_1\}+[K_1]\{U_1\}=-[M_b]\{\ddot{U}_{g1}\}-[C_b]\{\dot{U}_{g1}\}-[K_b]\{U_{g1}\} \qquad (3.18)$$

where the index *b* refers to the coupling terms between the freedom degrees of the support and the soil, $\{U_1\}$ are the unknown absolute displacements of the kinematic interaction and $\{U_{g1}\}$ the prescribed displacements at the supports.

By assuming the equally of all the displacements of the supports, Equation (3.18) can be transformed into:

$$[M_1]\{\ddot{X}_1'\}+[C_1]\{\dot{X}_1'\}+[K_1]\{X_1'\}=-([M_1]+[M_b])\{\ddot{U}_g\}-([C_1]+[C_b])\{\dot{U}_g\} \qquad (3.19)$$

The vector $\{U_g\}$ is the absolute displacements vector of the structure due to the displacement U_{g1} of the axis system connected to the base.

If, by simplification, the dashpot matrix of the system is considered to be proportional to the stiffness matrix, and the mass matrix is assumed to be a diagonal matrix, Equation (3.19) will be reduced to:

$$[M_1]\{\ddot{X}_1'\}+[C_1]\{\dot{X}_1'\}+[K_1]\{X_1'\}=-[M_1]\{\ddot{U}_g\} \qquad (3.20)$$

For the inertial equation of motion one has:

$$[M]\{\ddot{X}_2'\}+[C]\{\dot{X}_2'\}+[K]\{X_2'\}=-[M_2]\{\ddot{U}_1\}-[C_2]\{\dot{U}_1\}-[K_2]\{U_1\} \qquad (3.21)$$

As when the stiffness matrix of the structure undergoes itself a motion of a rigid body is null, then:

$$[K_2]\{U_g\}=\{0\}\Leftrightarrow[K_2]\{U_1\}=[K_2](\{X_1'\}-\{U_g\})=[K_2]\{X_1'\} \qquad (3.22)$$

and due to the proportionality between the damping and stiffness matrices:

$$[C_2]\{\ddot{U}_1\} = [C_2]\{\dot{X}_1'\} \qquad (3.23)$$

Equation (3.21) can then be rewritten as:

$$[M]\{\ddot{X}_2'\} + [C]\{\dot{X}_2'\} + [K]\{X_2'\} = -[M_2]\{\ddot{U}_1\} - [C_2]\{\dot{X}_1'\} - [K_2]\{X_1'\} \qquad (2.24)$$

From the sum of Equations (3.20) and (3.24) one will be led to Equation (3.10) once again:

$$[M_1]\left(\{\ddot{X}_1'\} + \{\ddot{U}_g\}\right) + [M_2]\{\ddot{U}_1\} + [M]\{\ddot{X}_2'\} + \left([C_1] + [C_2]\right)\{\dot{X}_1'\} + [C]\{\dot{X}_2'\} + \left([K_1] + [K_2]\right)\{X_1'\} + [K]\{X_2'\} = \{0\}$$

The sub-matrices of the system will be repartitioned as:

$$M_1 = \begin{bmatrix} M_{1G} & M_{1GC} \\ M_{1GC}^T & M_{1C} \end{bmatrix} \qquad M_2 = \begin{bmatrix} M_{2C} & M_{2SC} \\ M_{2SC}^T & M_{2S} \end{bmatrix}$$

$$M = \begin{bmatrix} M_{1G} & M_{1GC} & 0 \\ M_{1GC}^T & M_{1C} + M_{2C} & M_{2SC} \\ 0 & M_{2SC}^T & M_{2S} \end{bmatrix}$$

Where the index *G* refers to the freedom degrees due only to the soil, the *S* index refers exclusively to the structure and *C* refers to the common freedom degrees between the soil and the structure. The stiffness and damping matrices can be similarly repartitioned to the mass matrix, and the vectors $\{Y_1\}$ and $\{Y_2\}$ can be repartitioned according to the matrices of the system:

$$\{Y\} = \begin{Bmatrix} Y_G \\ Y_C \\ Y_S \end{Bmatrix}$$

As the freedom degrees of the structure are null for the kinematic interaction, the equation of the seismic interaction may be written as:

$$\begin{bmatrix} M_{1G} & M_{1GC} & 0 \\ M_{1GC}^T & M_{1C}+M_{2C} & M_{2SC} \\ 0 & M_{2SC}^T & M_{2S} \end{bmatrix} \begin{Bmatrix} \ddot{Y}_{2G} \\ \ddot{Y}_{2C} \\ \ddot{Y}_{2S} \end{Bmatrix} + \begin{bmatrix} C_{1G} & C_{1GC} & 0 \\ C_{1GC}^T & C_{1C}+C_{2C} & C_{2SC} \\ 0 & C_{2SC}^T & C_{2S} \end{bmatrix} \begin{Bmatrix} \dot{Y}_{2G} \\ \dot{Y}_{2C} \\ \dot{Y}_{2S} \end{Bmatrix} + \begin{bmatrix} K_{1G} & K_{1GC} & 0 \\ K_{1GC}^T & K_{1C}+K_{2C} & K_{2SC} \\ 0 & K_{2SC}^T & K_{2S} \end{bmatrix} \begin{Bmatrix} Y_{2G} \\ Y_{2C} \\ Y_{2S} \end{Bmatrix} =$$
$$= -\begin{bmatrix} 0 \\ M_{2C} \\ M_{2SC}^T \end{bmatrix} \{\ddot{U}_{1C}\} - \begin{bmatrix} 0 \\ C_{2C} \\ C_{2SC}^T \end{bmatrix} \{\dot{X}_{1C}'\} - \begin{bmatrix} 0 \\ K_{2C} \\ K_{2SC}^T \end{bmatrix} \{X_{1C}'\}$$

(3.25)

Assuming that the terms of the sub-matrices $[M_{2C}]$ and $[M_{2SC}]$ are too small, if compared to the terms of the sub-matrix $[M_{1C}]$, happening the same for the respective sub-matrices of stiffness and damping, the third equation will become uncoupled:

$$\begin{bmatrix} M_{1G} & M_{1GC} \\ M_{1GC}^T & M_{1C} \end{bmatrix} \begin{Bmatrix} \ddot{Y}_{2G} \\ \ddot{Y}_{2C} \end{Bmatrix} + \begin{bmatrix} C_{1G} & C_{1GC} \\ C_{1GC}^T & C_{1C} \end{bmatrix} \begin{Bmatrix} \dot{Y}_{2G} \\ \dot{Y}_{2C} \end{Bmatrix} + \begin{bmatrix} K_{1G} & K_{1GC} \\ K_{1GC}^T & K_{1C} \end{bmatrix} \begin{Bmatrix} Y_{2G} \\ Y_{2C} \end{Bmatrix} = \begin{Bmatrix} 0 \\ 0 \end{Bmatrix}$$
$$\Leftrightarrow \begin{Bmatrix} Y_{2G} \\ Y_{2C} \end{Bmatrix} = \begin{Bmatrix} 0 \\ 0 \end{Bmatrix}$$

(3.26)

$$[M_{2S}]\{\ddot{Y}_{2S}\} + [C_{2S}]\{\dot{Y}_{2S}\} + [K_{2S}]\{Y_{2S}\} = -[M_{2SC}]\{\ddot{U}_{1C}\} - [C_{2SC}]\{\dot{X}_{1C}'\} - [K_{2SC}]\{X_{2C}'\}$$

which means that the displacements induced in the soil may be neglected. Therefore, one concludes that for a much higher contribution of the terms concerning the soil, the problem can be uncoupled. Thus, the soil motion is determined for the kinematic interaction and the structure motion is determined for the inertial interaction.

It is only worth dividing the problem into steps if the assumed simplifications bring advantages over the direct solution like, for instance, a finite element model.

In turn, the number of degrees of freedom involved in each step may be much less than in the complete solution, once the structure is modeled grossly for the kinematic interaction and the soil is replaced by the mass-spring-damper systems.

4

Project Description and Measurements

4.1. INTRODUCTION

As stated in chapter 1, the case of study reports the construction of an elastically bedded building nearby a buried/tunneled train track. Despite the lower amplitudes of the train induced waves when compared to another types of ground vibrations, the higher frequencies and also the short distance between source and receiver require the use of an elastic material on the building foundation in order to avoid/decrease the effects of the rail traffic.

Furthermore, the two wide and 1 meter thick plates layered with the elastic material between (CIBATUR – Calenberg-Ingenieure), thereby featuring the elastic foundation, represent a solution never tested so far for such cases, which reveals an additional point of interest. The present chapter is devoted to the description of the used equipment and the measurements to be done and their processing. Ahead, modeling as well as theoretical and practical results analyses are presented.

Figure 4.1 – Elastic foundation of the building

4.2. EQUIPMENT DESCRIPTION

For the vibration analysis on the building site a system called VibroStar 3000 was used. This system mainly consists of a data logger with up to 256 channels and a velocity sensor (geophone). In turn, the data logger basically consists of a data-concentrator unit (Figure 4.2) and 3 single channels for input. Additionally, in every VibroStar unit an industry pc for controlling the unit and storing the data can be found.

Figure 4.2 – Data-concentrator unit

The velocity sensor used is a triaxial velocity one with a built-in amplifier. In the sensor case is for each of the three measuring directions an electro-dynamic velocity pickup with natural frequencies from 4.5Hz (Geophone) built-in.
For the same case, the electronic network built-in extends the lower frequency range to 1 Hz while the upper frequency range is limited at 315 Hz and the signal is amplified in accordance with the selected measuring range.
Figure 4.3 is a picture of the sensor used for the measurements at the building site.

Figure 4.3 – Sensor

Figure 4.4 – Measuring equipment set

4.3. DATA ACQUISITION AND PROCESSING

In Figure 4.5, a plant of the building site with the points where the measurements took place is schemed.

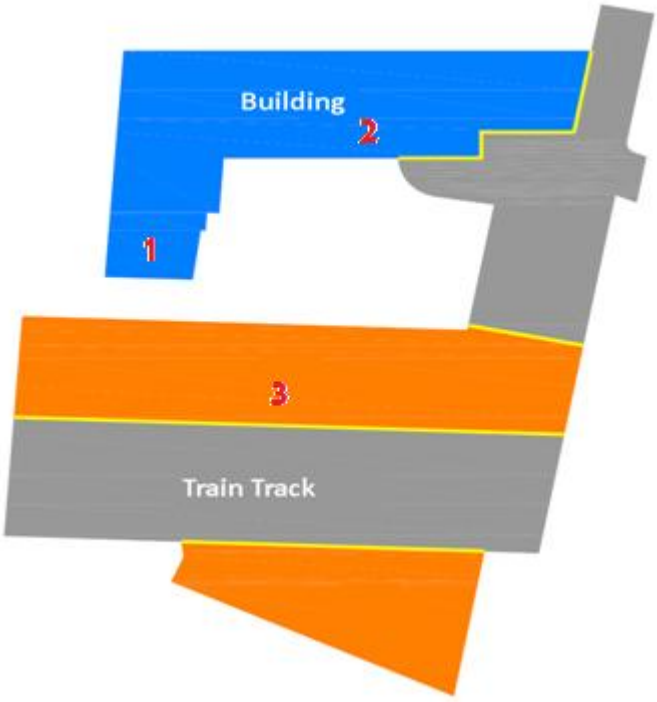

Figure 4.5 – Plant/scheme of the building site

In order to verify the efficiency of the adopted solution for the elastic foundation, the first measurements (points 1 and 2 of Figure 4.5) were taken twice after the hardening of the first concrete plate: due to its wide area, getting results for distant points is necessary so a linear (or non-linear) behavior of the plate can be admitted. In a second stage, the same measurements at points 1 and 2 were done for the upper plate. Also other points (point 3, for instance) in the ground were chosen to record the time series of the train vibrations: the ratio between the records of two different points was the adopted way for the analysis of the results (transfer function).

Figure 4.6 – Measuring equipment on the ground

For a good data collection, each measurement lasted around 2 hours, thus corresponding more or less to 20 trains recorded. The records had then to be filtered, depending on some factors:

- Records of which amplitudes of the time series were not enough high or not perceptible were not considered. For instance, a train stopping at the station near the building site is supposed to pass slower and the vibrations produced are not so high;
- Records with some other external interferences as, for instance, objects falling next to the geophones, were erased;
- Although the freight trains are much heavier than the passenger trains, their too slow speed lead them to produce too low amplitudes and so they were not taken into consideration either, unless when they passed nearby the station at the same time than any other train thereby increasing the total amplitudes measured.

Once the equipment was set up, the different time series recorded from each of the geophones were continuously stored on the computer, sorted in files of 2 minutes of length.

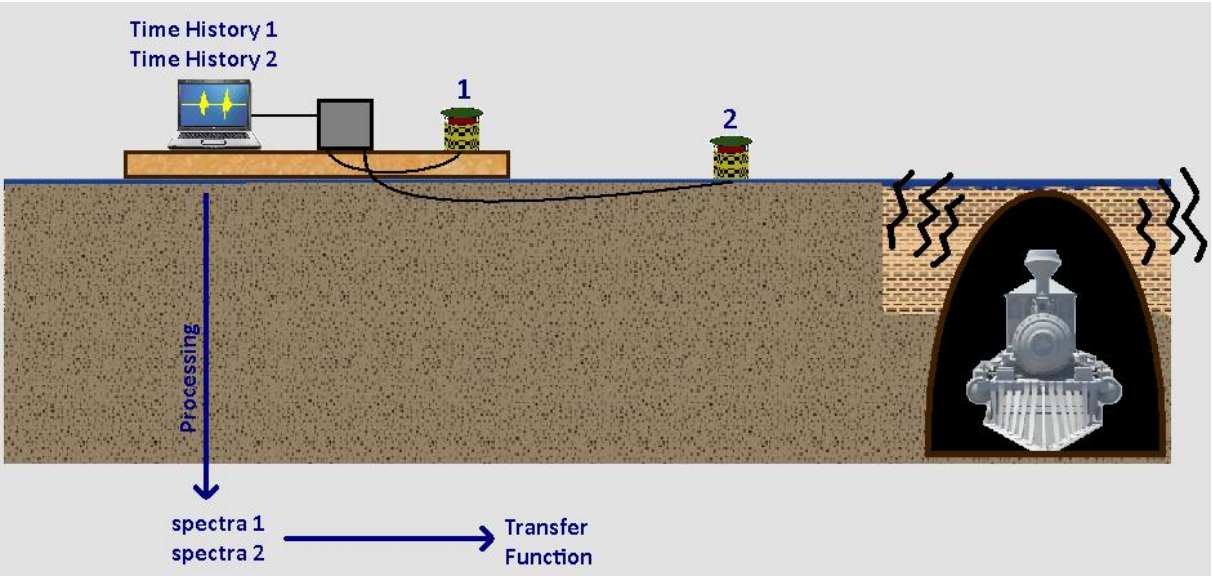

Figure 4.7 – Scheme of data recording and processing

Figure 4.8 is an example of a record of one of the geophones where it is possible to notice oscillations due to a train passage nearby the building site. Channel 3 is related to the z-coordinate.

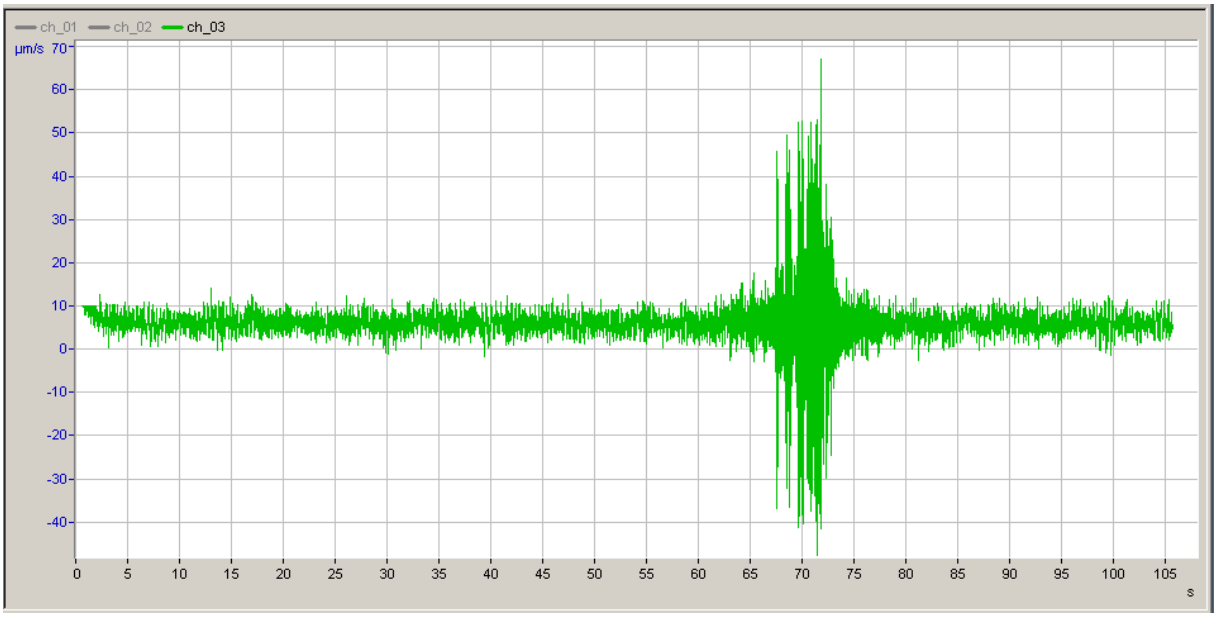

Figure 4.8 – Record containing a train induced vibration

Through the auxiliary software (which algorithm follows what is described in sub-chapter 2.2) of signal analysis previously described they had then to be converted into the frequency domain. With the filtered records at any measured point, the average of the amplitudes for each frequency point (note that the conversion into the frequency domain results in a discrete function) was then used to obtain the transfer functions.

4.4. GEOTECHNICAL CONDITION OF THE SITE – SOIL PROPERTIES

The knowledge of static and dynamic soil properties is required for the analysis of vibration problems. Due to its particulate material in solid particles, water and gas, the soil parameters are affected by mineral properties, particle shape, size, and composition, and porosity. As stated in chapter 2, soil parameters as shear modulus, soil density, Poisson's ratio and material damping represent those that are usually required when analyzing vibration problems. In turn, the most important factors which influence soil behavior during vibratory loading are the strain level, material degradation (effect of loading cycles), loading rate and material damping (absorption of energy). In Table 4.1 generalized dynamic properties of the soil in Vienna (Austria) are shown. Figure 4.9 gives an estimation of damping values for different soils.

Table 4.1 – General characterization of the soil next to the building site (IC Consulenten, 2002)

Layer	Weight [kg/m^3]	P-wave velocity [m/s]	S-wave velocity [m/s]	K-Modulus [Pa]	G-Modulus [Pa]	Damping [%]	Depth [m]
clay	1800	250	120	5.118E7	1.156E8	2	0
bedrock							13

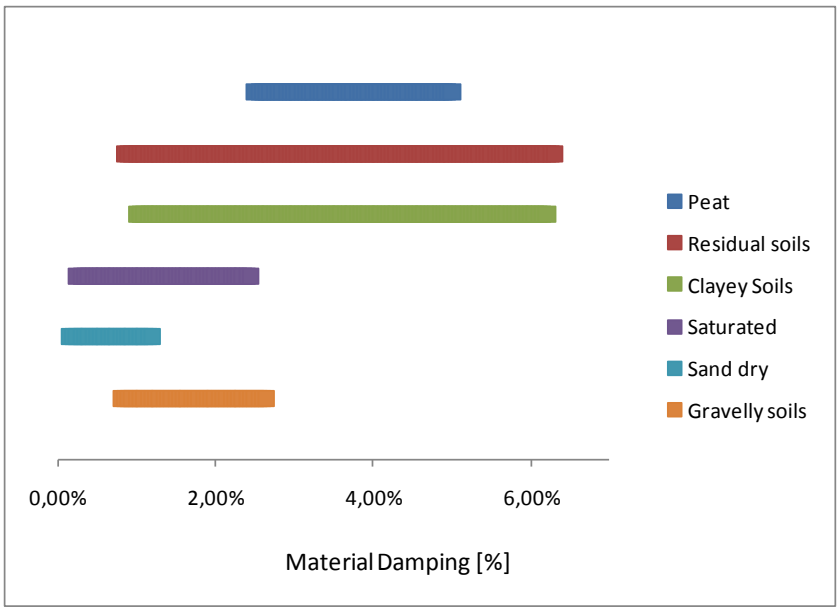

Figure 4.9 – Damping values for different soils (IC Consulenten, 2002)

5

Modeling and Analysis

For the analysis of the results and prediction of the train vibration effects in the meant building structure, the modeling had to be focused on two main aspects: the elastic material and the influence of the dynamic soil structure interaction. Therefore, two sub-models were adopted and a third one involving the whole system tested afterwards. Since the measurements were done both at the free-field, first and second plates of the elastic foundation, the two sub-models can be performed apart and the complete one concerning all the system tested at last. Additional analysis involving the entire building, which storeys are not yet built, was also done in order to approach mainly the human perception.

5.1. ELASTIC FOUNDATION MODELING

By opting for a material such as CIBATUR it is expected that the vibrations measured upon the upper plate record lower amplitudes than those measured on the lower plate, as the rubber material lies between the two concrete plates.

5.1.1. PRODUCT DESCRIPTION

The chosen product (CIBATUR) consists of a fabric reinforced elastomeric plate having underneath truncated cone shape spring elements. Natural rubber of high quality is used for the spring elements which have excellent dynamic properties resistance to abrasion, oil and ozone is ensured by the top layer, as well as resistance to temperatures ranged from -40ºC up to +70ºC.

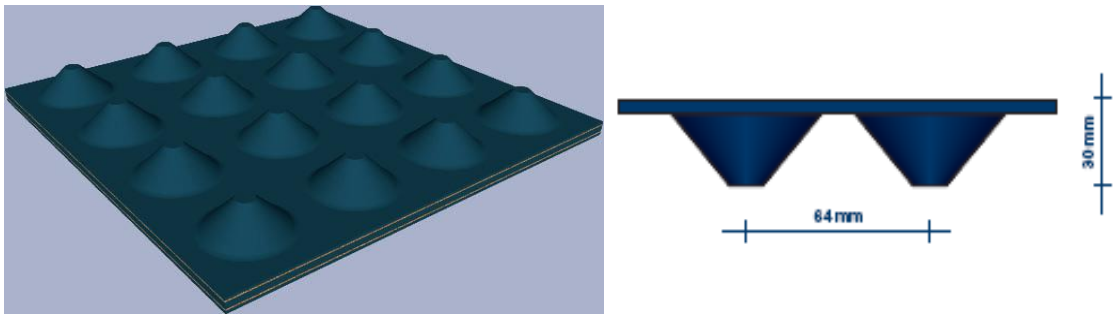

Figure 5.1 – Elastic material applied between the two concrete plates of the foundation. URL http://calenberg-ingenieure.de

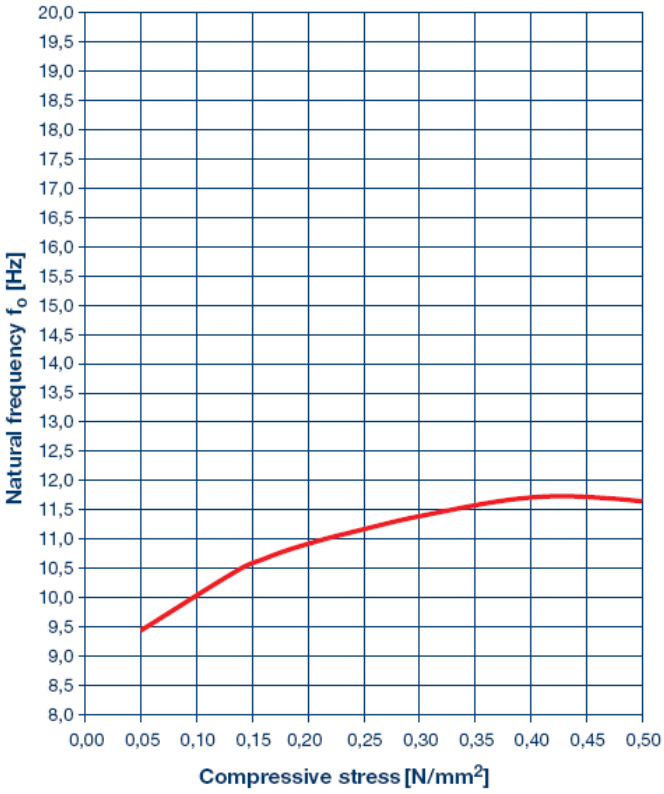

Figure 5.2 – *Compressive stress versus natural frequency of the system (CIBATUR plus concrete structure)* experimental test results for the elastic material. URL http://calenberg-ingenieure.de

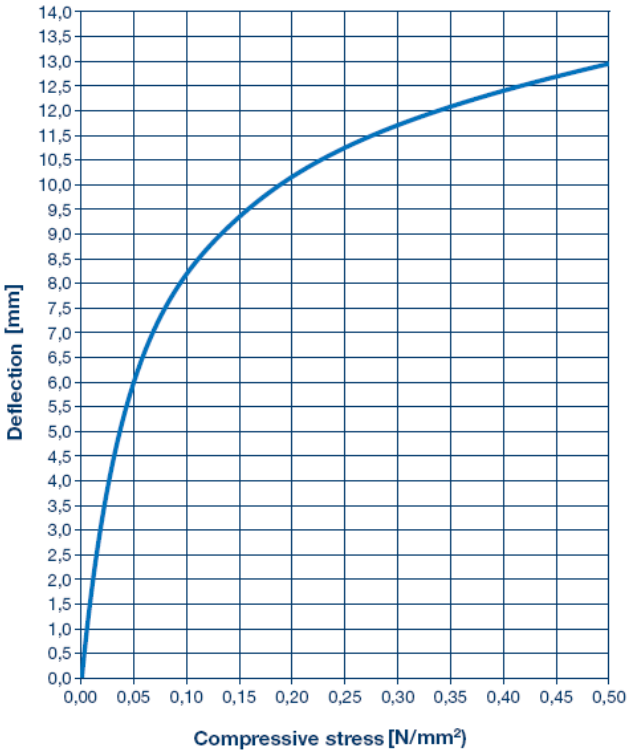

Figure 5.3 – *Compressive stress versus deflection* experimental test results for the elastic material. URL http://www.calenberg-ingenieure.de

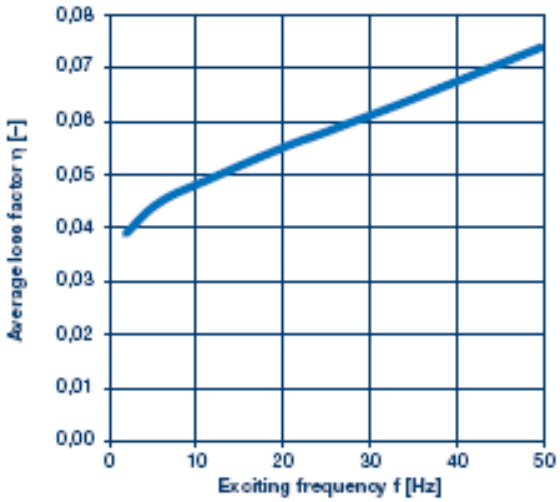

Figure 5.4 – *Exciting frequency versus angular loss factor* experimental test results for the elastic material. URL http://www.calenberg-ingenieure.de

Figures 5.2, 5.3 represent the results by means of natural frequencies and static deflections obtained from the laboratory experiments.

From Figure 5.4 and by taking the approximation

$$\eta \approx 0.5\zeta \qquad (5.1)$$

the degree of damping at the frequency domain can be estimated.

5.1.2. MODELING

Modeling the rubber material constituted the main issue in this first step. To idealize a valid model that later ensures reliable results, the charts obtained from experimental tests might represent a solid base.

The used software, SOFISTIK, provides, like many others, the user the option to define spring elements. For some long lengths, several spring elements ought to be considered, in order to avoid eventual bending effects. Hence, instead of only one spring element, a system of parallel springs must be adopted.

This first model took a length of, 20 m, divided into forty segments of 0.5 m each, i.e., 41 spring elements. Thus, the stiffness of either spring element has to be a forty-first of the determined spring constant (kN/m) times the length (20 meters). The transverse stiffness of each spring was empirically estimated of 10% of the axial stiffness. A thickness of 1 m and the concrete C20/25 were considered. The presence of any reinforcement, S500 for instance, could be neglected, as this sort of dynamic analysis concerns more on the mass, which is a very small percentage in the case of steel, and even for any deflections the steel is not expected to act, as they are too small.

Figure 5.5 illustrates the system adopted for the elastic foundation.

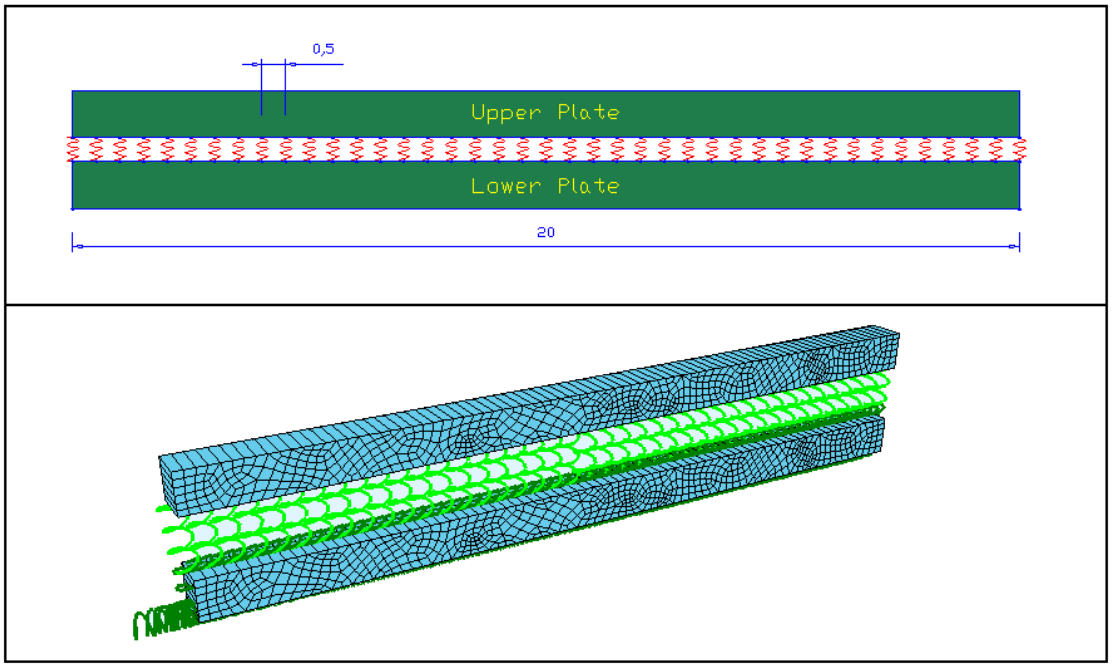

Figure 5.5 – Elastic foundation modeling

To verify whether or not the adopted model seems to be ideal, only one plate was considered at first for a dead load case, which maximum compressive stress obtained was 0.0243 N/mm^2.

The chart from Figure 5.3 states that in the range of 0.00 – 0.05 kPa the variation of the deflection is approximately linear. However, if one considers the whole building together with the higher-valued static loads, the deflections obtained are expected to be out of the linear variation range. Anyway, as the displacements resulting from a train vibration are too small, also a linear law can be defined for the spring elements, as from the slope at the intended point.

A pressure of 0.0243 kPa led one to admit a value of 8333 kN/m/m, which means 4065 kN/m for each spring element over the 20 m of length.

The second plate was then added together with the spring elements. To confirm the operation, the obtained natural frequency for the vertical vibration mode must fit in the chart of Figure 5.2. The value of 9.208 Hz proves that the assumption is valid.

5.1.2.1. Damping modeling and Rayleigh Damping

If no damping is set to the defined spring system that constitutes the rubber layer, the results expected for the dynamic action will result in much higher values for the amplification factor. Together, the chart plotted in Figure 5.4 and the relationship between the loss factor and the frequency feature a

damping factor that varies all over the frequency domain. In chapter 2, it was shown for a singly mass system, by Equations (2.29), and (2.30), that the dashpot value is function of, among others, a damping factor that is assumed to be constant.

In a system with n degrees of freedom it is known that the modal mass participation decreases with increasing modes thus meaning a decrease of the critical damping. In fact, a constant damping ratio is a valid assumption whenever the contribution of the first modes achieves nearly 100%. For a system where higher mode contribution is more significant the results based on a fixed damping ratio will not be realistic anymore.

When it comes to dynamic analysis of soil, structures and foundations, the way to treat damping within modal analysis framework is to consider the damping value as an equivalent Rayleigh Damping in form of:

$$[C] = \alpha[M] + \beta[K] \qquad (5.2)$$

in which [C] is the damping matrix of the physical system; [M] is the mass matrix of the physical system; [K] is the stiffness matrix of the system and α and β are pre-defined constants.

Equation (1.22), when describing the motion of a system with multi-degrees of freedom, can be reduced to n-uncoupled equations by orthogonal transformation:

$$\{\phi\}^T[M]\{\phi\}\{\ddot{y}\} + \{\phi\}^T[C]\{\phi\}\{\dot{y}\} + \{\phi\}^T[K]\{\phi\}\{y\} = \{\phi\}^T\{F\} \qquad (5.3)$$

$$\{\ddot{y}_i\} + 2\zeta_i\omega_{ni}\{\dot{y}_i\} + \omega_{ni}^2\{y_i\} = \{F_i\} \qquad (5.4)$$

in which {y} is the displacement of the structure in the transformed co-ordinate; ζ is the damping ratio in uncoupled mode; ω_n is the natural angular frequency of the system; {F} is the modified force vector in transformed co-ordinate and {ϕ} is the normalized eigen vector of the system.

The orthogonal transformation is valid only when the damping matrix is proportional. In other words, the damping matrix has to be function of the mass and stiffness matrices. Therefore, the damping in its Rayleigh form reduces to:

$$\{\phi\}^T[C]\{\phi\} = \begin{bmatrix} \alpha+\beta\omega_{n1}^2 & 0 & .. & 0 \\ 0 & \alpha+\beta\omega_{n2}^2 & .. & 0 \\ . & . & .. & . \\ 0 & . & .. & \alpha+\beta\omega_{nn}^2 \end{bmatrix} \qquad (5.5)$$

and from symmetry:

$$2\zeta_i\omega_{ni} = \alpha + \beta\omega_{ni}^2 \qquad (5.6)$$

This, on simplification reduces to

$$\zeta_i = \frac{\alpha}{2\omega_{ni}} + \frac{\beta\omega_{ni}}{2} \qquad (5.7)$$

or

$$\zeta_i = \frac{\alpha}{4\pi f_i} + \beta\pi f_i \qquad (5.8)$$

The values of α and β, for the elastic layer, can be determined by choosing two points from the chart in Figure 5.4 and relating them with the damping factor . Thus, for the pairs:

P_1: (10 Hz; 0.096)

P_2: (20 Hz; 0.11)

one has

$\alpha = 6.86962\ \text{sec}^{-1}$

$\beta = 0.001316\ \text{sec}$

and the degree of damping can be plotted in the frequency domain in (see Figure 5.6).

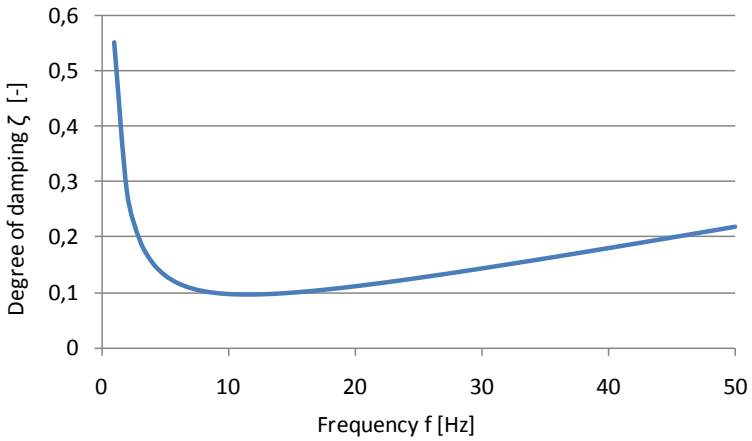

Figure 5.6 – Graphical representation of the Rayleigh damping for the elastic material

5.1.3. RESULTS

For the confirmation of the experimental tests concerning the natural frequency versus compressive stress relationship, a sampling from the time series measured upon the second plate, where no any disturbances happen, was taken. Such sample provides one an approximated value of the natural frequency (Figure 5.7).

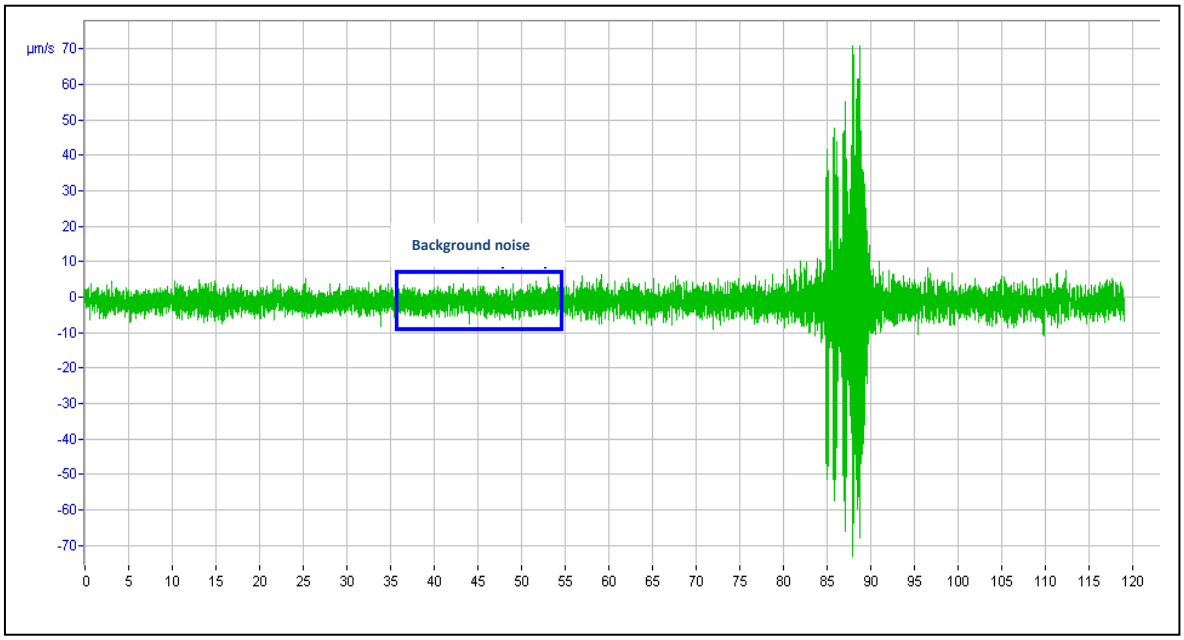

Figure 5.7 – Time series on the second plate

By using the FFT, the frequency chart is composed (Figure 5.8), where the peak of the amplitudes leads to assume that the natural frequency lies within the range of 8 Hz to 10 Hz, which is in accordance with the previous analysis.

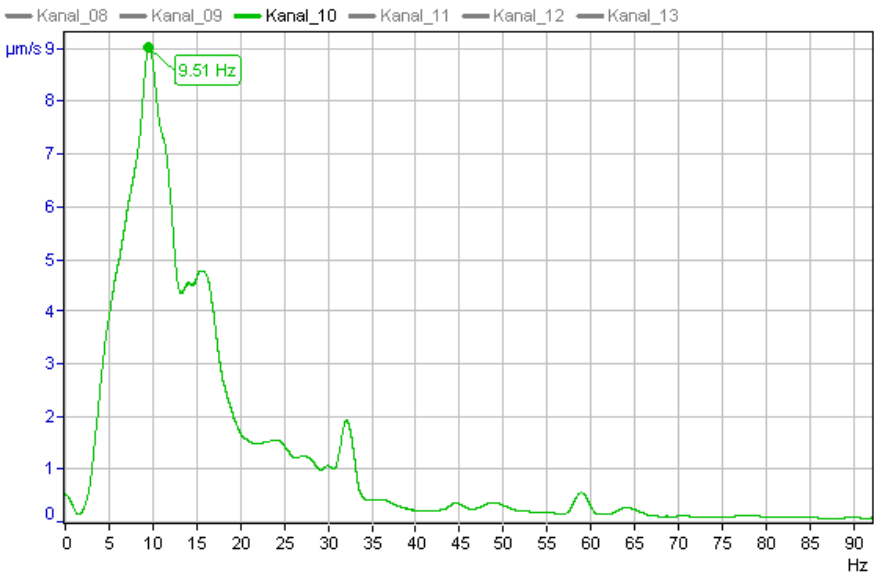

Figure 5.8 – Natural frequency spectrum corresponding to a timeframe with background noise

The attenuation effects due to the elastic material could be predicted from a train time series applied to the lower plate. For the comparison between theoretical and practical results transfer functions must be used, since the dynamic load factor is unknown. Thus, despite the time series applied to the bottom of

the lower plate is set by means of displacements for a load factor of 1 kN, a new series record from the top of the lower plate has to be output, as well as another one from the upper plate. It is worth to refer that due to linearity a time series by means of velocity can be used as if it is a force.

```
Load Case    11
Factor forces and moments          1.000
Factor dead weight       DL-XX     0.000
Factor dead weight       DL-YY     0.000
```

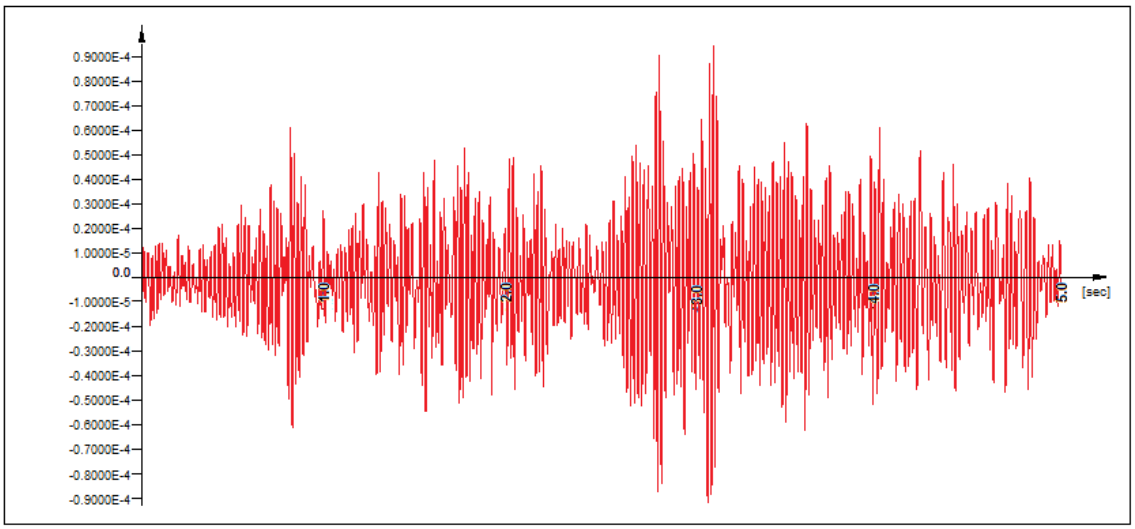

Figure 5.9 – Train time series

The two output records have then to be converted into the frequency domain whence the transfer function results.

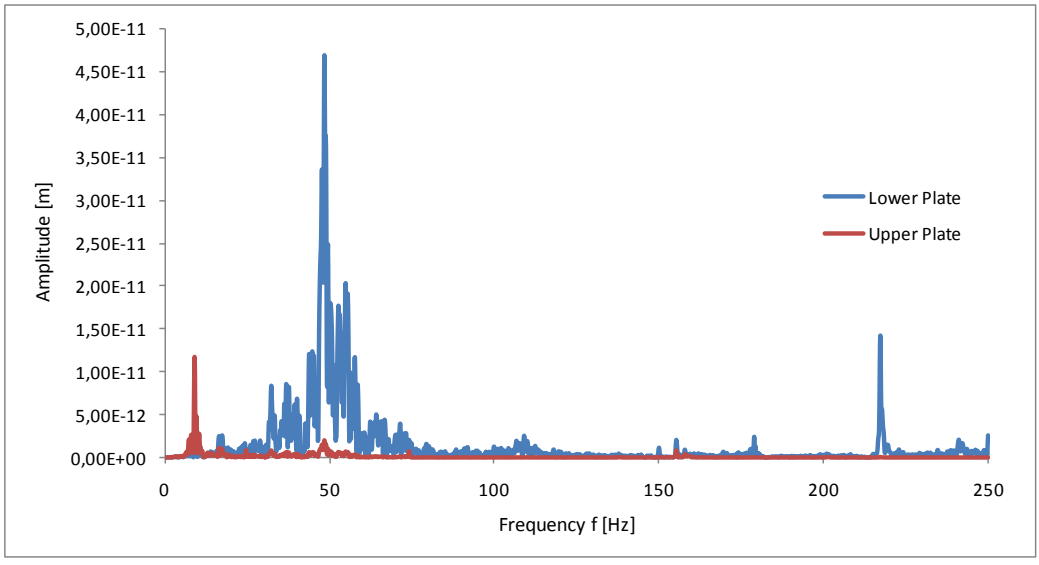

Figure 5.10 – Frequency spectra obtained in both foundation plates for a train vibration with a factor of 1 kN

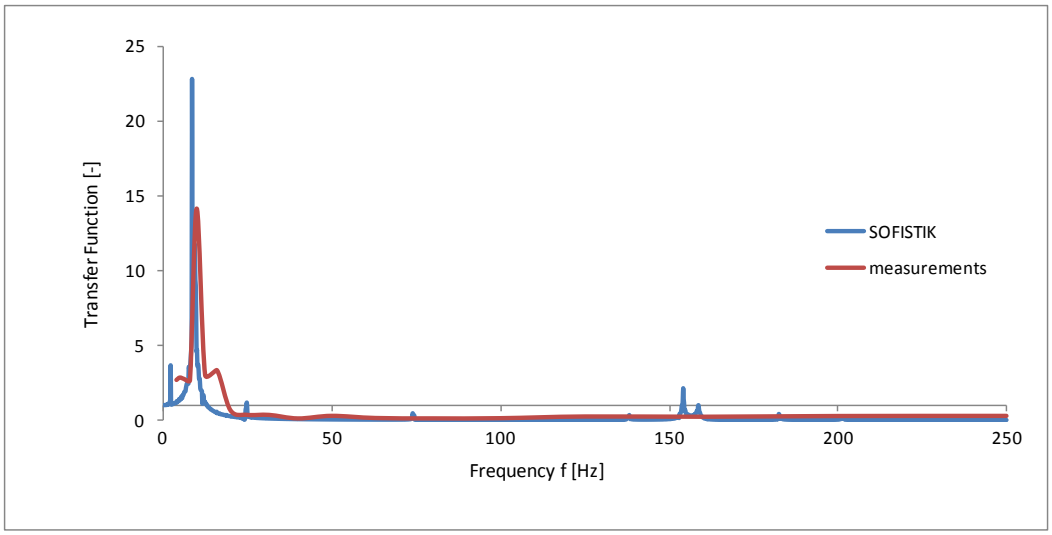

Figure 5.11 – Comparison between the lower plate – upper plate of the elastic foundation transfer functions for the measured and theoretical results (frequency range up to 250 Hz)

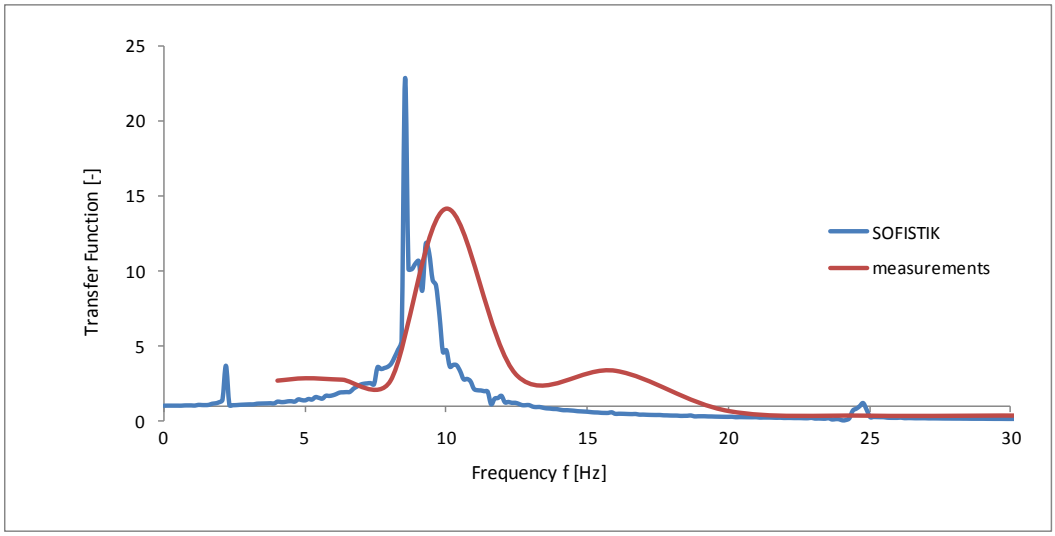

Figure 5.12 – Comparison between the lower plate – upper plate of the elastic foundation transfer functions for the measured and theoretical results (frequency range up to 30 Hz)

As it is visible in Figures 5.11 and 5.12 the close results verify the accuracy of the set model.

5.2. SOIL-FOUNDATION SYSTEM MODELING

For a FE model involving soil and structure together, the central issue resided in the formulation of the interface between these two sub systems. The kinematic and inertial phenomena make the modeling more complex than only replace the soil by a system of springs and dampers with the soil properties.

Furthermore, the definition of a halfspace implies some boundary conditions in order, for instance, to process/simulate any wave propagation through the elastic media without any reflections.

5.2.1. INTERFACE FORMULATION

An interface is represented as normal and shear stiffness between two planes which may contact one another (see Figure 5.13 scheme).

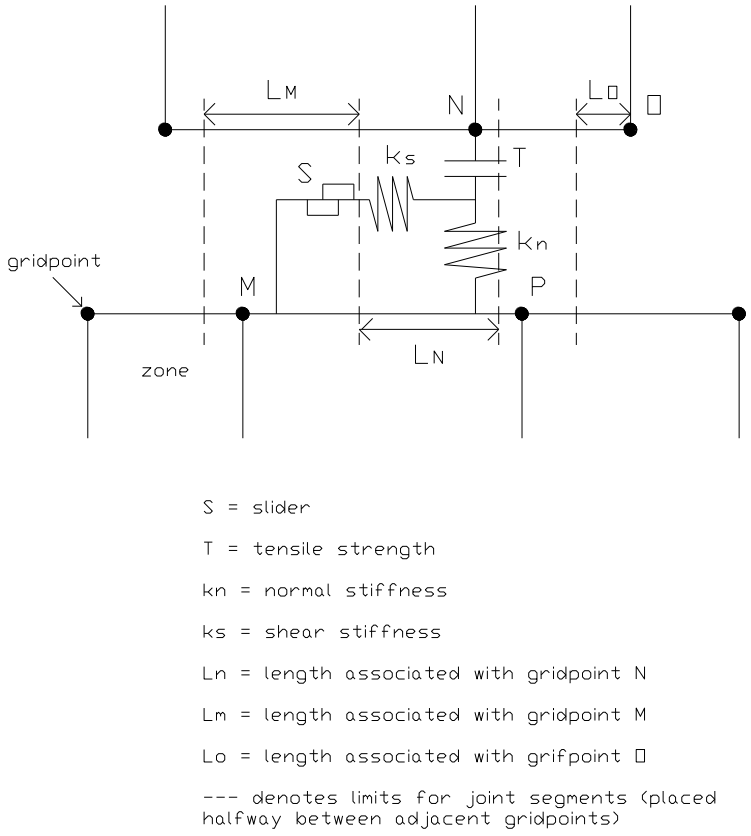

Figure 5.13 – Interface formulation (FLAC formulation)

The considered logic is described as following:

A list of grid points (i,j) lying on each side of any particular surface is considered. In turn each point is taken and checked for contact with its closest neighboring point on the opposite side of the interface. If contact is detected, the normal vector to the grid point is computed. A “length” is also defined for the contact along the interface. This length is equal to the half distance to the nearest grid point to the left of the checked point plus half the distance to the nearest point to the right, irrespective of whether the neighboring grid point is on the same side of the interface or on the opposite side of the checked point. In this way, the entire interface is divided into contiguous segments, each controlled by a grid point.

During each time step, the velocity, $\dot{u}_i$, of each grid point is determined. Since the limits of velocity are displacement per time step, and the calculating time step has been scaled to unity to speed convergence, then the incremental displacement for any given time step is:

$$\Delta x_i \equiv \dot{x}_i \qquad (5.9)$$

The incremental relative displacement vector at the contact point is resolved into the normal and shear forces determined by:

$$\begin{aligned} F_n^{(t+\Delta t)} &= F_n^{(t)} - k_n \Delta x_n^{\left(t+(1/2)\Delta t\right)} L \\ F_s^{(t+\Delta t)} &= F_s^{(t)} - k_s \Delta x_s^{\left(t+(1/2)\Delta t\right)} L \end{aligned} \qquad (5.10)$$

where the stiffness, k_n and k_s, have the units of [stress/displacement].

To specify the conditions of the interface which may require an adjustment of the contact forces the interfaces can be declared glued, in accordance with the Coulomb shear-strength criterion, or bonded (this last can be defined either as bonded interface or slip while bonded).

The Coulomb shear-strength criterion is defined by the relation:

$$F_{s\max} = c' \cdot L + \tan\phi \cdot F_n \qquad (5.11)$$

where *c'* is the cohesion along the interface, *L* the effective contact length and ø the friction angle of interface surfaces. For a real interface that is stiff compared to the surrounding material, but which can slip and perhaps open in response to the anticipated loading, only a means for one sub-grid to slide and/or open relative to another sub-grid need to be provided the friction (and perhaps cohesion and tensile strength) is important, but the elastic stiffness is not. The Coulomb criterion looks to be suitable for such approach that considers only the slip and separation phenomena, but not to the interface formulation of the required model and respective analysis.

A bonded interface, in turn, suits better a real interface that is soft enough to influence the behavior of the system (like, for instance, a joint soft clay filling or a dike containing heavily fractured material), which is not the case either.

An artificial device to connect two "sub-grids" together is then formulated. Although for glued interfaces, no slip or opening is allowed, the elastic displacement still occurs, according to the given stiffness. Anyway, the too small displacements expected to be obtained in the present analysis do not constitute a problem at all and hence slip or opening phenomena can be neglected.

Values of friction, cohesion and tensile strength are not necessary and only shear and normal stiffness must be provided. The apparent stiffness of a zone in the normal direction is

$$\max\left[\frac{\left(K + \frac{4}{3}G\right)}{\Delta z_{\min}}\right] \qquad (5.12)$$

where *K* and *G* are the bulk and shear modules, respectively, and Δz_{min} is the smallest width of an adjoining zone in the normal direction. The max [ ] notation indicates that the maximum value of all zones adjacent to the interface is to be used.

The interface elements adjacent to the interface were set to a minimum size of 0.25 m. the value of ($K + {}^{4}/_{3}G$) is 33.29 GPa (concrete shear and bulk moduli values – see ahead sub-chapter 5.2.2). Hence both shear stiffness and normal stiffness were set to be 133.16 x 10^9 Pa/m. Similarly to sub-chapter 5.1, a system of 41 parallel springs of 324.79 x 10^5 kN/m either ($k_n = k_s$), throughout a length of 10 m, was used. Figures 5.14 and 5.15 represent the adopted scheme for a transverse section to the train tunnel.

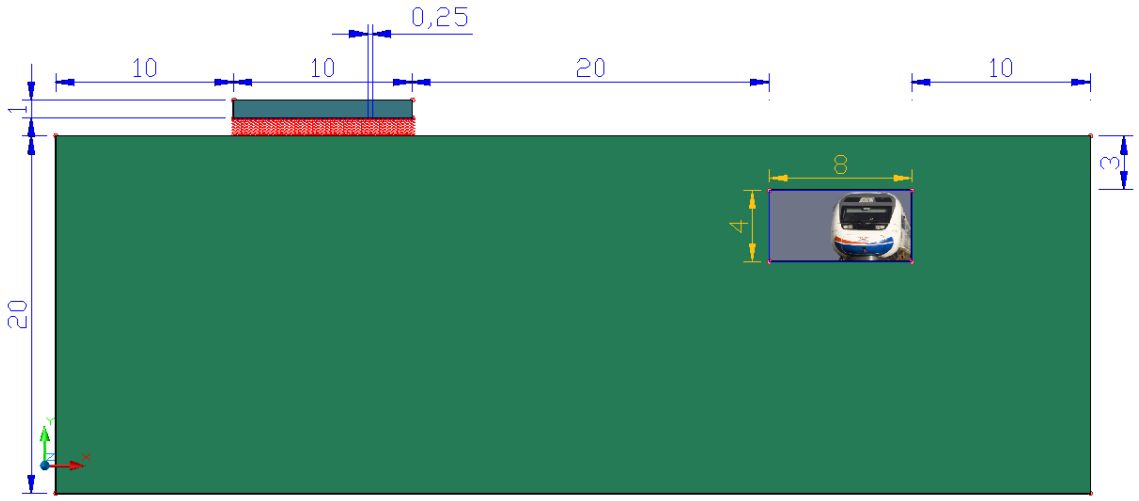

Figure 5.14 – Transverse section to the train tunnel (scheme)

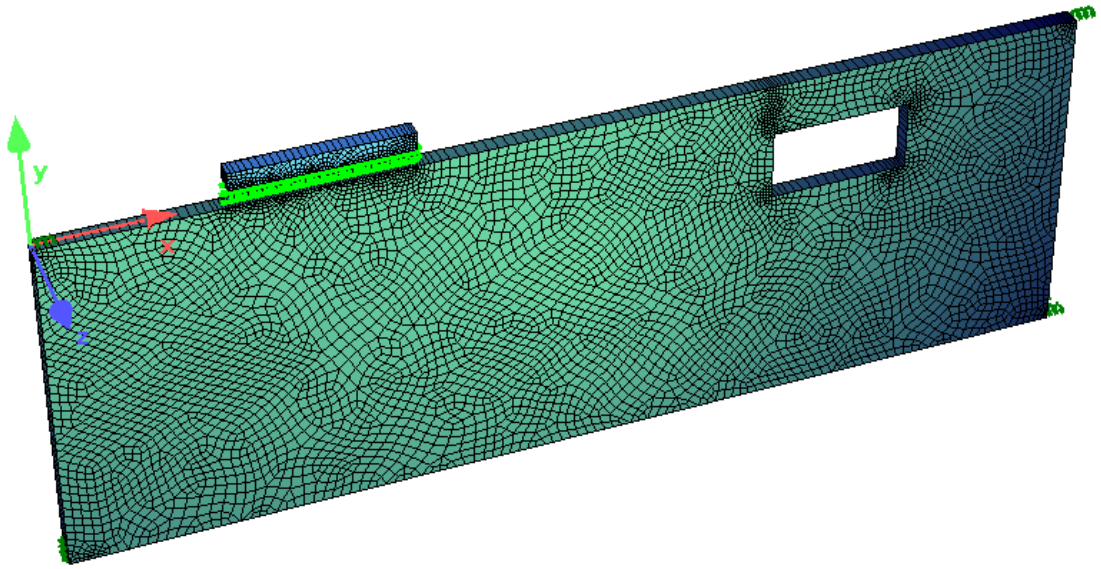

Figure 5.15 – SOFISTIK halfspace model

5.2.2. HALFSPACE MODELING

The software SOFISTIK usually determines stiffness matrices for any structure size that are assembled either from finite elements or they can be described analytically, for example, as elastic halfspace with appropriate soil parameters. These stiffness matrices represent elastic substructures, linked via defined connection nodes. The statics calculation determines then the soil-structure interaction. However, for

calculations concerning dynamics, the halfspace module has at least one limitation that disables its appliance to the present issue: especially designed for static calculations, where most of the effects occur nearby the structure foundation and decrease with the distance from it, the user is not provided the possibility to apply any static or dynamic loads directly on the halfspace.

If proper, the use of this module would release any interface formulation, as described in sub-chapter 5.2.1.

Replacing the halfspace by a structure with the soil settings was hence the adopted way. To turn such substructure into a similar one to the halfspace, a few more settings had to be defined:

- At first, any soil subjected to dynamic loads will undergo motion. Thus, the support conditions of the structure representing the halfspace have to be set in a way that allows the soil to move. Hence, boundary elements such as bedding elements (kN/m^2) may be adopted, working as springs. As no any information about which values should be given to the bedding elements, one must study the influence of their stiffness over the system. Because of the experimental results showing the insignificance of the tried displacements of the system and the big dimensions of the "halfspace" structure when compared to the foundation structure, the importance of how the stiffness of the bedding elements influences the results for such actions might be analyzed by means of natural frequencies variation/non-variation (first six modes of vibration). Figure 5.16 features the behavior of the model for stiffness values (vertical) ranging from 1000 to 1E7 kN/m^2. The lateral beddings were considered to be 10 times the bottom bedding, since the vertical component of the excitations measured is much higher than the horizontal ones.

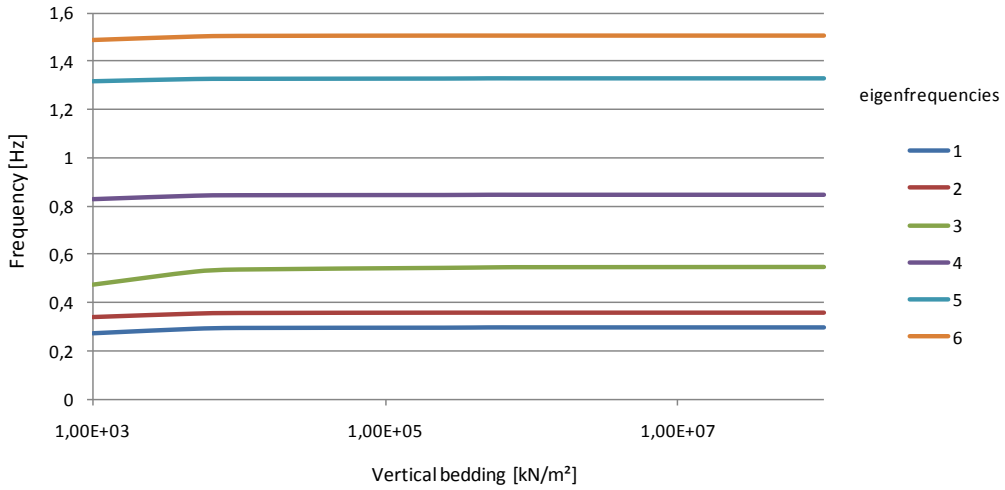

Figure 5.16 – First six natural frequencies variation with vertical bedding (SOFISTIK halfspace model)

As the chart of Figure 5.16 demonstrates, the value of the natural frequency corresponding to the vertical vibration mode remains practically constant, meaning thereby the small influence of the stiffness value of the bedding elements for any train induced vibrations. Hence, the values 20000 kN/m^2 and 200000 kN/m^2 were set for vertical and lateral bedding, respectively.

- Another aspect to take into account in this halfspace modeling is the possibility of wave reflection. Once a wave reaches the "bounds of the halfspace" it is expected to reflect itself,

which does not correspond to the truth. In order to prevent this situation, the scheme illustrated in Figures 5.14 and 5.15 had already additional boundary elements consisting of dampers with very high damping values. The use of such elements was supposed to simulate the wave propagation over the infinity. Note that also these dampers do not influence the results by means of frequencies.

What led one to assume a halfspace was that the depth of the bedrock when compared with the distance between the tunnel and the foundation. The halfspace was then considered to be homogeneous due to the high depth of the first layer. The set values were the following:

Table 5.1 – Halfspace dynamic properties

Parameter	Value
Weight [kN/m^3]	18.13
Poisson's ratio [-]	0.395
Elastic modulus [MPa]	322.52
Shear modulus [MPa]	115.6
Bulk modulus [MPa]	511.94

As a system with large degrees of freedom, guessing meaningful values of Rayleigh damping coefficients α and β may not be so clear for the soil. Digressing from the determination of such parameters in the case of elastic foundation, where the two chosen points were taken from a chart plotted according to experimental tests, the halfspace α and β had to be calculated from an estimated minimum of the function. For the concerned soil, a minimum value of 2% for a frequency of 25 Hz seemed to be a plausible value. For other sorts of soils, different values can be conferred in Table 5.2.

Table 5.2 – Rayleigh damping for different soils (IC Consulenten, 2002)

Material	Density [kg/m^3]	Bulk [Pa]	Shear [Pa]	Fmin [Hz]	Damp [%]
gravel	2100	2.67E+07	1.60E+07	30	2.5
sand	1700	1.67E+07	1.00E+07	30	2.5
silt	1750	2.67E+06	1.60E+06	25	2
clay	1800	6.67E+05	4.00E+05	20	2
rock	2700	2.26E+10	1.10E+10	50	1.5

***from FLAC material database**

To determinate α and β from a given minimum, the second equation of the system is the derivate of Equation (5.8) and its value for the given frequency must be zero.

$$\left(\frac{\alpha}{4\pi f}+\beta\pi f\right)\frac{\partial\zeta}{\partial f}=\frac{-\alpha}{4\pi f^2}+\pi\beta \qquad (5.13)$$

Thus one has the system:

$$\begin{cases}0.02=\dfrac{\alpha}{4\pi\times 25}+\beta\times 25\pi\\ 0=\dfrac{-\alpha}{4\pi\times 25^2}+\pi\beta\end{cases} \qquad (5.14)$$

and α and β are:

$$\begin{cases}\alpha=3.1415927\,\mathrm{sec}^{-1}\\ \beta=0.00012732\,\mathrm{sec}\end{cases} \qquad (5.15)$$

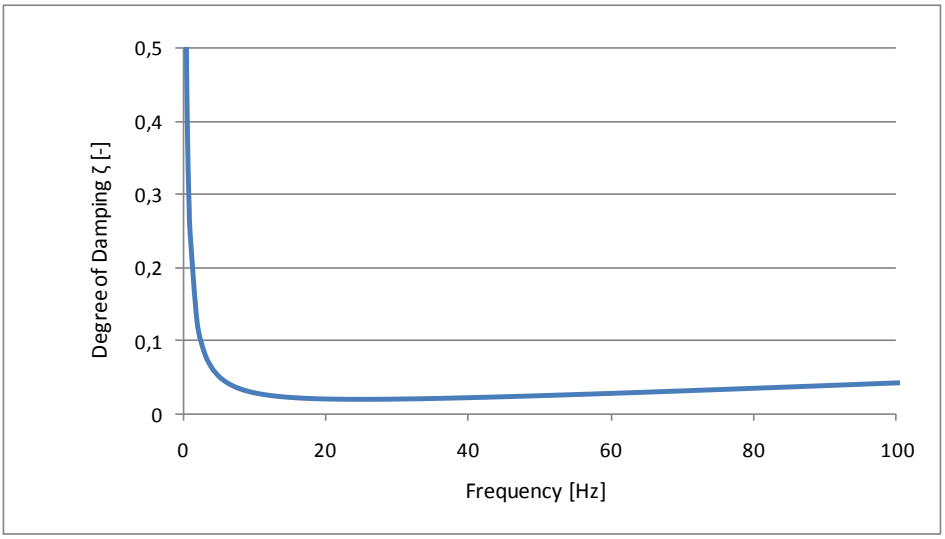

Figure 5.17 – Estimated Rayleigh damping for the soil

5.2.3. RESULTS

Similarly to the testing of the elastic foundation, the comparison of the theoretical and experimental tests was made, by the same reasons, in terms of transfer functions. This time, the train series (Figure 5.9) was applied on the bottom of the set opening of the halfspace that represents the tunnel.

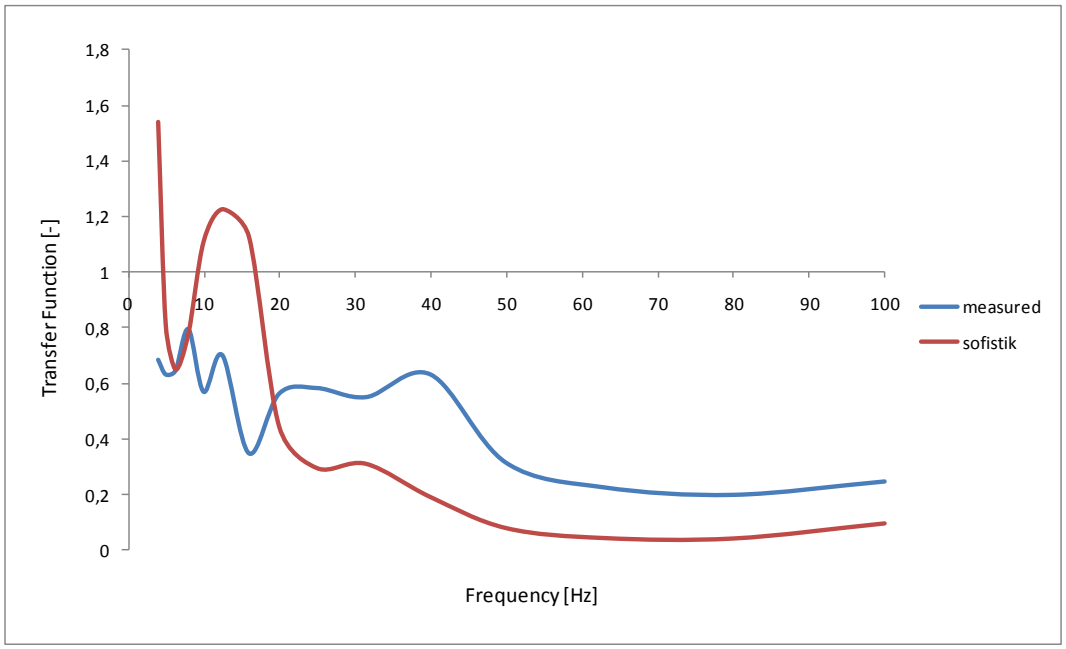

Figure 5.18 – Comparison between the measured and SOFISTIK soil-foundation transfer functions

The results obtained from the SOFISTIK model are not satisfactory at all. Not only the behavior of the transfer function is different than the measured, but also the theoretical models were expected to be more conservative. In order to verify whether or not the system is performing as elastic, a new analysis was tried for a triangular load, described in Figure 5.19.

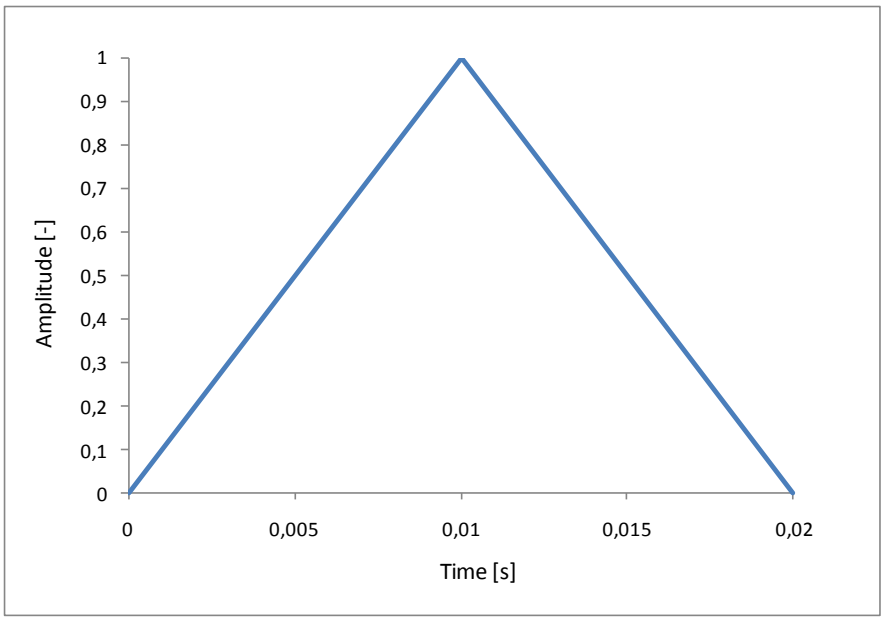

Figure 5.19 – Dynamic triangular load

The two transfer functions for the two different loads are ahead plotted together (see Figure 5.20).

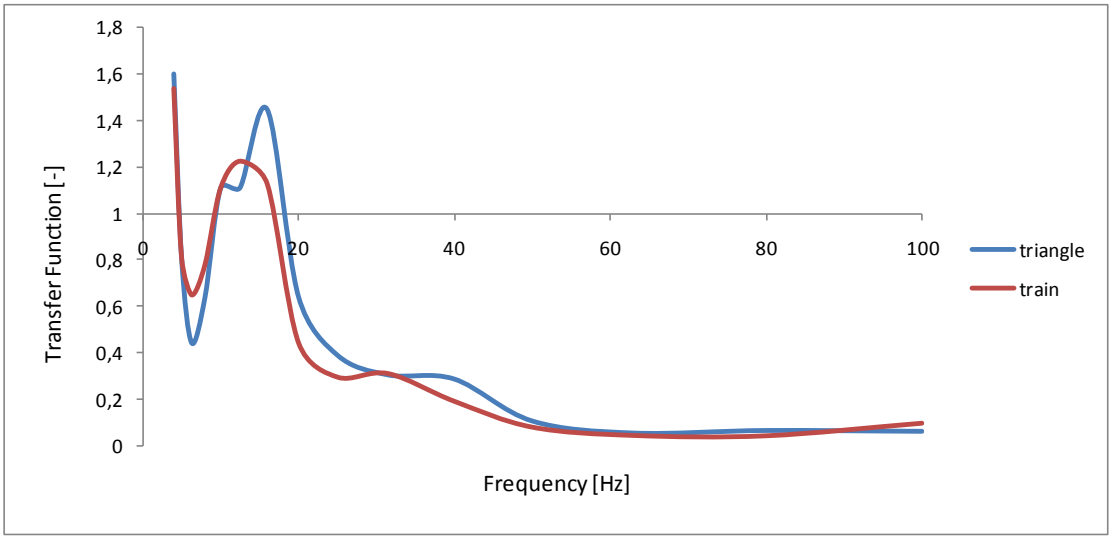

Figure 5.20 – Comparison between the triangle and the train load

As it is easy to conclude, when using two loads of different natures very close transfer functions are generated and so the linearity of the model is proved. Nevertheless, the described procedure for a SOFISTIC model does not show accuracy to such sort of calculations involving the elastic media. Hence, the software FLAC, proven software for SSI dynamic analysis, even though for simple models, was used for the same purpose, taking the same assumptions as the SOFISTIK model. The model is illustrated in Figure 5.21 and the results are shown in Figure 5.22.

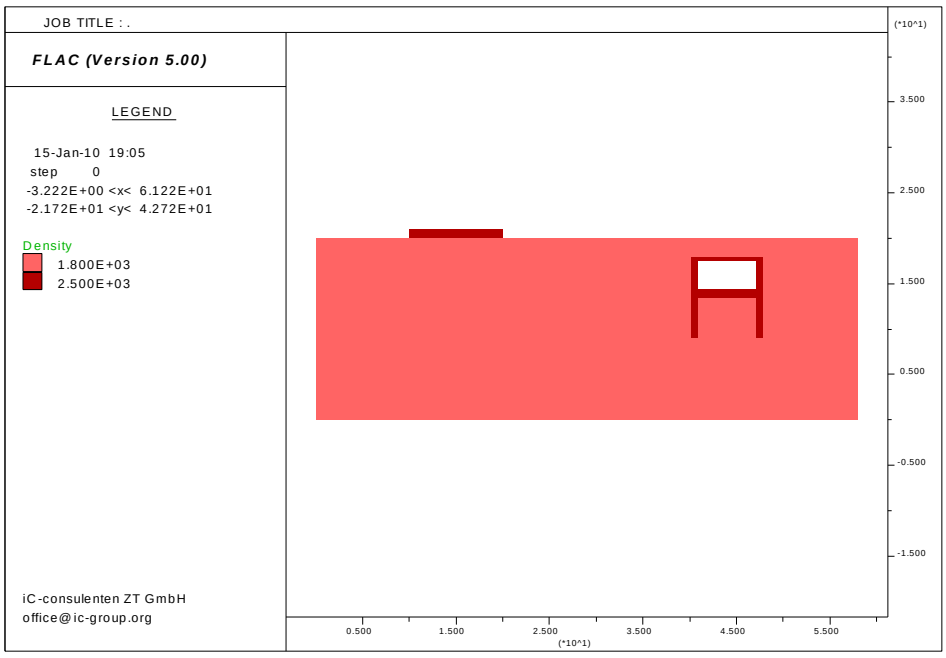

Figure 5.21 – FLAC (Fast Lagrangian Analysis of Continua) halfspace model

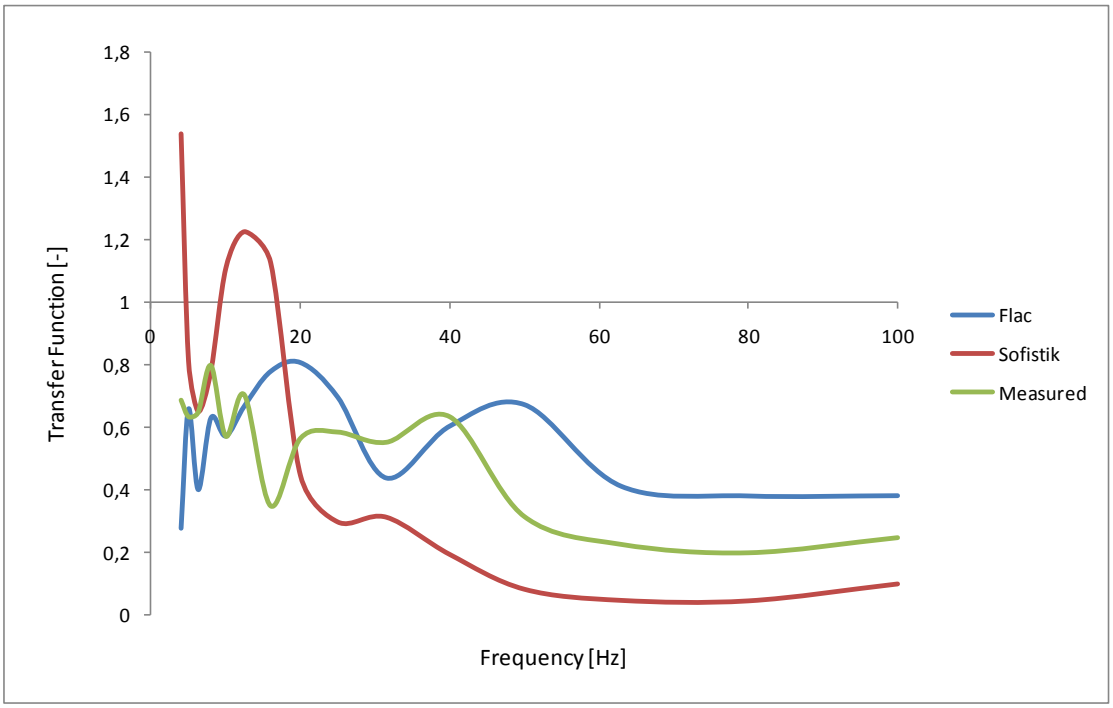

Figure 5.22 – Comparison between the different soil-foundation transfer functions (FLAC, SOFISTIK and measured results)

The FLAC graphic brings out closer and conservative results. Therefore, the assumptions for this software can be taken as valid. For the complete model concerning the whole building structure, a SOFISTIK model could still be used as the model for the elastic foundation has demonstrated to be credible. However, for this software, whatever are the time series applied to the tunnel, they must be transformed into the loads that are expected to act over the foundation of the building, through the transfer functions computed in the FLAC model.

5.2.3.1. FLAC's theory and background

In the finite difference method, every derivate in the set of governing equations is replaced directly by an algebraic expression written in terms of field variables (for instance, stress or displacements) at a discrete point in space. These variables are undefined within elements. In contrast, the finite element method has a central requirement that the field quantities (stress, displacement) vary throughout each element in a prescribed fashion, using specific functions controlled by parameters. Both methods produce a set of algebraic equations to solve. Even though these equations are derived in quite different ways, it is easy to show (in specific cases) that the resulting equations are identical for the two methods. However, over the years, certain "traditional ways" of doing things have taken root, such as finite element programs that combine the element matrices into a global stiffness matrix,

whereas this is not normally done with finite differences because it is relatively efficient to regenerate the finite difference equations at each step. FLAC uses an "explicit", time-marching method to solve the algebraic equations, but implicit, matrix oriented solution schemes are more common in finite elements.

The calculation sequence combined in FLAC is illustrated in Figure 5.23:

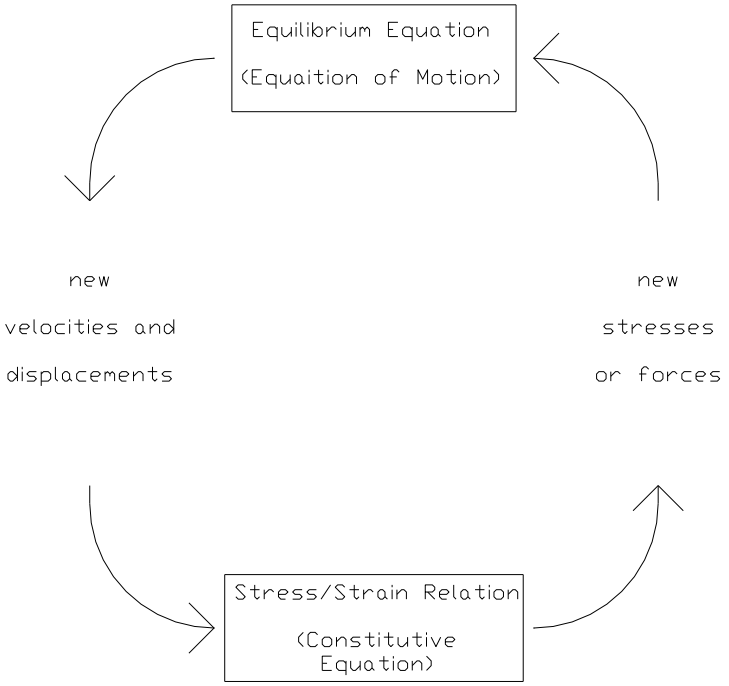

Figure 5.23 – Basic explicit calculation cycle (FLAC, 2005)

This procedure first invokes the equations of motion to derive new velocities and displacements from stresses and forces. Then, the strain rates are derived from velocities and the new stresses from strain rates. One timestep for every cycle around the loop is taken. The important thing to realize is that each box in Figure 5.23 updates all of its grid variables from known values that remain fixed while control is within the box. This might seem unreasonable because it is known that if a stress changes somewhere, it will influence its neighbors and change their velocities. However, the chosen timestep is so small that information cannot physically pass from one element to another in that interval.

Since it is not needed to form a global stiffness matrix, it is a trivial matter to update at each timestep in large-strain mode. The incremental displacements are added to the coordinates so that the grid moves and deforms with the material it represents. This "Lagrangian" formulation contrasts to an "Eulerian", in which the material moves and deforms relative to a fixed grid.

The method presented by *Wilkins* (1964) consisting of deriving difference equations for elements of any shape (also known as the "finite volume method") is used in FLAC. Using Wilkins' method, boundaries can be any shape, and any element can have any property value – just like finite elements.

The solid body is divided by the user into a finite difference mesh composed of quadrilateral elements. Internally, FLAC subdivides each element into two overlaid sets of constant-strain triangular elements, as shown in Figure 5.24:

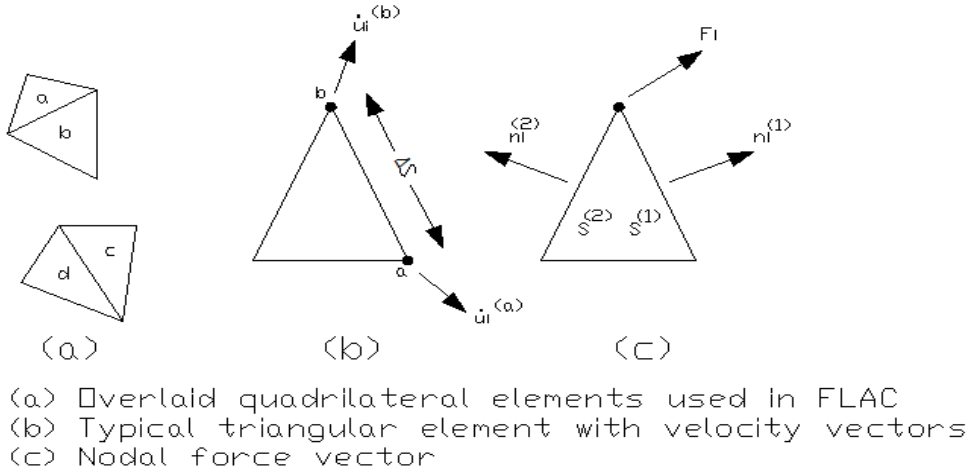

Figure 5.24 – FLAC's quadrilateral elements subdivision (FLAC, 2005)

The deviatoric stress components of each triangle are maintained independently, requiring sixteen stress components to be stored for each quadrilateral (4 x σ_{xx}, σ_{yy}, σ_{zz}, σ_{xy}). The force vector exerted on each mode is taken to be the mean of the two force vectors exerted by the two overlaid quadrilaterals. In this way, the response of the composite element is symmetric, for symmetric loading. If one pair of triangles becomes badly distorted then the quadrilateral are used. If both overlaid sets of triangles are badly distorted, FLAC complains with an error message.

5.3. WAVE PROPAGATION

The FLAC model, specifically designed for the soil subsystem, also describes the wave propagation through the media. In Figure 5.25 different times after the train vibration acts can be observed.

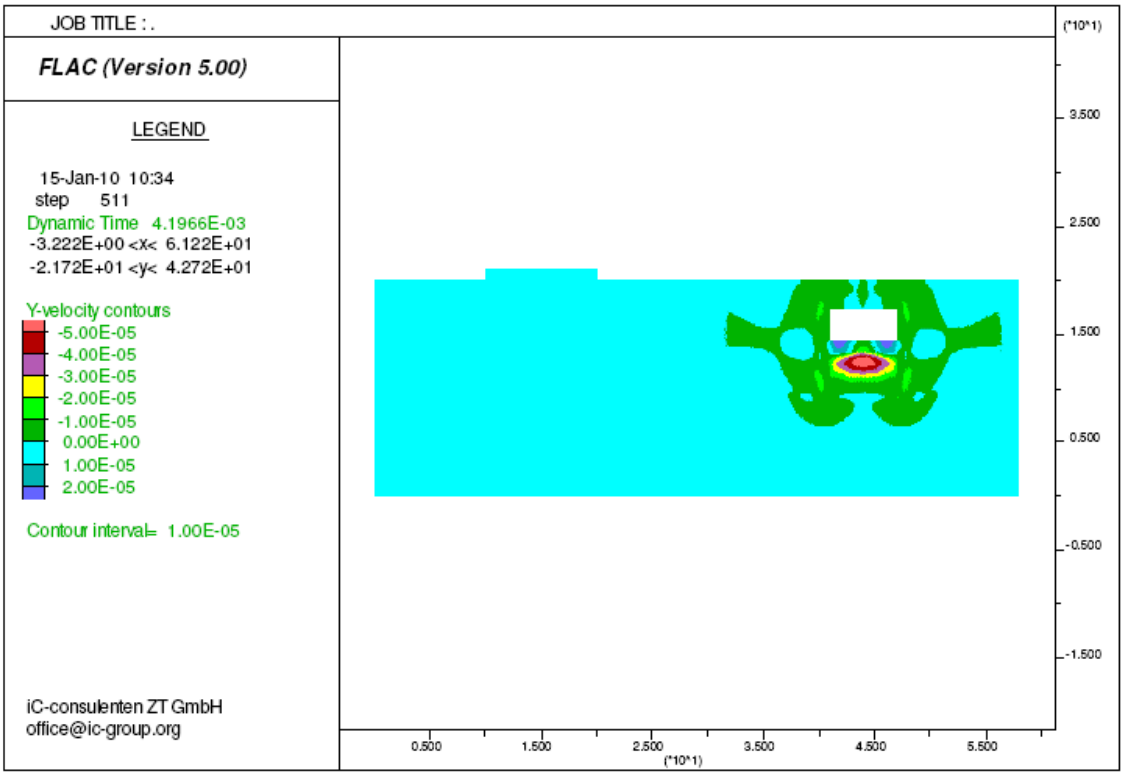

Figure 5.25a – wave propagation over the halfspace (I)

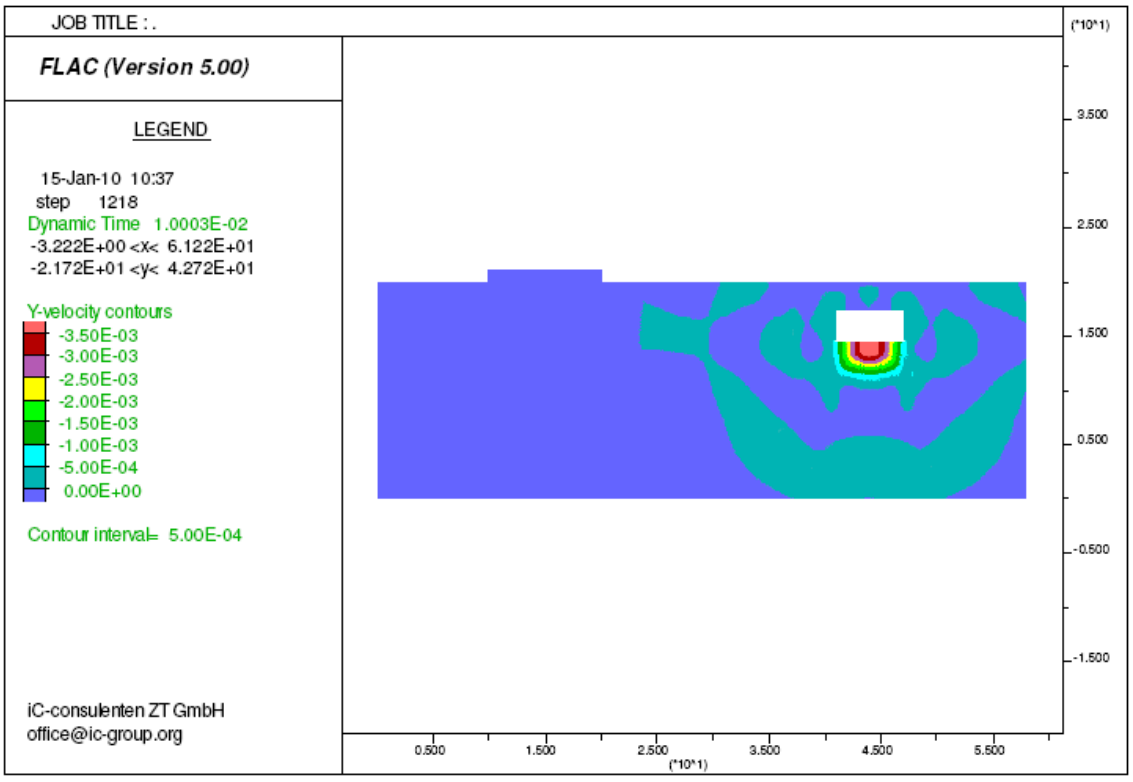

Figure 5.25b – wave propagation over the halfspace (II)

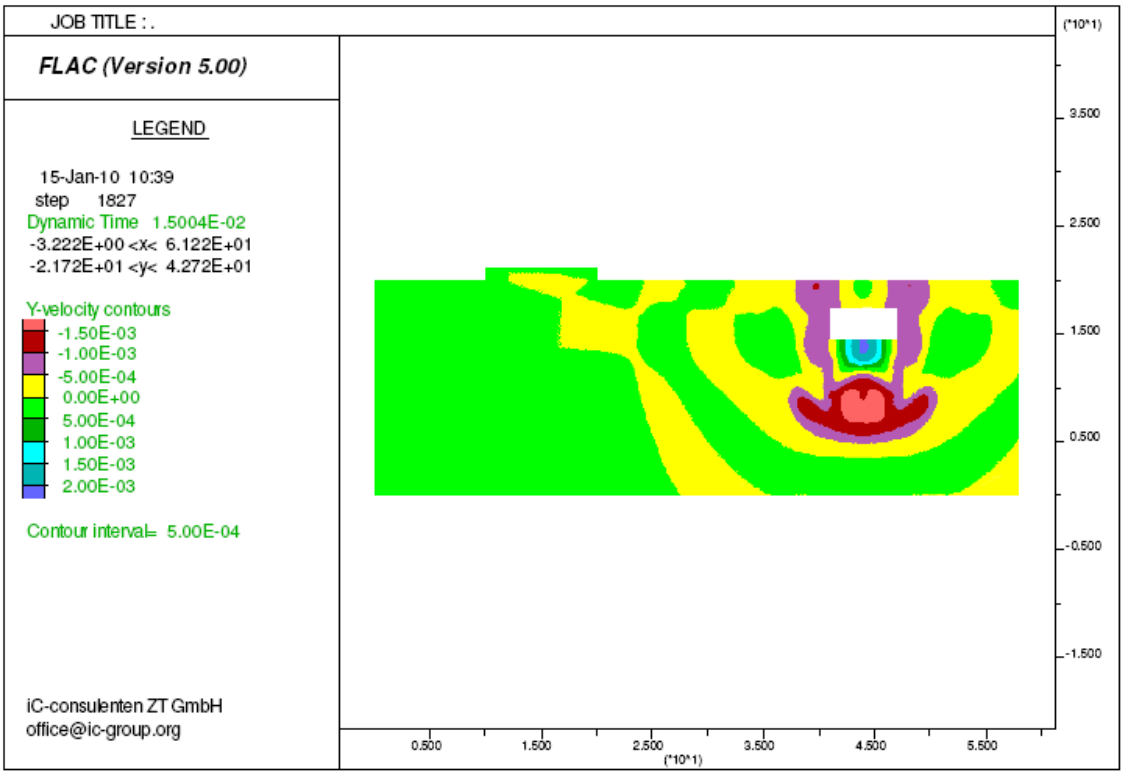

Figure 5.25c – wave propagation over the halfspace (III)

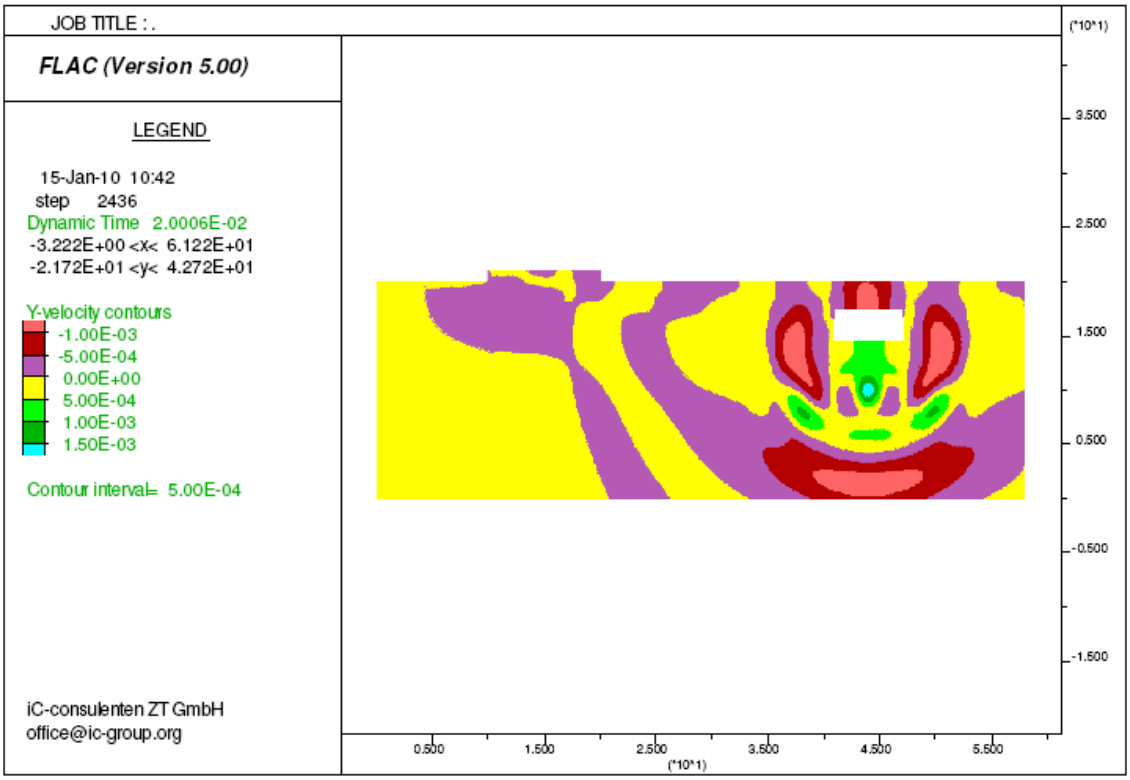

Figure 5.25d – wave propagation over the halfspace (IV)

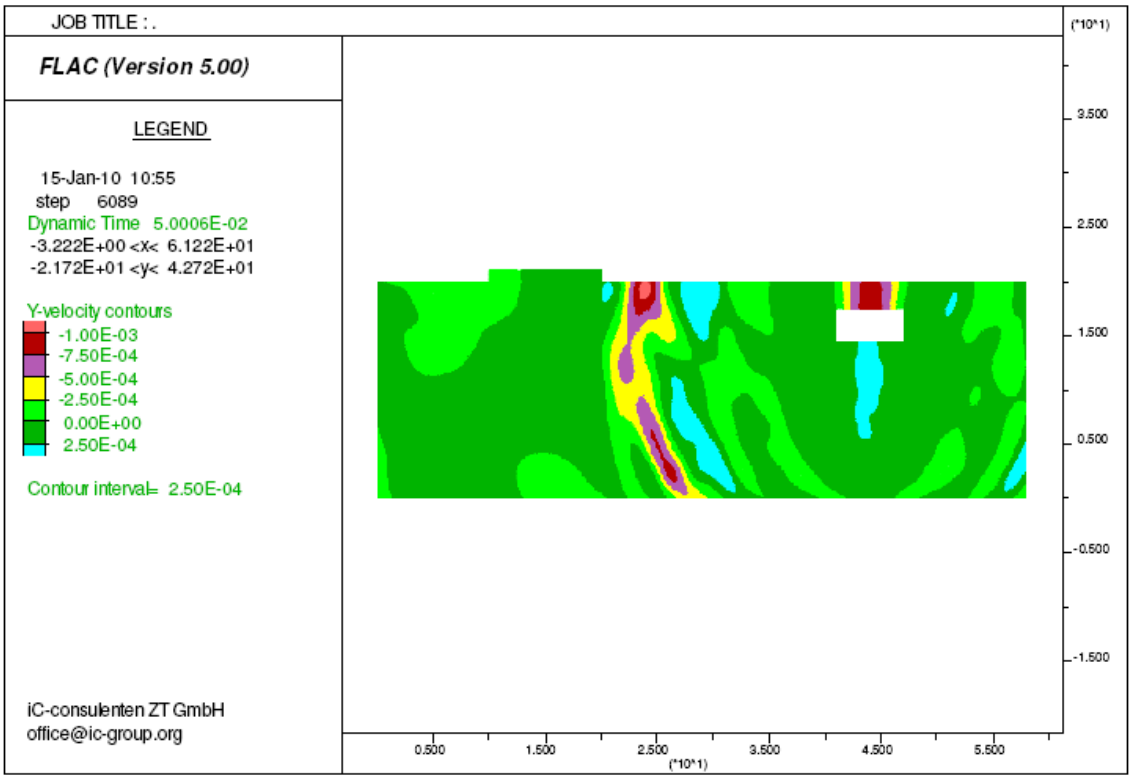

Figure 5.25e – wave propagation over the halfspace (V)

It is possible to observe from the velocity contours the generation of longitudinal, shear and Rayleigh waves. It is clearly visible that the propagation in the longitudinal direction is faster than in the vertical one, as described in chapter 2. The R-waves, in turn, are perceptible from the lower velocity propagation at shallow depths.

5.4. ANALYSIS OF THE HUMAN RESPONSE EXPECTED INSIDE THE BUILDING

5.4.1. BACKGROUND

Although some external dynamic loads can damage the structure of the building significantly, the importance of analyzing the vibrations induced by trains lies especially at the human response criteria. As long as the structural criteria are related to the ultimate limit state, the human comfort has to do with the serviceability limit state. The human perception of vibration actions varies from person to person and hence the value of the vibration limits should be seen as reference values and not fixed values. Also some other factors can influence the human perception and sensibility: the age, gender, activity, the vibration length, frequency and direction.

A simple way to evaluate the human sensibility to different vibration levels, according to several authors, is indicated in Table 5.3.

Table 5.3 – Human perception limits to vibrations (upright position)

Effects of vibration on Humans	Frequencies from 1 to 10 Hz a_{max}[mm/s^2]	Frequencies from 10 to 100 Hz a_{max}[mm/s^2]
Imperceptible	10	0.16
Barely perceptible	40	0.64
Clearly perceptible	125	2.0
Bothersome	400	6.4
Very unpleasant	1000	16
Intolerable	>1000	>16

The vibration values in Table 5.3 are supposed to be of harmonic nature, which amplitudes are less than 1 mm, and they are distinguished, by means of frequencies, into two groups.

Nevertheless, some standards establishing limits to vibration levels in structures in order to satisfy the human comfort are already known.

The DIN 4150-2 establishes admissible values for frequencies ranged from 1 to 80 Hz, using a parameter KB, defined as:

$$K_B = d\,\frac{0.8f^2}{\sqrt{1+0.032f^2}} \qquad (5.16)$$

where d is the amplitude and f is the frequency.

Some limits for the value of KB are shown in Table 5.4:

Table 5.4 – Acceptable values of vibrations in buildings, evaluated in K_B, suggested by the norm DIN 4150-2

Building location	Period	Acceptable KB	
		Continuous or repeated vibrations	Infrequent vibrations
Purely residential areas, property rental and resorts	Day	0.2 (0.15*)	4
	Night	0.15 (0.1*)	0.15
Villages, small office areas and shopping centers	Day	0.3 (0.2*)	8
	Night	0.2	0.2
Office areas and general trade	Day	0.4	12
	Night	0.3	0.3
Industrial areas	Day	0.6	12
	Night	0.4	0.4
Particularly sensitive areas to vibrations	Day	0.1 – 0.6	4 – 12
	Night	0.1 – 0.4	0.15 – 0.4

(*) adopted values for horizontally excited buildings which frequencies are lower than 5 Hz

The norm ISO 2631, in turn, evaluates the human response in a certain direction, for vibrations transmitted through a rigid support surface. This standard considers 3 discomfort levels and a crest factor which is a ratio between the peak value and the effective value of the measured signal. This last one is given by:

$$a_{eff} = \sqrt{\frac{1}{T}\int_0^T a^2(t)dt} \qquad (5.17)$$

where a is the acceleration and t is the timeframe.

The considered system of axis is schemed in figure 5.26:

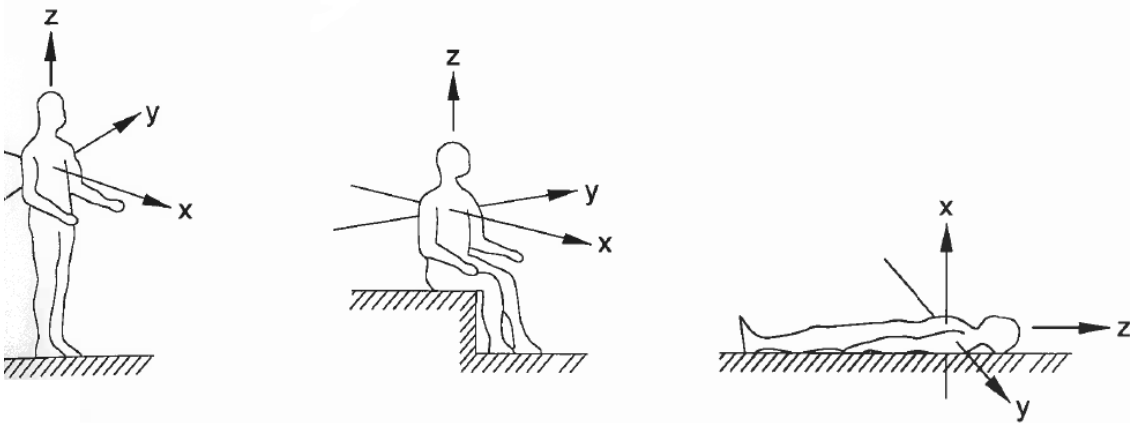

Figure 5.26 – System of axis considered by the norm ISO 2631

The limits for the loss of efficiency level are shown in Figures 5.27 and 5.28 and the same levels for the discomfort level and the maximum exposure level can be obtained by reduction factors of 3.15 and 2, respectively, applied to the values of Figures 5.27 and 5.28. For non-harmonic vibrations, the evaluation is carried out according to one-third octave bands.

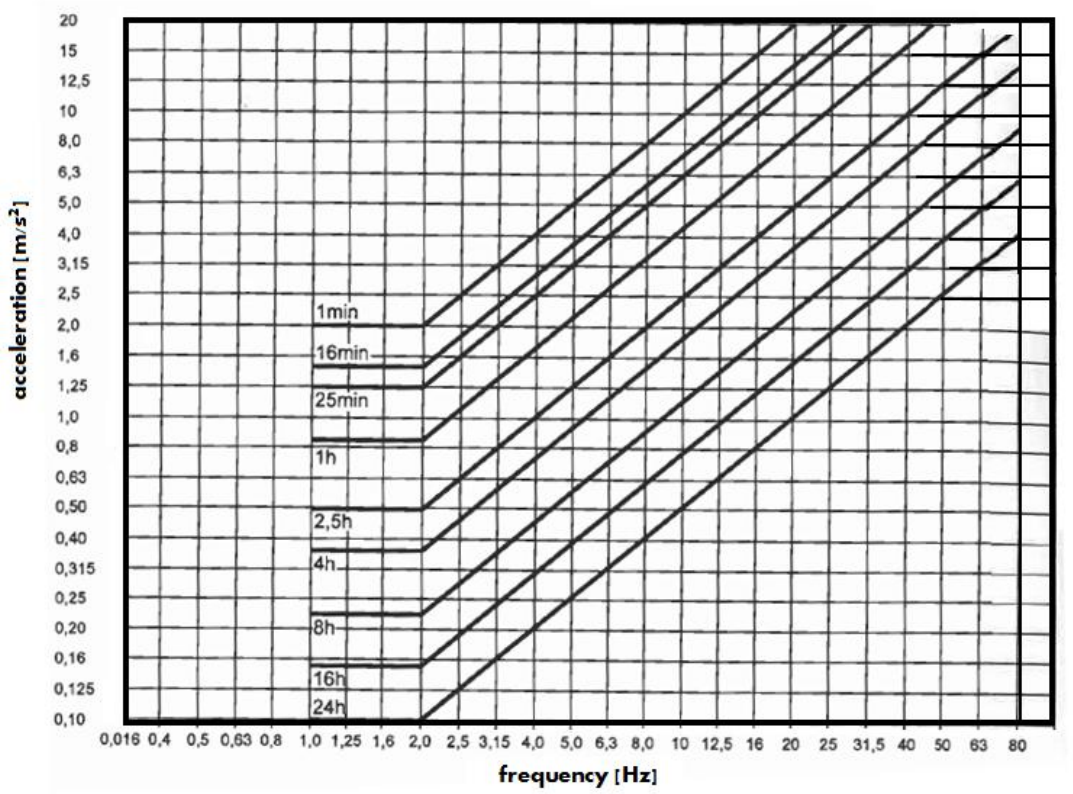

Figure 5.27 – Limits of the loss of efficiency by fatigue associated with direction z (ISO 2631)

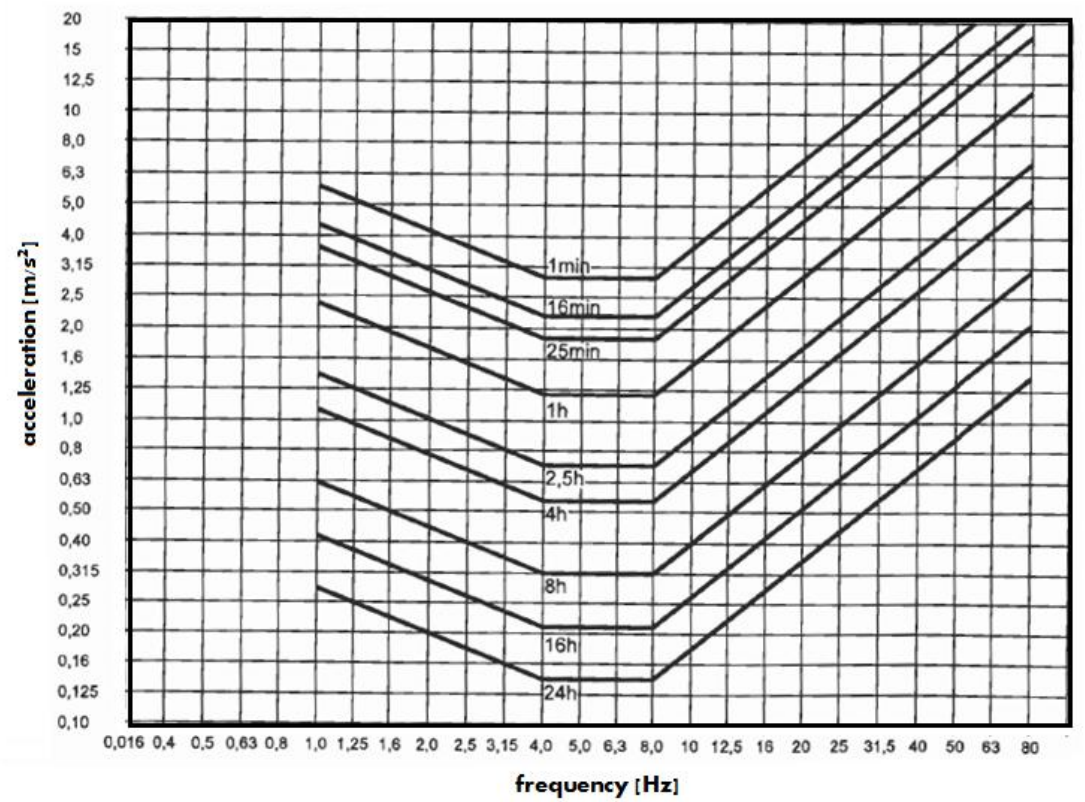

Figure 5.28 – Limits of the loss of efficiency by fatigue associated with directions x and y (ISO 2631)

Table 5.5 – Third octave bands characterization

Band number	Central Frequency [Hz]	1/3 octave [Hz]		Band number	Central Frequency [Hz]	1/3 octave [Hz]	
		f_1	f_2			f_1	f_2
1	1.25	1.12	1.41	11	12.5	11.2	14.1
2	1.6	1.41	1.78	12	16	14.1	17.8
3	2	1.78	2.24	13	20	17.8	22.4
4	2.5	2.24	2.82	14	25	22.4	28.2
5	3.15	2.82	3.55	15	31.5	28.2	35.5
6	4	3.55	4.47	16	40	35.5	44.7
7	5	4.47	5.62	17	50	44.7	56.2
8	6.3	5.62	7.08	18	62	56.2	70.8
9	8	7.08	8.91	19	80	70.8	89.1
10	10	8.91	11.2	20	100	89.1	112

The central frequency is given by

$$f_0 = \sqrt{f_1 \times f_2} \qquad (5.18)$$

where f_1 and f_2 are the lower and the upper limits for each third octave band (Table 5.5).

Some improvements have been done over the past years to norm ISO 2631. Whereas this norm takes a frequency range of [1; 80] Hz and a crest factor of 3, recent added chapters/new standards define a range from 0.1 to 0.5 Hz for the incidence of sickness and motion and from 0.5 to 80 Hz for the other effects (health, vibration perception and comfort) and the crest value is 9 (ISO 2631-1).

The Austrian standard is based on the ISO 2631 standard and the study case can be analyzed under it.

In case the vibrations have a wide spectra content, the effects of the vibrations of different frequencies are superposed, which contradicts the methods suggested in ISO 2631 whereby the vibration levels should be evaluated by means of the central frequency of each third octave band. While the new methods suggest that several weighting functions must be used according to several criteria, the Austrian standard uses a general weighting function whatever is the case. Such weighting function is shown in Figure 5.29 and Table 5.6.

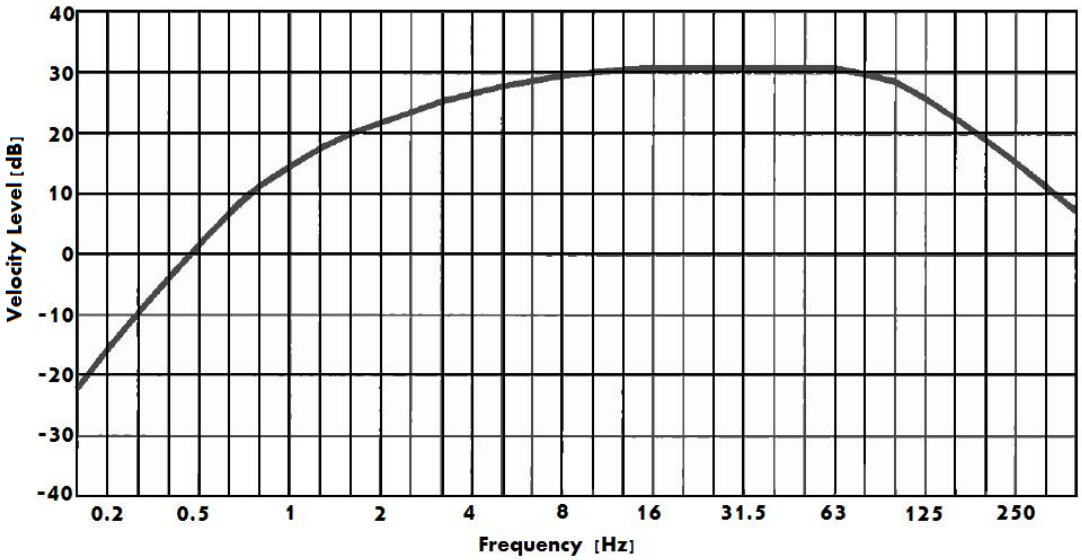

Figure 5.29 – Weighting function (Austrian standard)

Table 5.6 – Weighting function values

x	Frequency [Hz]		W_m	W_m
	nominal	exact	Factor	dB
-7	0.2	0.1995	0.0788	-22.06
-6	0.25	0.2512	0.157	-16.08
-5	0.315	0.3162	0.310	-10.18
-4	0.4	0.3981	0.608	-4.32
-3	0.5	0.5012	1.16	1.28
-2	0.63	0.6310	2.10	6.44
-1	0.8	0.7943	3.49	10.86
0	1	1.000	5.23	14.38
1	1.25	1.259	7.17	17.12
2	1.6	1.585	9.30	19.38
3	2	1.995	11.7	21.36
4	2.5	2.512	14.4	23.14
5	3.15	3.162	17.3	24.78
6	4	3.981	20.5	26.22
7	5	5.012	23.6	27.46
8	6.3	6.310	26.5	28.48
9	8	7.943	29.0	29.26
10	10	10.00	31.0	29.84
11	12.5	12.59	32.5	30.24
12	16	15.85	33.6	30.52
13	20	19.95	34.3	30.72
14	25	25.12	34.7	30.82
15	31.5	31.62	35.0	30.88
16	40	39.81	35.0	30.88

17	50	50.12	34.3	30.72
18	63	63.10	33.1	30.38
19	80	79.43	30.1	29.58
20	100	100.0	25.3	28.02
21	125	125.9	19.1	25.60
22	160	158.5	13.2	22.44
23	200	199.5	8.70	18.78
24	250	251.2	5.59	14.94
25	315	316.2	3.56	11.02
26	400	398.1	2.25	7.04

*NOTE: x is the frequency band number according to IEC 61260: 1995

5.4.2. MODELING AND RESULTS

For an estimation of what to expect inside the building when subjected to the train vibrations, a 2D frame was idealized as following:

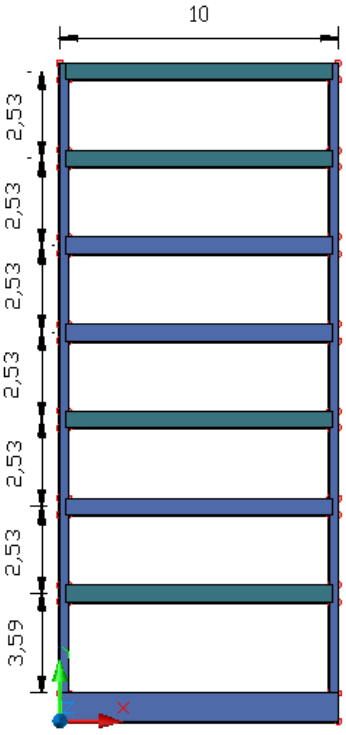

Figure 5.30 – 2D frame scheme

- Beams section: 0.3 x 0.6 m^2;

- Columns section: 0.3 x 0.3 m^2;
- Concrete C20/25 (EN 1992).

Regarding the model in 5.1, a new value for the spring elements had to be set, as the compressive stress was out of the linear range variation (Figure 5.3). To calculate the maximum compressive stress on the plate the following assumptions were taken:

- Distributed static loads of 165 kN/m^2, corresponding to an estimation of the weight of the slabs plus the defined values in Eurocode for habitation buildings type, applied to each beam element;
- Dead load factor of 1.0 (self weight).

The value obtained was 0.166 N/mm^2. Although this value is in a non-linear variation range, linear springs were assumed due to the very small displacements verified for this kind of actions. The slope at the intended point in the chart led one to define a spring stiffness of 56521.7 kN/m/m, i.e. 26915.1 kN/m for each of the 21 spring elements along the two plates interface (10 m).

Another digression from the elastic foundation model is that damping must be defined for the building structure, as the mass is more significant. Table 5.7 shows the first 25 vibration modes for the building structure (using Lanczos method):

Table 5.7 – First 25 vibration modes for the building structure

No.	Frequency [Hertz]	Activated Mass [%]	No.	Frequency [Hertz]	Activated Mass [%]
1	**1.433**	**32.71**	**14**	20.028	29.00
2	4.362	33.64	**15**	24.303	22.72
3	7.541	35.44	**16**	36.080	14.13
4	10.869	32.35	**17**	40.490	11.80
5	12.021	4.51	**18**	42.568	10.55
6	12.888	9.69	**19**	43.739	5.99
7	12.249	7.37	**20**	44.951	10.31
8	13.841	10.68	**21**	63.648	14.61
9	14.295	32.09	**22**	76.014	15.52
10	14.584	9.10	**23**	93.960	5.76

11	15.328	7.32	**24**	138.250	3.82
12	**15.696**	**7.88**	**25**	169.976	19.31
13	17.525	30.19			

To know up to which vibration mode is worth to take the eigenfrequencies into consideration, in order to determine α and β, not only the mass contribution is important, but also the modes have to correspond to a vertical vibration. Therefore the first 12 vibration modes were considered:

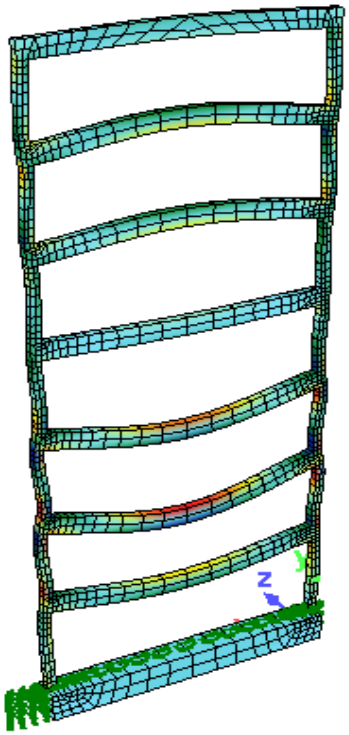

Figure 5.31 – 12th vibration mode of the 2D frame

It was assumed that the significant dynamic response of the system would die down within the first twelve modes with damping ratios varying between 1.5% and 2%. Note that these damping values correspond to the concrete damping values and not to the whole structure ones. The damping ratios ranges concerning the structures usually have higher upper limits, as factors as the connection between structural elements increase the damping value and hence this is a conservative assumption. The values obtained for α and β were 0.23923 sec^{-1} and 0.000381 sec, respectively.

The complete model scheme is shown in Figure 5.32:

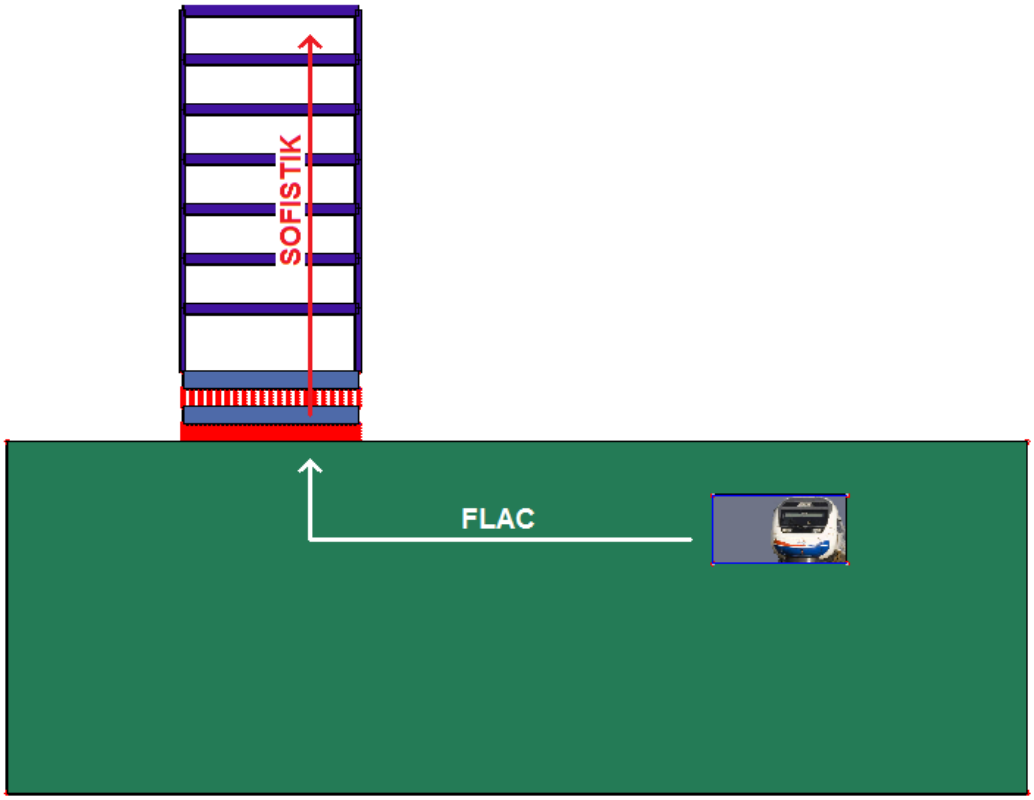

Figure 5.32 – Global modeling scheme

For an expected dynamic train load applied on the tunnel (Figure 5.9, for instance), the following transfer functions between the upper plate of the foundation and the first two floors were obtained:

Table 5.8 – Transfer functions for the 2D frame

Frequency [Hz]	TF foundation-1st floor [dB]	TF foundation-2st floor [dB]	TF foundation-1st floor	TF foundation-2st floor
4	3.5	6.1	1,49623566	2,01836636
5	6.682	11.876	2,15824131	3,92464157
6.3	-1.871	-7.91	0,80621338	0,40225366
8	4.21	3.08	1,62367835	1,42560759
10	-4.36	-0.33	0,60534087	0,96272001
12.5	-4.09	-3.48	0,62445335	0,66988461
16	-0.42	-2.13	0,95279616	0,78252821
20	-3.09	0.56	0,70064818	1,06659612

25	-1.323	-3.487	0,85871688	0,66934496
31.5	-15.786	-22.359	0,16244263	0,07621668
40	-21.774	-33.118	0,08152673	0,02208513
50	-24.44	-34.409	0,05997911	0,0107041
63	-27.69	-44.04	0,04125722	0,00628058
80	-30.053	-41.963	0,03143041	0,00797719
100	-30.42	-35.28	0,03013006	0,01721869

In Figure 5.33 a range of records from track for trains passing nearby the building provides one the data that is needed for the human response analysis.

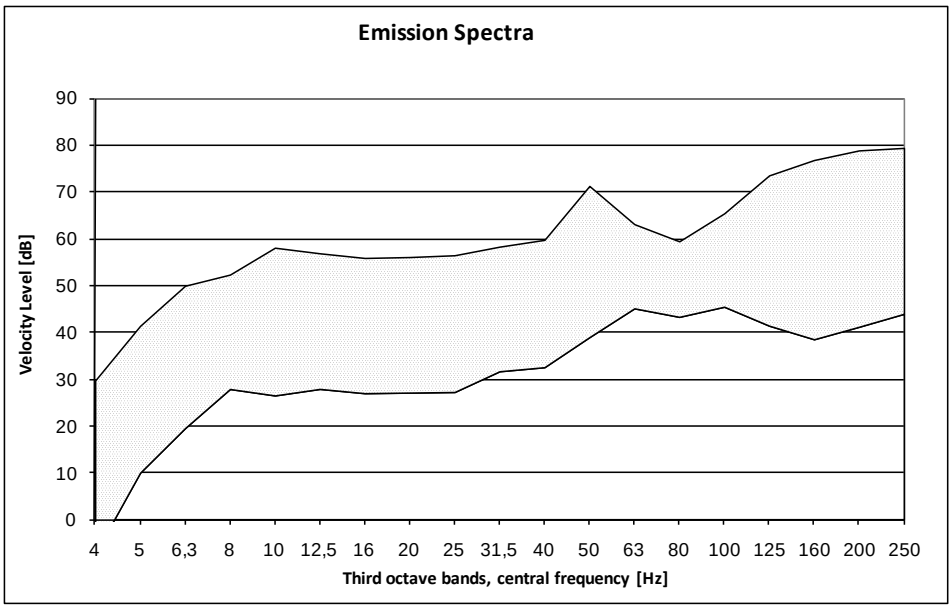

Figure 5.33 – Train vibrations measured on the train track

The following relationships shall be presented:

$$v\left[dB\right] = 20 \cdot \log\left(\frac{v\left[m/s\right]}{5\times10^{-8}}\right) \qquad (5.19)$$

$$v\left[m/s\right] = 10^{\frac{v\left[dB\right]}{20}} \times 5\times10^{-8} \qquad (5.20)$$

In Table 5.9, the predicted results are shown based on average values from Figure 5.33 and the Austrian standard.

Table 5.9 – Accelerations on the first two floors

Train vibration [dB]	Train vibration [mm/s]	1st floor	2nd floor
15.2911111	0.00029075	0.00244219	0.00329442
27.4553333	0.00117961	0.03937755	0.07160588
36.9837778	0.00353312	0.0299816	0.01495908
42.1145556	0.00637819	0.18818967	0.16523262
43.563	0.00753564	0.08044178	0.12793274
45.6736667	0.00960845	0.12972889	0.13916714
42.8305556	0.00692624	0.17192422	0.14120077
44.6253333	0.00851602	0.16444883	0.25034031
45.3097778	0.00921423	0.19016841	0.14823077
45.8404444	0.00979472	0.02419693	0.01135299
53.3825556	0.02333984	0.03999133	0.01083343
57.6231111	0.03802993	0.05235036	0.00934264
54.4104444	0.02627195	0.01463256	0.00222751
50.9747778	0.01768923	0.0063114	0.00160186
54.6813333	0.0271042	0.00777924	0.00444567
Energetic sum – acceleration (mm/s^2)		**0.39896926**	**0.4163403**

The Austrian norm establishes a value of 0.00357 mm/s^2 from which the human perception is noticeable and an admissible limit of 0.00714 mm/s^2. The obtained values for the first two floors are practically the and smaller than the noticeable limit of a factor of 10 (!). According to these results, the adopted solution for the elastic foundation model seems to be efficient.

As the vibrations decrease with area of propagation, no additional analysis is needed for the upper floors since the accelerations are supposed to be lower and the first two floors already fulfill the standards requirements.

6

Closing remarks

During this work, an attempt to achieve a FE model that yielded consistent results for a dynamic SSI was tried. Even within the dynamic analysis domain several assumptions may be taken depending on the nature of the problem. For instance, the damping defined as Rayleigh damping for many subsystems could not be the best assumption if it came to seismic analysis, as the produced frequencies of the ground would be in a lower range corresponding to the left branch of the analytical Rayleigh curve.

SOFISTIK® is a proven software in what concerns static analysis, static calculations involving the soil and even dynamic analysis for structures. Nevertheless, the halfspace module of this software is not able to carry out any analysis for the soil under motion. The described steps meant to replace the halfspace by a structure with the soil characteristics have proved to be unsuitable. Despite the formulation for the soil-structure interface that is based on the theoretical modeling behind proven software in dynamic SSI such as FLAC, thus representing a credible approach, the soil subsystem did not perform as expected, as a soil. Moreover, the current SOFISTIK versions do not provide the user the visualization of any wave propagation over the "soil" as FLAC does, which turns even harder to figure out what the behaving of such substructure is and therefore to take any conclusions.

The adaptation that was taken afterwards ensures acceptable results. However, FLAC's modeling requires much time to spend on and the complexity of the models is limited. The main challenge for coming works with the same subject would reside on the improvement or rather another tries to generate FE models where calculations ensure not only reliable results, but also less time and the whole model assembled in the same program and calculated at once. It is known that some other software that can be capable to fulfill these requirements are already in use. The SASSI 2000 could be one of them. However, it was not possible to get this program for the current work.

Concerning the expected results for the human perception, the obtained values of a factor of 10 times below the perception limits are plausible. The accelerations for the first and the second floor are approximately the same. As the modeling was done by using a 2D frame the energy dissipation between the floors is much lower than in a 3D frame, due to the smaller area. There are also cases where the experimental records show higher signals for a second floor. In some measurements for similar and previous projects it was often tried to achieve a factor of 4 (to get a safety value for the prognosis) below the perception limit as higher value. Furthermore, one must considerate that the chosen values were average values and not the most critical ones, which would increase the accelerations from 10 times less to around 5. Besides that, the Austrian standard uses the third octave band analysis of just the maximum timeframe (max-eff method) which gives even higher results (4-10 dB) than the third octave analysis for the whole signal (the one that was taken).

The results at the frequency domain for different sub-models were obtained in different ways. As long as the system involving only the elastic foundation is theoretically similar to a singly mass system, where the natural frequency has a low value, the soil is more often compared to a multi degree of freedom system where the natural frequencies can reach high values. The aliasing can be a limitation of the FFT when converting signals with very high frequencies and therefore unexpected peaks of the transfer functions can wrongly result for such high frequencies. Another issue is that the Austrian standard works with the third octave band analysis. Thus, to get the human response in the building, the terz analysis must be used for the soil.

Using the terz analysis mixed up with the FFT is not possible, not only because it is very hard to get the terz from the FFT, but also because it is impossible to get the FFT from the terz.

Compared to the "normal" frequency analysis often based on a FFT algorithm by Cooley & Turkey, the third octave band analysis does not use equally spaced bandwidth for the analysis. In case of the frequency analysis, the bandwidth between two lines in the spectrum depends on the Nyquist frequency of the signal and the length of the signal respectively. For the third octave band analysis the situation is completely different. In the third octave band analysis, the relationship of the lower (f_1) and the upper (f_2) frequency limit of the bandwidth is constant, as shown below:

$$\frac{f_2}{f_1} = \sqrt[3]{2} = 1.26 \qquad (6.1)$$

As obvious from Equation (6.1), the bandwidth increases with increasing frequency whereas the ratio between the upper and the lower frequency remains constant.

The charts in Figure 6.1 are examples of a third octave band analysis and a frequency analysis, respectively:

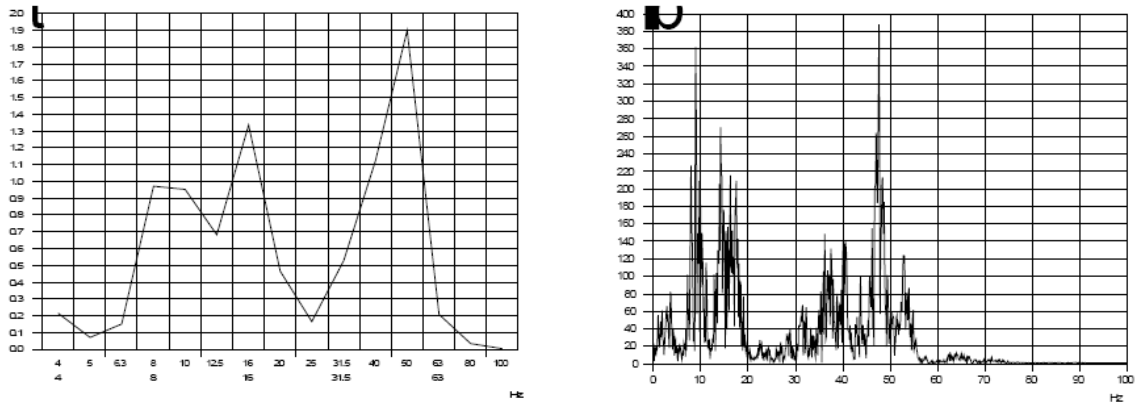

Figure 6.1 – Third octave band (left) and frequency chart (right)

The calculation of the third octave band spectrum is mainly done by digital filters. Practically in digital signal process applications the filters are added to filter bank tool.

At last, for the comparisons between practical and theoretical results that were considered to be satisfactory, some high differences at some points in the charts may bring out some doubts. It should be taken into account that theoretical models represent ideal models and the reality involves many other factors that are not considered in theory. For instance, from previous experimental tests it was proven that difference of just 10 cm in the geophone positioning can sometimes result in errors up to 100%.

To conclude, according to the work results it can be assumed that, regarding the human comfort, the adopted elastic foundation model will avoid eventual issues from induced train vibrations and so similar elastic foundations can be taken into consideration for future projects under similar conditions (it shall be referred that this building represents the first of a series of buildings to be built in the same area along the path of the train track in a period of around 2 years).

BIBLIOGRAPHY

Baguelin, F., Jézéquel, J., Shields, D., *The Pressuremeter and Foundation Engineering*, Trans Tech Publications, 1978.

Bahrekazemi, M., *Train Induced Ground Vibrations and its Prediction*, Dissertation, Stockholm, 2004.

Cavalcanty, D., *Análise da Interacção Solo Estrutura através do Emprego Conjunto dos Métodos dos Elementos de Contorno e Elementos Finitos*, Dissertation, Maceió–AL , 2006.

Colares, G., *Programa para Análise da Interacção Solo-Estrutura no Projecto de Edifícios*, Dissertation, São Carlos, 2006.

Danziger, B., Carvalho, E., Costa, R., *Estudo de Caso de Obra com Análise da Interacção Solo Estrutura*, 2005.

Fang, H., *Foundation Engineering Handbook*. Chapman & Hall, New York, 1991.

Flesh, R., *Baydynamik Praxis Grecht*, Editor, Wien, 1993.

IC Consulenten, *Arcade Meidling*, Wien, 2002.

Itasca Consulting Group, *FLAC version 5.0 Optional Features*, Minneapolis, 2005.

Itasca Consulting Group, *FLAC version 5.0 Background and Theory*, Minneapolis, 2005.

Mita, A., Yoshida, K., Kumagai, S., Shioya, K., *Soil Structure Interaction Using Impulse Response – Earthquake Engineering and Structural Dynamics, vol.18*, Tokio, 1989.

Moutinho, C., *Controlo de Vibrações em Estruturas de Engenharia Civil*, Dissertation, Univ. Porto, Porto, 2007.

Rao, S., *Mechanical Vibrations*. Pearson Education, New Dehli, 1991.

Richart, F., Hall, J., Woods, R., *Vibrations of Soils and Foundations*. Prentice Hall, Cidade de publicação.

Sanayei, M. *Predicting Train Induced Vibrations Propagation in Multy-Story Buildings*. http://engineering.tufts.edu/cee/people/hines/Sanayeieetal2008.pdf , 17-10-2009.

Santos, S., *Um Modelo Semi-Analítico em Elementos Finitos Para Interacção Inercial em Análise Sísmica*, Dissertation, Rio de Janeiro, 1980.

Smekal, A., Bodare, A., Massarch, K., *PrognosVib, Effects of Vibration from Railway Traffic*, 2002.

Stewart, J. *Seismic Soil-Structure Interaction in Buildings*. 01-01-1999, http://www.escholarship.org/uc/item/7qp9w0tb 16-10-2009, 06-10-2009.

Tsudik, E., *Analysis of Beams and Frames on Elastic Foundation*. Trafford, 2006.

Zeevaert, L., *Foundation Engineering for Difficult Subsoil Conditions*. Krieger, New York, 1979.

Zeevaert, L., *Interacción Suelo-Estructura de Cimentación*. Limusa, Mexico, 1980.

http://www.ejge.com/2003/Ppr0318/Ppr0318.pdf , 05-10-2009

http://cp.literature.agilent.com/litweb/pdf/5952-8898E.pdf, 05-10-2009

http://bssa.geoscienceworld.org/cgi/content/abstract/99/2A/611, 06-10-2009

http://www.csiberkeley.com/Tech_Info/16.pdf, 06-10-2009

http://linkinghub.elsevier.com/retrieve/pii/S0022460X0800878X, 06-10-2009

http://www.calenberg-ingenieure.de/eng/pdf/Cibatur_englisch.pdf, 07-10-2009

http://en.wikipedia.org/wiki/Ground-structure_interaction, 10-10-2009

http://www.memory-uae.com/image/sap2000/demo3.gif, 10-10-2009

http://www.icivilengineer.com/Software_Guide/product.php?id=82, 11-10-2009

http://en.wikipedia.org/wiki/Body_wave_(seismology), 12-10-2009

http://en.wikipedia.org/wiki/Rayleigh_wave, 12-10-2009

http://www.norsonic.com/index.php?sideID=7195&ledd1=7181, 12-10-2009

http://www.mms.gov/tarprojects/125/125AG.PDF, 20-02-2010